2020

Single Droplet Drying Technology for the Optimization of the Dairy Ingredients with Best Quality and Functionality

Hiral Narendrabhai Vora
South Dakota State University

SINGLE DROPLET DRYING TECHNOLOGY FOR THE OPTIMIZATION OF THE DAIRY INGREDIENTS WITH BEST QUALITY AND FUNCTIONALITY

BY

HIRAL NARENDRABHAI VORA

A dissertation submitted in partial fulfillment of the requirements for the

Doctor of Philosophy

Major in Biological Sciences

Specialization in Dairy Science

South Dakota State University

2020

DISSERTATION ACCEPTANCE PAGE

Hiral Narendrabhai Vora

This dissertation is approved as a creditable and independent investigation by a candidate for the Doctor of Philosophy degree and is acceptable for meeting the dissertation requirements for this degree. Acceptance of this does not imply that the conclusions reached by the candidate are necessarily the conclusions of the major department.

Joseph P Cassady
Advisor Date

Joseph P Cassady
Department Head Date

Nicole Lounsbery, PhD
Director, Graduate School Date

This dissertation is dedicated to my parents.

For their endless love, support, encouragement, and belief in me

ACKNOWLEDGEMENTS

I would sincerely like to thank my advisor, Dr. Lloyd Metzger, for this guidance and support throughout the Ph.D. program, and especially for his confidence in me. He also provided me with an excellent work environment, freedom to work, financial assistantship, and thought-provoking discussions. Without his constant motivation, it would have been impossible for me to complete my thesis writing. It is an honor to work with him.

I would like to thank Dr. Joseph Cassady for promptly accepting to be on my committee and serve as an advisor. I want to extend my gratitude to Dr. Vikram Mistry for his encouragement, help, and insightful comments. Further, I want to thank Dr. Sanjeev Anand for his advice and moral support. I would like to thank Dr. Jessica Meendering for serving on my committee. I would like to thank Dr. Hasmukh Patel for starting my Ph.D. project and hiring me. I would like to thank SDSU for providing an atmosphere for my scientific inquisitiveness.

I am indebted to Dr. Nan Fu and Dr. Xia Dong Chen for providing training at Soochow University (China) on Single Droplet Drying equipment, without which I would have never been able to start the project work. Also, for providing some supplies throughout the study at no cost. I would like to extend my thanks to my advisor Dr. Lloyd Metzger and our department for facilitating this training in China.

Thanks to Dr. Aditya Putranto, Dr. Meng Woo, Dr. Cordelia Selomulya from Monash University, for been research partners on this project.

Help received from Steve Beckman and his team during plant trials is highly appreciated. Thank you, Kristi, Jayne, Akki, John, for your support. I would like to show my gratitude to my friends, Dr. Hari, Dr. Suja, Suresh, Dr. Ananya, Dr. Salunke, Kartik, Krupali, Ahmed, and fellow graduate students and labmates for their help and comments on my work. I am thankful to Dr. Tom and Dorris, for making me part of the FTA group.

Thanks to Valley Queen Cheese factory for providing Whey Protein Concentrate samples for my study. Financial assistance from Midwest Dairy Food Research Centre and National Dairy Council for funding my research project is highly acknowledged. I would also like to thank Dairy Education and Foundation for providing me scholarships for two consecutive years.

I want to thank my parents, Narendra and Daksha Vora for their unconditional love and support throughout my life. Thank you for giving me the courage to chase my dreams and reach for the stars. My thanks go to my husband, Kunal for his constant support during my thesis writing. My sisters, Ulka and Maitri, and my brother-in-law's for constant faith and wholehearted moral support. My niece, Aashi and my nephew, Yug for their fun and frolic phone calls to cheer me up. Last but not the least, I would like to thank all my friends, extended family members and mentors that contributed to my success and led me where I am today.

Thank you, Lord, for always being there for me.

This dissertation is only the beginning of my next journey.

Hiral Vora

CONTENTS

ABBREVIATIONS

MPI	Milk Protein Isolates
MPH	Milk Protein Hydrolysates
WPI	Whey Protein Isolates
WPH	Whey Protein Hydrolysates
SMP	Skim Milk Powder
% (w/w)	Percent weight by weight
RO	Reverse Osmosis
UF	Ultrafiltration
MF	Microfiltration
NF	Nanofiltration
MPa	Megapascal
kDa	Kilo Dalton
kV	Kilo Volt
µm	Micrometer
µL	Microliter
MCC	Micellar casein concentrate
MMCC	Mineral-reduced micellar casein concentrate
CO_2	Carbon dioxide
SDD	Single Droplet Dryer/ Drying
WPC80	Whey Protein Concentrate with 80% protein on dry basis
SEM	Standard Error of Mean
mL	Milliliter

°C	Degree Celsius
kg/m^2	Kilogram per meter square
L/m^3	Liters per cubic meter
g/ml	Gram per milliliter
m/s	Meter per second
vs.	Versus
Cp	Centipoise
SDSU	South Dakota State University

LIST OF FIGURES

CHAPTER 1

LIST OF TABLES

ABSTRACT

SINGLE DROPLET DRYING TECHNOLOGY FOR THE OPTIMIZATION OF THE DAIRY INGREDIENTS WITH BEST QUALITY AND FUNCTIONALITY

HIRAL NARENDRABHAI VORA

2020

As a result of their extended shelf-life, dried dairy ingredients constitute a significant category produced for global markets. During the development of dairy ingredients, several drying trials are typically conducted to determine optimum drying conditions. The results of these trials can be critical in determining optimum dryer design. However, these trials can be expensive and time-consuming. An alternative that has recently been developed using a new technique called single droplet drying (SDD). The SDD technique involves a single droplet suspended on the tip of a glass filament, where changes in droplet diameter, mass, and temperature are measured during drying. SDD makes it possible to create a pictorial view of the drying process. Once the drying process is complete, particle morphology can be determined using microscopy, or the rehydration behavior can be visually studied. A predictive model generated using SDD can then be used to optimize the drying conditions and dryer design. The modeling will help reduce costly plant trials and accelerate the development of new ingredients with novel functionalities. Hence, the Single Droplet Dryer (SDD) was installed at SDSU to conduct the bench-top trials.

The aim of the first study was to study the effect of different solids concentration on the drying kinetics of whey protein concentrate by using SDD. There was a significant

($P<0.01$) change in the diameter, mass, and temperature change profiles during the drying run between 10%, 20%, and 30% total solids level for the WPC80. These activation curves are independent of the initial droplet sizes and constant drying conditions but dependent on the initial total solids' concentration, hence calculated separately for each level of total solids. The viscosity of the WPC80 solution significantly ($P < 0.01$) increases with an increase in the total solids level. There is a correlation between the particles obtained from the semi-commercial spray dryer and the particle generated on the SDD. Scanning electron microscopy, in conjunction with SDD, completely avoids commercial spray drying run to observe a particle and study the morphology of newer materials.

The second study was conducted to compare the differences in the drying kinetics of Micellar Casein Concentrate (MCC) vs. Modified (CO_2 induced) MCC, due to the difference in the composition of both the materials. Due to the differences in the pH and mineral balance between MCC (pH ~ 6.7) and Modified MCC (pH ~ 5.7); and the presence of the higher amount of de-aggregated casein micelle in the modified MCC, there was a significant difference ($P<0.01$) observed in the drying properties like change in moisture removal pattern, mass change of the particle, and temperature change pattern during the drying run. Materials with higher viscosities, higher total protein, and higher total solids, and minor differences in composition can be compared and studied on SDD.

The objective of the third study was to understand the dissolution behavior of the dried particle of the infant formula at two different temperatures, viz: 70°C and 110°C. The outlet temperatures of the dryer have a significant effect ($P<0.01$) on the rehydration properties of dried powder. We have observed a significant difference ($P<0.01$) in the

diameter change/ moisture removal pattern, mass change, and temperature change between 70°C and 110°C, two different temperatures of drying at all the solids level viz., 15%, 40%, and 50%. The change in total solids for each temperature had a significant ($P<0.01$) effect on the properties of the dried particle. We observed better rehydration/ higher solubility ($P<0.01$) of the powder particle of Infant Milk formula dried at 70°C temperature compared to those dried at 110°C. The dissolution times for each total solid at 70°C are significantly ($P<0.01$) different than those at 110°C for corresponding total solid values. Hence, the functionality of dairy powders is affected by the outlet temperatures of the dryer.

CHAPTER 1

REVIEW OF LITERATURE

INTRODUCTION

"No matter how black a cow is, the milk is always white," as the old saying goes. Milk is considered among the essential staple foods, is an integral part of a balanced diet, and contains a high percentage of calcium, among other vital nutrients. Milk is included in the daily diet as such and can be used in a variety of food preparations (Barton, 2000).

There are numerous benefits of consuming dairy products that provide health benefits – significantly improved bone health. Foods in the Dairy category provide nutrients vital for the health and maintenance of the human body. The essential nutrients available from the dairy products include calcium, potassium, vitamin D, and protein (USDA, 2019).

Nutrients

- Calcium is a very important nutrient for building bones and teeth and in maintaining bone mass. In typical American diets, dairy products are the primary source of calcium. Diets that provide three cups or the equivalent of dairy products per day can improve bone mass.
- Diets rich in potassium are vital in maintaining healthy blood pressure. Dairy products, like yogurt, fluid milk, and cheese, are rich in potassium.
- Proper calcium and phosphorous levels are maintained in the body with the help of Vitamin D, thereby helping to build and maintain bones.

Milk, yogurt, and milk-based beverages fortified with vitamin D are good sources of these nutrients.

(Ross et al., 2011)

Health benefits

- Consuming dairy products in daily diet is linked to improved bone health, and the risk of osteoporosis is also reduced.
- During the childhood and adolescence stage of growth for humans, when bone mass is being built, the intake of dairy products has become very important to bone health.
- In adults, the intake of dairy products is associated with a reduced risk of cardiovascular disease and type 2 diabetes, and with the lowering of blood pressure.

(Rozenberg et al., 2016)

CONSUMER PERCEPTION OF MILK AND MILK-BASED POWDERS

The worldwide milk production in 2017 amounted to about 502.82 million metric tons. The United States was ranked second in the world with a milk production amounting to over 98.8 million metric tons in 2018, amongst the major producers (Shahbandeh, 2019).

A recent survey in 2017 on the consumer side revealed that 58 percent of Americans use milk and dairy as a high-quality source of protein. Still, a massive decline has been observed in the per capita consumption of skim milk in the United States from 2000 to 2017. The per capita consumption of milk, in general, is projected to decline

significantly from 194.9 pounds in 2010 to 167.1 pounds in 2019 to 155.3 pounds by 2028 (www.statista.com).

According to the report compiled from the USDA database, the United States per capita consumption of skim milk amounted to 29.7 pounds in the year 2000, which declined to 27.2 in 2010 and a further decline to 13.7 pounds in 2017 (Shahbandeh, 2020).

Contrary to the decline, premium-priced milk categories such as organic, plant-based, or flavored products should assist in increasing American consumption once again.

FASTER GROWTH OF DAIRY INGREDIENT AND PRODUCTS BEYOND TRADITIONAL DAIRY/ REDEFINING DAIRY GROWTH

The dairy market in the United States has a stagnant and sometimes declining growth in recent years, particularly for fluid milk and commodity cheese. To access higher growth in segments outside their historic wheelhouse, dairy manufacturers can start thinking of ways to redefine their identities as more than just traditional dairy processors. (Carbonneau and Meilhac, 2016). However, this is not an easy transition. There are examples of many companies that have excelled at redefining their identities, while numerous companies also fell short.

Dairy products are losing share to non-traditional alternatives, such as almond and soy milk (see Figure 1), and innovations within the dairy sector. Amidst this reality, dairy companies can redefine their identity to add non-traditional alternatives to their product portfolio and serve a broader consumer base. Executing this strategy requires companies

to deploy the appropriate amount of capital and resources to new fast-growing businesses (Carbonneau and Meilhac, 2016).

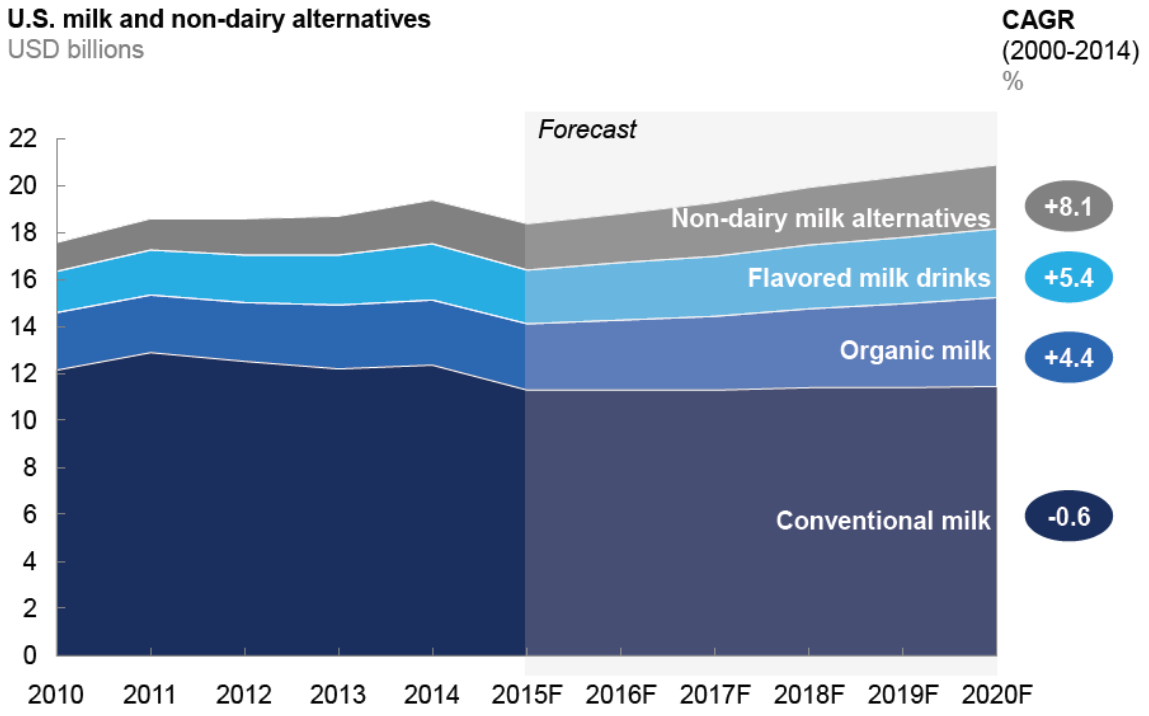

Figure 1. The projected growth for U.S. dairy milk and non-dairy alternatives. (Source: McKinsey and Company, 2016)

The next closest adjacency for milk and cheese players today are dairy ingredients, such as whey protein. Over the last several decades, dairy byproducts have evolved into high-value fractions with large markets both in volume and sales. Two reasons explain this phenomenon. On the manufacturing side, new sophisticated and cost-effective technology allows milk and cheese processors to develop high-functional products by fractionating milk components at a micro-nutrient level (e.g., MPI, MPH, WPI, WPH). On the consumer side, food makers now are more and more using dairy ingredients for their physical characteristics, while end-consumers continue to increase

demand for high protein content foods, such as snack bars and baking ingredient mixes (see Figure 2).

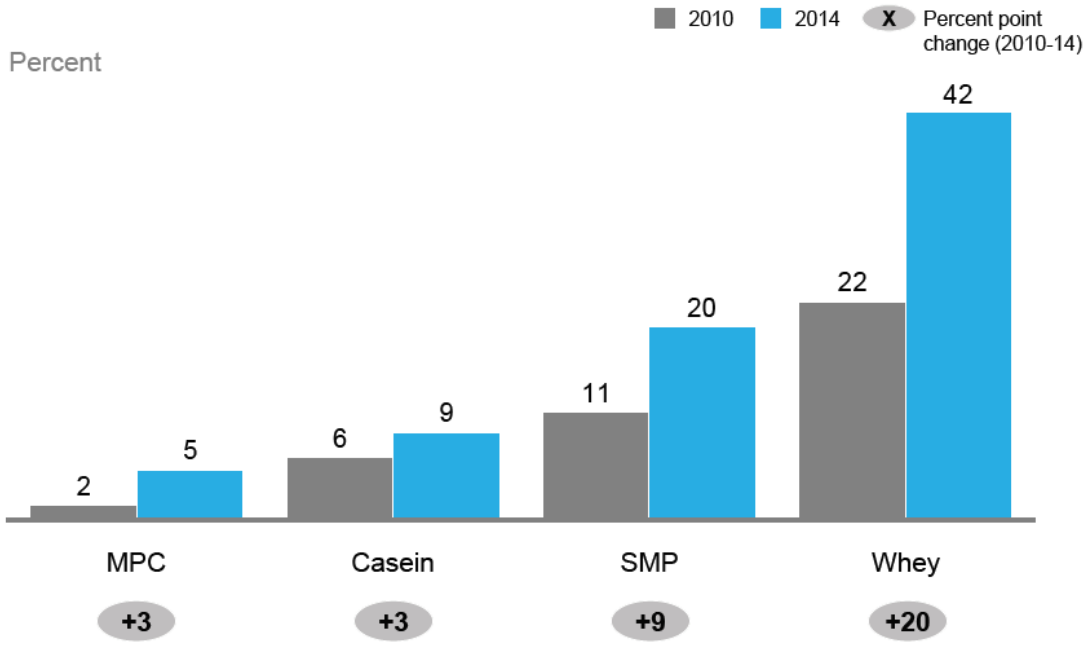

Figure 2. Increased demand for protein in foods. (Source: McKinsey and Company, 2016).

Because of the growing demand for ingredients from food manufacturers, most dairy ingredients' markets are projected to grow faster than world milk production (see Figure 3).

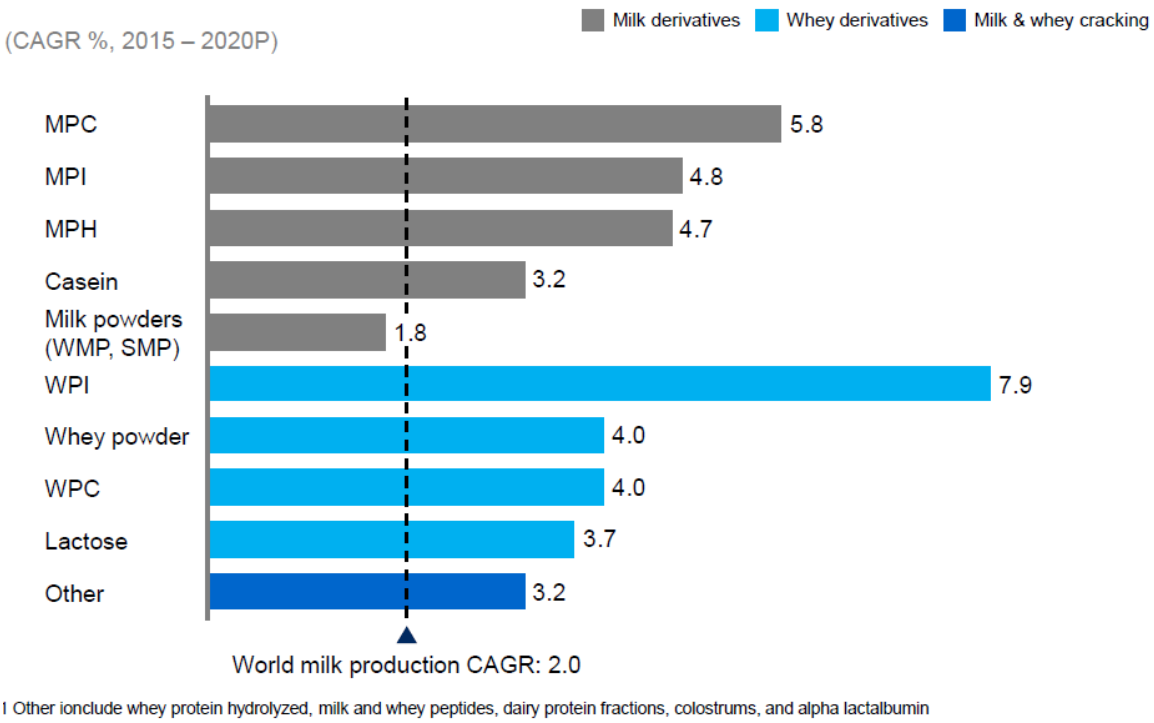

Figure 3. The projected growth of Milk and Whey derivatives (Source: McKinsey and Company, 2016).

Milk and, particularly, milk proteins are mesmerizing and complex systems designed by nature. Milk proteins can be processed into a wide range of nutritious and great-tasting food products and beverages. With the evolution of dairy technology and science, researchers are continually working to utilize the potential of milk proteins to formulate products that provide increased nutritional and functional benefits for the consumers. Today's food consumers are becoming ever more aware and perceptive, demanding new products with improved flavors and texture and nutrient values, with ingredient labels that are clear to understand and simple. Milk ingredients specifically are uniquely positioned to provide an ever-widening opportunity for food researchers/ developers to meet consumer expectations (DiRienzo, 2016).

MILK PROTEINS

Protein is an essential dietary component, and an adequate amount of protein intake is vital for a balanced and healthy diet. Consumers nowadays are even more conscious of and informed about the benefits of the protein in the daily diet. They are knowledgeable about the important role it plays in helping manage hunger, sustain energy, and maximize performance. Dairy is an important source of high-quality, versatile, and multifunctional protein. Many beverage and food manufacturers are trying to include dairy protein in their products. Milk proteins are not only an excellent source of nutrition, but they also offer the clean label desired by the consumers. Milk proteins also provide a range of functional benefits in finished products: viz. solubility, heat stability, gel formation, emulsification, and foaming (Patel et al., 2015). Milk is a dynamic and complex system that provides several functional and nutritional benefits. The degree of processing will affect the properties of milk and milk protein and how it will behave in the food systems. The proteins in milk are specifically complex and readily affected by several processing conditions used in the dairy and food industry (e.g., heat treatment, shear). Processing of the products results in changes to the structure of the milk protein, causing the denaturation, aggregation, and interactions of milk proteins. The extent and type of protein interactions can vary depending on several factors such as processing conditions (e.g., product composition, protein concentration, time-temperature combination, pH, and ionic strength). The functional properties of the dairy ingredients, such as gelation, solubility, heat stability, and emulsification, are affected by these changes in the proteins, which ultimately affect their outcome of the finished products. Whereas on the other hand, the heat-induced changes in milk protein contribute to the

substantial improvement of the sensory characteristics of dairy and food products, like yogurt, baked goods, and sweets/confectionaries. Therefore, it is very imperative to understand the dairy proteins and their functionality that can help to bring tailored functional properties to dairy ingredients as well as to their applications in dairy and food products for consumer uses.

Milk is a complex biological liquid consisting of water, fat, proteins, lactose, and minerals/ash (Table 1). Water is present as a continuous liquid phase in which other constituents and nutrients are either dissolved or suspended. Protein and a portion of the mineral salts are found in the colloidal solution, while lactose and the remaining of the minerals are found in a soluble phase with water.

Table 1. The average composition of Raw Bovine Milk.

Component	% (w/w) in milk
Water	87.30
Lactose	4.60
Fat	3.90
Proteins	3.30
Casein proteins 2.60	
Whey proteins 0.70	
Minerals	0.70
Organic acids	0.20

(Walstra and Jenness, 1984)

Bovine milk contains 3.0 to 3.5 grams of protein per 100 grams, broadly classified into two main categories, viz. casein and whey proteins. Casein exists primarily in the colloidal state, while whey proteins exist in the soluble state (Walstra and Jenness, 1984). The casein and whey proteins impart different functional properties and play different roles depending on their state and structure in the aqueous solution. Caseins and whey proteins have very different and unique structures and, hence different physicochemical properties that constitute the basis for the manufacture of many dairy and food products (Fox, 2003). The comparison of the properties of casein and whey proteins are summarized in Table 2. Based on the properties of casein and whey proteins mentioned in the table, it is apparent that milk proteins' properties influence their behavior in food products.

A typical example is the precipitation of casein. Lowering the pH of milk via fermentation or direct acidification yields products such as yogurt and cottage cheese. Coagulation of kappa-casein (κ-casein) with rennet leads to the production of cheese. κ-casein is one of four main parts of casein molecules, including alpha-s1-, alpha-s2- and beta-caseins. The alpha- and beta-caseins are hydrophobic proteins that are readily precipitated by calcium. κ-casein is a distinctly different molecule; it is not calcium-precipitable. As the caseins get secreted, they self-associate into aggregates called micelles in which the alpha- and beta-caseins are prevented from precipitating by their interactions with κ-casein. In a nutshell, κ-casein keeps the majority of milk protein soluble typically and prevents it from spontaneously coagulating.

Table 2. Comparison of selected physicochemical properties of casein and whey proteins.

PROPERTIES	CASEINS	WHEY PROTEINS
Structure	Lack of well-defined secondary, tertiary and quaternary structure; possess random coil structure	Well-defined tertiary and quaternary structure
Amino acid composition	Low in sulfur-containing amino acids; high in proline	Relatively high in sulfur-containing amino acids; low in proline
Physical state	Exist as large colloidal aggregates called casein micelles	Exist as globular proteins in the form of monomer-octamers, depending on pH
Solubility at pH 4.6	Insoluble at pH 4.6	Soluble at pH 4.6
Heat stability	Very heat-stable (can withstand severe heat treatment such as sterilization, ultrahigh temperature (UHT) or retort processing)	Heat-labile (can be completely denatured, particularly when heating at 90°C or higher)
Coagulation by limited proteolysis or ethanol	Can be coagulated by specific, limited proteolysis (e.g., rennet coagulation) or ethanol	Cannot be readily coagulated by the enzymes or limited proteolysis or ethanol

(Patel et al., 2015)

Casein

Caseins comprise approximately 80% of milk proteins and precipitate at the isoelectric point of pH 4.6 (Walstra and Jenness, 1984). Caseins form approximately 2.5% of the milk weight but hold 10% of the volume because they are highly hydrated (Dalgleish and Corredig, 2012). In milk, caseins are found as colloidally dispersed particles known as micelles. The casein micelles are often very poly-dispersed; however, casein micelles of single cows are quite mono-dispersed and extremely constant in time (de Kruif et al., 2012). The micelles are dispersed throughout the milk and are the main source of its whiteness. All casein fractions differ in primary structure and type and degree of post-translational modification (Swaisgood, 2003). The remainder of the micellar solids consist of inorganic material, collectively referred to as colloidal calcium phosphate (CCP) or micellar calcium phosphate (MCP), which is about 7% on a dry matter basis (de Kruif et al., 2012). Milk contains 30 mM calcium; about 65% exist in the casein micelles, while 10% is present as free calcium (Swasigood, 1992). Because casein molecules are phosphoproteins, these colloidal particles have been referred to as calcium phosphocaseinate. The caseins can undergo post-translational modification such as phosphorylation (αS1-casein), glycosylation (κ-casein), and proteolysis (β-casein) (Swaisgood, 1992). Furthermore, the proteolytic action of plasmin on β-casein yields various fractions of γ-casein and proteose peptone (Swaisgood, 1992). Salunke et al. (2010) demonstrated that casein content increases over time, and casein content decreases due to hydrolysis in the presence of endogenous enzymes, even though milk is stored at refrigerated temperature.

At any given time, the milk will have approximately 7 to 12% soluble casein in the serum phase (Rollema, 1992) depending on the temperature and degree of proteolysis or abuse it undergoes. The major casein fractions may have several genetic variants, contain various phophoseryl residues, and have different hydrophilic and hydrophobic regions in a polypeptide (Swaisgood, 1992). Both α-casein and β-casein are sensitive to calcium and precipitated by the calcium ions in milk if κ-casein is not present in the complex. The κ-casein renders the complex stable. The removal of Calcium leads to reversible dissociation of β-casein without micellular disintegration. The addition of calcium leads to aggregation. The caseins contain too many proline residues, affecting its structure (especially β-casein) as it disrupts the formation of α-helical and β-sheet required in secondary and higher structures (Swaisgood, 1992). From a product, technological, and industry point of view, caseins are by far the most important and valuable component of milk (de Kruif et al., 2012). The main dairy products of liquid milk, cheese, and yogurt derive their textural, sensory, and nutritional properties from caseins. These proteins have excellent surfactant properties in emulsions and foams, gelling properties, and thermal resistance to denaturation (Fox and McSweeney, 1998) because of their lack of complex secondary and tertiary structure. Casein micelles can withstand moderate heat and cold temperatures without aggregation or disruption of the basic structure (Dalgleish and Corredig, 2012). Although the casein micelle is quite stable, there are four major pathways in which aggregation can be induced: acid, heat, age gelation, and chymosin.

Casein micelle structure

Casein exists in a micelle form. Various models of caseins have been proposed (Waugh, 1958; Rose, 1969; Schmidt, 1982; Walstra, 1990, and 1999; Horne, 2003, 2006; Holt, 1992). A recently, de Kruif et al. (2012) have reviewed all casein micelle models (Figure 4). The oldest and most frequently cited model is the sub-micelle model based on the idea that caseins form micelles, which are then glued together by colloidal calcium phosphate. A widely accepted model by Holt (1992), based on experiments with casein nanoclusters, views the casein micelle as a matrix of CASEINs in which the CCP nanoclusters are dispersed (Figure 5). In this model, it is proposed that there is an uneven distribution of casein fractions throughout the micelle. Particularly, κ-casein is located principally on the surface of the micelle. The glycomacropeptide (GMP) portion of κ-casein is rich in carbohydrates and provides a negative charge, which in turn provides stability to the casein micelle via electrostatic repulsion of adjacent micelles (Holt, 1992). All models agree that the micellar surface is more or less completely covered by κ-casein. The κ-casein does not cover the micelle fully but is predominant on the surface; β-casein is mostly interior; and αS1-casein is found throughout the structure (Dalgleish and Corredig, 2012). Casein micelle stability is due to the surface zeta potential of -20 mV at pH 6.7 and steric stabilization due to protruding κ-casein hairs (Fox and McSweeney, 1998). Invariably, κ-casein is thought to limit the process of self-association, leading to the stabilization of the native casein micelle (de Kruif et al. 2012; Dalgleish and Corredig, 2012). The κ-casein stabilizes the micelles and prevents them from aggregating together in the presence of calcium. If it was not for κ-casein, the other highly phosphorylated caseins would aggregate together. As discussed earlier (Table 5), caseins

provide various functional properties. Most functional properties of the micelle depend on its surface properties rather than its interior makeup (de Kruif, 1999; Dalgleish and Corredig, 2012). Processing and drying techniques, in general, do not modify the casein micelles and have similar structures and properties to native micelles; however, no proper studies have been carried out (Dalgleish and Corredig, 2012).

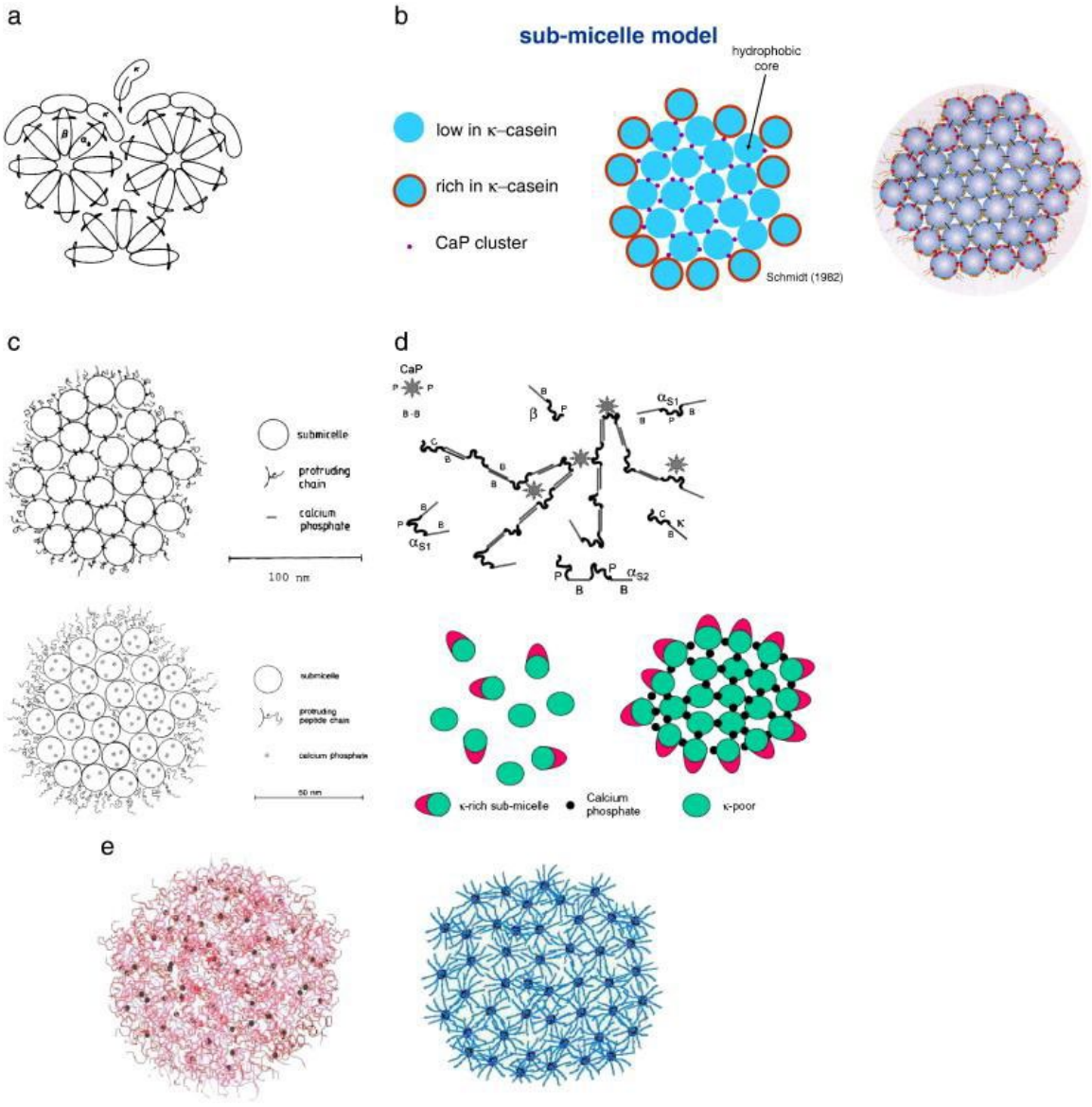

a. Model of casein micelles proposed by Waugh 1958. b. Representations of the model of casein micelles proposed by Schmidt. c. Representations of the model of casein micelles proposed by Walstra 1990 and 1999. d. Representation of the dual binding model proposed by Horne 2003, and the interpretation of Schmidt's model in a review 2005. e. Representations of the model of casein micelles proposed by Holt.

Figure 4. Collection of (artists) impressions of the casein micelle particle. (from de Kruif et al., 2012)

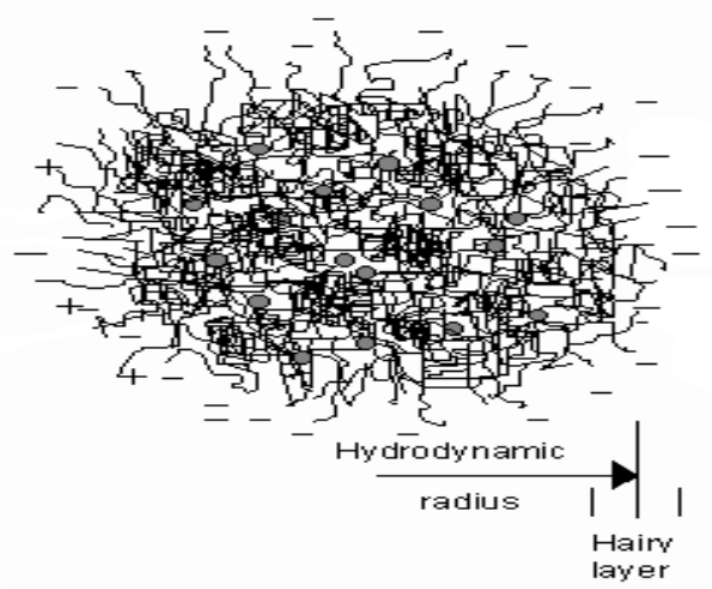

Figure 5. Hairy casein micelle model proposed by Holt, where a tangled web and open structure of polypeptide chains cross-linked by calcium phosphate nanocluster (colloidal calcium phosphate) in the core provides rise to an external region of lower segment density known as the hairy layer. The gray circles represent the calcium phosphate nanoclusters. (Adapted from http://www.foodsci.uoguelph.ca/deicon/casein.html)

Since the initial reports in 1969, various models of the casein micelle structure have been proposed (Huppertz, 2013). Casein has excellent surface-active and emulsification properties due to its amphiphilic nature. Caseins have a relatively higher charge and contain many proline residues but few cysteine residues (Swaisgood, 2003). As discussed earlier, a detailed overview of the structure and properties of casein micelles has been published (de Kruit et al., 2003). Caseins have lower levels of secondary and tertiary structures; this feature contributes to their remarkable stability at high temperatures. However, when casein is subjected to severe heat treatment, they undergo

changes, like dephosphorylation and proteolysis. Polymerization of caseins can happen as a result of condensation reactions (e.g., Maillard-type reactions) and the formation of lysinoalanine complex. The changes that occur in casein micelles upon heat treatment comprises of an increase in hydrodynamic diameter, a decrease in zeta potential and hydration, and the dissociation of caseins from micelles, which have been reviewed in detail. Casein micelle may undergo association and dissociation based on pH, processing conditions, and ionic environment (Singh and Creamer, 1992; Singh, 1995). The formation of various products and functional dairy ingredients such as yogurt, cheese, and caseinates (Figure 4) is based on this very important property of casein micelle. Many technically important properties of milk, such as rennet coagulability, heat stability, and the strength of rennet curd and syneresis properties of rennet gels, are strongly influenced by calcium ions (Ca^{+2}). The binding of Ca^{+2} to caseins is mainly through phosphoryl residues and by the carboxylic acid side chains (Fox, 1982).

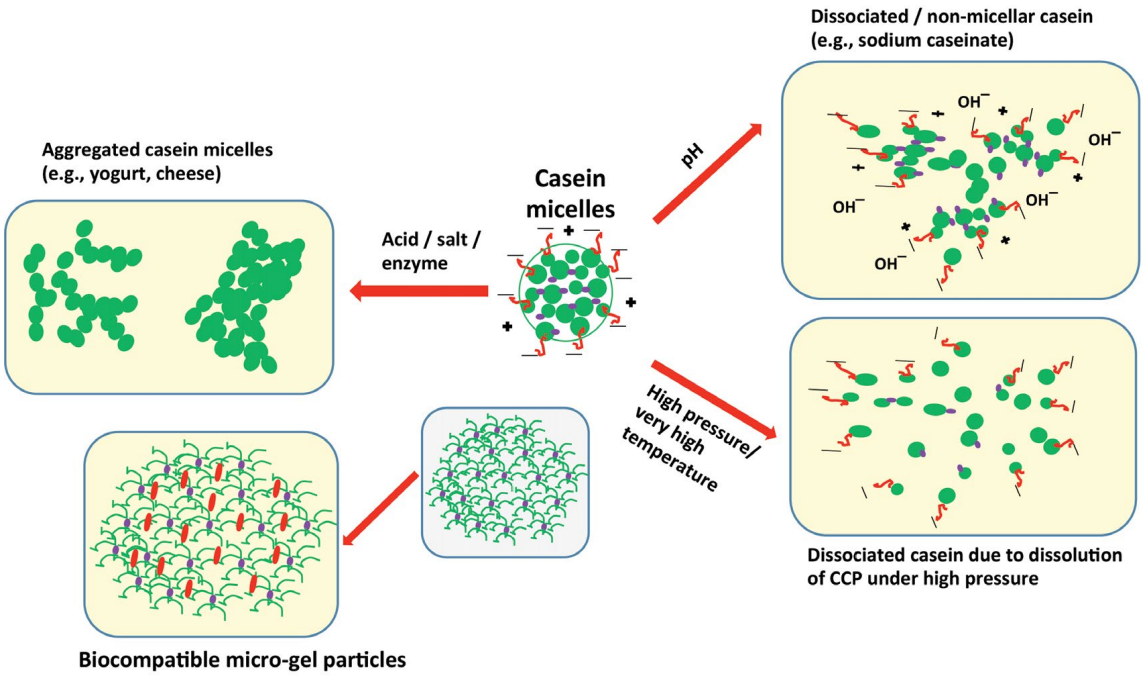

(Adapted from Patel et al., 2015)

Figure 6. Different approaches to modify the functionality of milk proteins. Schematic diagram showing changes in the casein micelle as affected by the change in processing and formulation conditions.

Whey Proteins

After the isoelectric precipitation of casein at pH 4.6 at 20°C to produce acid whey or the coagulation of casein by limited proteolysis with rennet to produce sweet whey, whey proteins, or milk serum proteins are the proteins that remain soluble after the precipitation (Donavan and Mulvihill, 1987; Jelen and Rattray, 1995). The average compositions of acid whey and sweet whey are shown in Table 3. Whey proteins represent about 20% (i.e., 5 to 7 grams per liter) of the total nitrogenous material in bovine milk. The principal whey proteins are β-lactoglobulin (β-LG), α-lactalbumin (α-LA), bovine serum albumin (BSA), and immunoglobulins (IG's) in decreasing order of

whey protein concentration. Whey proteins are predominantly globular with a rather uniform distribution of hydrophobic/hydrophilic amino acids along their polypeptide chains (in contrast to caseins) (Pearce, 1989).

They lack the amphiphilic nature of casein monomer subunits, a feature that confers on them many unique functional properties (Singh and Havea, 2003). The substantially lower proline content of the whey protein molecules permits a globular conformation with a large amount of helical content, which explains their strong susceptibility to denaturation by heat (Sawyer, 2003). Whey proteins are sold commercially as food and nutritional ingredients, such as whey powders, whey protein concentrates (WPCs), and whey protein isolates (WPIs). WPCs and WPIs are valuable ingredients in the food industry because of their exceptional nutritional value and critical functional properties, such as emulsification, solubility, and ability to form heat- or pressure-induced gels (de Wit, 1984; 1989; 1990). The composition of commercial WPCs varies widely, affected by various factors such as concentration, seasonal variation, the type of whey (whey source) (Moor, 1990), and the processing methods used to manufacture the WPC (Table 4). The denaturation of whey protein occurs when hydrogen, hydrophobic or covalent bonds are affected (Huffman, 1996). This phenomenon often exposes hydrophobic amino acid side chains that are generally buried within the native three-dimensional structure and, thus, causes increased reactivity of such groups (Mulvihill, 1992). Through sulfhydryl-disulfide interchange and hydrophobic interactions, the unfolded protein molecules may associate with each other to form aggregates (Figure 6), which will become insoluble as they increase in size. Severe heat treatments can lead to interactions with other protein molecules, which result

in intermolecular association and aggregation and, finally, precipitation or gelation, depending on several factors, including the protein concentration, heating and cooling rates, pH, and ionic strength. Protein denaturation is any modification or changes in the secondary, tertiary, or quaternary structure that is not followed by the rupture of peptide bonds involved in the primary structure. The final confirmation after denaturation can correspond to a totally (random coil) or partially unfolded polypeptide structure. Aggregation or polymerization: The terms precipitation, aggregation or polymerization, coagulation, and flocculation refer to unspecified protein-protein interactions that are resulting in the formation of large complexes with higher molecular weights. Gelation is an orderly aggregation of native and/ or (partially) denatured proteins, forming a three-dimensional network structure in which protein-protein and protein-solvent interactions are balanced to produce a well-ordered matrix that can hold significant amounts of water (de Wit, 1984; 1989).

Table 3. Protein compositions of Sweet Whey and Acid Whey.

Protein	Approximate % of Total Whey Protein	
	Acid Whey	Sweet Whey
β-lactoglobulin	54	45
α-lactalbumin	23	18
Bovine Serum Albumin (BSA)	6	5
Immunoglobulins	6	5
Casein-derived peptides	2	20
Enzymes	2	2
Phospholipid-protein complexes	5	5

(Patel et al., 2015)

MEMBRANE FILTRATION

Membrane filtration is a widely used processing technology in the dairy industry to physically separate and selectively concentrate milk components viz., caseins, whey proteins, fat globules, lactose, and minerals. By manipulating the ratio between these components, obtaining a liquid or powdered ingredient with the desired composition and henceforth functionality is possible (IDF, 2019).

Membrane processing involves a range of separation technologies broadly applied within dairy processing for the de-fatting of milk and whey, protein isolation and enrichment, partial demineralization, the removal of bacteria and bacterial spores' concentration of dry matter, and recovery of water.

The membrane filtration process is a pressure-driven system, where (in crossflow mode) the feed runs in parallel to the membrane surface. At the same time, the permeate is transmitted perpendicularly to the direction of flow. The characteristics of the membrane, design of the processing plant, concentration factors, applied properties of the feed material, and its propensity to form a secondary filtration layer by way of fouling govern the partition dynamics and performance of a given process. The membrane types used in the dairy industry are differentiated based on their fabrication material and design. E.g., tubular ceramic or spiral wound polymeric) and their ability to reject components based on specific molecular weight cut-offs (MWCO) or nominal pore sizes. Figure 7 illustrates the spectrum of rejection based on membrane selectivity relative to milk components.

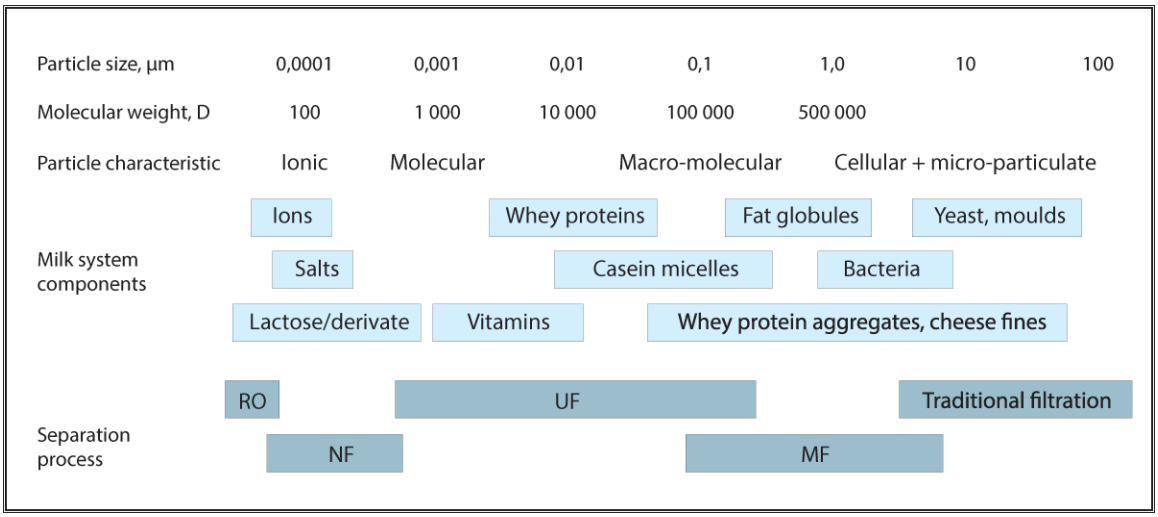

Figure 7. The spectrum of application of membrane separation processes in the dairy processing industry. (Adapted from Dairy Processing Handbook by Tetrapak, 2005).

Membrane performance

Typical reverse osmosis (RO) membranes with MWCO of approximately <150 Da show NaCl rejections of about 98%. During the RO process, high pressures (typically >3 MPa) are generated within the membrane plant to overcome osmotic pressure resistance, driving water from the retentate to the membrane's permeate side, hence concentrating the product. It is possible to achieve a high rejection of milk components, and concentration levels above 30% of dry matter content are possible. The high concentration of milk components depends on the desired characteristics of the product (pretreatment, viscosity, osmotic potential, fouling potential, etc.) and the type of membrane (feed spacer configuration, pressure limitations, etc.) (Bylund, 2005).

Nanofiltration (NF), as a progression of RO, is also a high-pressure filtration process, although normally operating in the range of 2-2.5 MPa. Contrasting to RO, NF membranes typically operate within a MWCO ranging from 150-300 Da; however, MWCO of 500-800 Da is also available for custom-made applications. Rejection rates for NaCl are approximately 40-60% commonly during NF. In contrast, rejection rates of 98-99% for MgSO4 and lactose are attainable, which indicates some loss of low molecular weight components will also happen during concentration by NF.

Ultrafiltration (UF), unlike RO and NF, is a low-pressure filtration process normally operated at pressures of <1MPa, with operating conditions depending on the number of membranes per housing, the plant configuration, and the existence of intermediate booster pumps for membranes joined in the series. MWCOs for UF ranges typically from 1-500 kDa, and the size of the macromolecules to be separated drives the rejection. However, for milk, all proteins are typically rejected by the UF membrane. The

10 kDa (polyethersulfone - PES) UF membranes are mostly used in the dairy industry to manufacture various milk protein and whey protein fractions known as concentrate. The smaller molecular weight components such as non-protein nitrogen, lactose, and soluble minerals are permeated selectively through the membrane as a byproduct stream known as permeate (Vora, 2008).

Microfiltration (MF) was originally only available in ceramic (aluminum/titanium oxides) membranes, has advanced over time from using uniform transmembrane pressure systems for control of pressure drop (and hence fouling) across the membrane. Nowadays, in dairy applications, specifically configured spiral-wound polymeric MF membranes are widely used (Metzger et al., 2012). MF membranes used in dairy processing have pore sizes in the range of 0.08-2 μm and have usually been utilized for reducing bacterial content. However, MF membranes and more recently used for the selective concentration of micellar casein through fractionation of serum proteins and other soluble components.

Diafiltration is an essential step during membrane filtration, a process essential in the manufacture of protein isolates and concentrates. During DF, water is added sequentially at different stages within the membrane plant, diluting the concentrated retentate, reducing viscosity, altering fouling dynamics, improving permeate flux, and allowing residual permeable transmission components (IDF, 2019). The extent of diafiltration, which is governed by many product and equipment-based factors, determines the final ratio of proteins versus other non-protein lower molecular weight solids. UF and MF's use with subsequent DF are the key to producing milk protein concentrates (MPCs) and isolates (MPIs).

WHEY PROTEIN CONCENTRATES

Whey protein concentrate (WPC) is a pale white to a light cream-colored product with a clean and bland flavor. WPC is manufactured by the removal of an adequate amount of non-protein constituents from pasteurized whey using membrane filtration and further drying the retentate resulting from the filtration process. The finished dry product WPC contains 25% or more protein. The non-protein constituents were removed by physical separation techniques such as precipitation, filtration, or dialysis. Further acidity of WPC is adjusted using safe and suitable pH-adjusting ingredients (ADPI, 2020).

MILK PROTEIN CONCENTRATES AND ISOLATES

UF or MF membranes are selectively used to concentrate milk proteins (Metzger, 2007) (Figure 8). The major milk proteins, namely caseins, are present in a micellar form. Caseins are colloidally suspended within a soluble phase containing serum proteins, non-protein nitrogenous compounds, lactose, and minerals. Depending upon MWCO and membrane pore size, the selective concentration of the protein is accomplished. Using typical MF membranes with larger pore sizes of about 0.1-0.2 μm, it is possible to separate/ pass through the membrane a fraction of the serum proteins (65-95% dependent upon equipment design). Hence, a retentate stream is created of micellar casein, and a permeate stream is obtained consisting of serum proteins. In this scenario, the retentate generated is called Micellar Casein Concentrate/Isolate (MCC/MCI). These MCC/ MCI concentrates have very definite use as the altered casein to serum protein ratio favors applications such as cheese milk standardization, yogurt, and structured dairy products, sports nutrition, and medical, nutritional products (IDF, 2019).

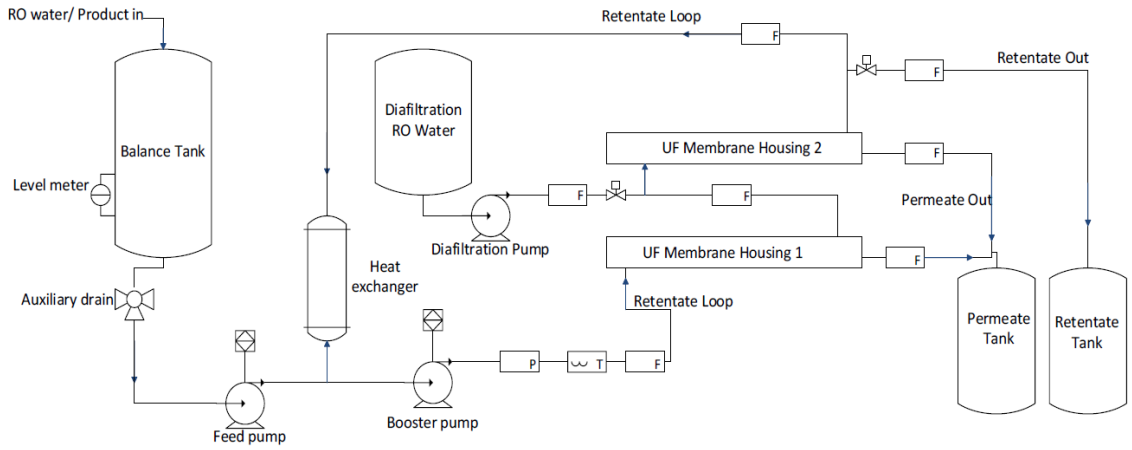

Figure 8. Ultrafiltration (UF) plant design for Milk Protein Concentrate manufacture and supplementary 'in series' connected membrane modules and sequential addition of diafiltration water (Adapted from IDF, 2019).

Generally, conventional milk protein concentrates are obtained using UF, coupled with a custom-made DF step. The greater the DF ratio, the higher is the ratio of protein to remaining solids in the finished product. During the UF process, the ratio of casein to serum proteins in skim milk is maintained, whereas lactose, non-protein nitrogen, and soluble minerals permeate through the membrane. It is imperative to note that the colloidal portion of the minerals in milk are retained in the retentate during concentration, thus changing the ratio between colloidal and serum ions. Milk protein concentrates contain 40% to 87% (w/w) protein in dry matter - once the protein value approaches 90% dry matter, the ingredients are known as "isolates." The increased protein content is associated with a corresponding decrease in soluble phase components.

MPC, MPI, and MCC can be used as ingredients in a variety of food preparations. Depending of the type of food they are added in, they act as flavor enhancers, emulsifiers,

formulation aids, texturizers, humectants, stabilizers and thickeners, and excellent sources of high-quality protein.

Composition of MPC and MPI

Several different MPC and MPI products are commercially available, each of which is identified by a number which represents the protein content of the product, as shown in the Table 4.

Table 4. Composition of various MPC and MPI.

Product	Protein %	Fat %	Lactose %	Ash %	Moisture %
MPC 40	39.5 min	1.25 max	52.0 max	10.0 max	5.0 max
MPC 42	41.5 min	1.25 max	51.0 max	10.0 max	5.0 max
MPC 56	55.5 min	1.50 max	36.0 max	10.0 max	5.0 max
MPC 70	69.5 min	2.50 max	20.0 max	10.0 max	6.0 max
MPC 80	79.5 min	2.50 max	9.0 max	8.0 max	6.0 max
MPC 85	85.0 min*	2.50 max	8.0 max	8.0 max	6.0 max
MPI	89.5 min*	2.50 max	5.0 max	8.0 max	6.0 max

* Protein content ≥ 85.0% is reported on dry basis, all other parameters are reported “as is”

Adapted from ADPI (2020)

MICELLAR CASEIN CONCENTRATES

Milk Protein products Concentrates are produced by concentrating skim milk through MF filtration processes so that the final product contains 40% or more protein by weight of the finished dry product.

Milk Protein Isolate (MPI) and Milk Protein Concentrate (MPC) is made by applying a combination of filtration methods viz. Ultrafiltration and Diafiltration, which

fundamentally retain all the casein and whey proteins available in the skim milk stream in the finished product, resulting in a casein-to-whey protein ratio 80:20 similar to that of the original milk used.

Concentrated Milk Protein products may also be manufactured using the Microfiltration process, which alters the casein-to-whey protein ratio similar to that observed in milk. The casein-to-whey protein ratio typically ranges between 82:18 and 95:5 for commercially available microfiltered products. The Microfiltration process is used in the manufacture of protein concentrates; the resulting product is called Microfiltered Milk Protein (MMP) or Micellar Casein Concentrate (MCC).

Composition of MCC

Several different MCC products are commercially available, each of which is identified by a number that represents the protein content of the product, as shown in the Table 5.

Table 5. Composition of MCC.

Product	Protein %	Fat %	Lactose %	Ash %	Moisture %
MCC42	41.5 min	1.25 max	51.0 max	6.0 max	5.0 max
MCC70	69.5 min	2.50 max	16.0 max	8.0 max	6.0 max
MCC80	79.5 min	3.00 max	10.0 max	8.0 max	6.0 max
MCC85	85.0 min*	3.00 max	3.0 max	8.0 max	6.0 max
MCC90	89.5 min*	3.00 max	1.0 max	8.0 max	7.0 max

* Protein content ≥ 85.0% is reported on dry basis, all other parameters are reported “as is”

Adapted from ADPI (2020)

MINERAL-REDUCED MICELLAR CASEIN CONCENTRATES

Mineral-reduced micellar casein concentrate (MMCC) is a product by introducing carbon dioxide during the manufacturing of micellar casein concentrate, as mentioned above (Marella et al., 2015). Due to the introduction of CO_2, there is a de-aggregation of casein micelle, as shown in Figure 9.

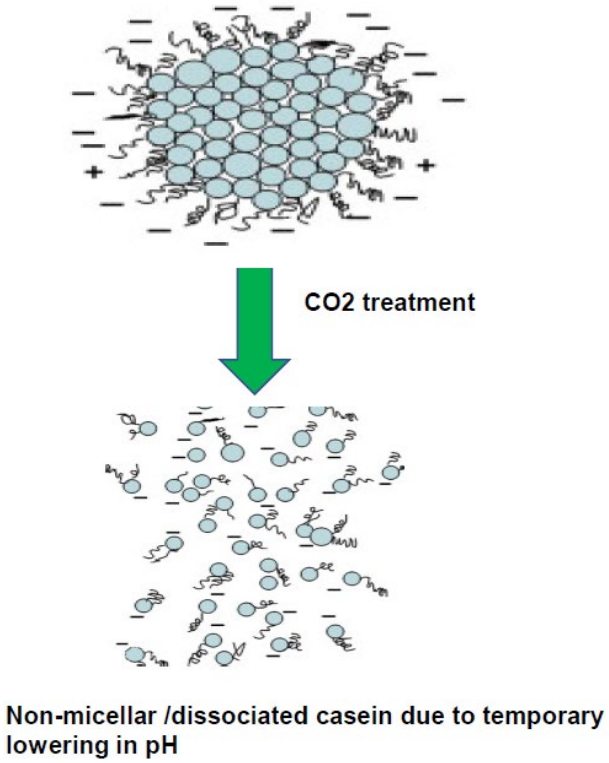

Fig 9. Changes in the casein micelle structure due to the introduction of Carbon dioxide.

INFANT MILK FORMULA

The Federal Food, Drug, and Cosmetic Act (FFDCA) defines infant formula as "a food which purports to be or is represented for special dietary use solely as a food for infants because it simulates human milk or its suitability as a complete or partial substitute for human milk" (FFDCA 201(z)). FDA regulations define infants as persons not more than 12 months old (Title 21, Code of Federal Regulations 21 CFR 105.3(e)) (Bagalman et al., 2014).

Infant formula or baby formula is food designed, manufactured, and marketed for feeding to infants under the age of 12 months. It is generally prepared for bottle-feeding or cup-feeding from powder reconstituted with water.

Manufacturers mention that the composition of infant formula is formulated to be roughly based on human milk at about one to three months postpartum; however, there are significant differences in the nutrient content of different baby formula products available in the market. The most widely used infant formulas contain cow milk casein and whey as a source of protein, a vegetable oil blends as a source of fat, lactose as a source of carbohydrate, a mineral-vitamin mix, and other ingredients depending on the producer of the product. Besides, there are infant formulas using soybean as a protein source in place of cow milk proteins (mostly in the United States and Great Britain). Also, for infants who are allergic to other proteins, some formulas use hydrolyzed protein converted into its component amino acids.

The ratio of casein to whey in breast milk is roughly 40:60 with 1% protein; milk formulas match this ratio except that they are 2-2.5% higher in protein. Cows’ milk is not

recommended until the age of one year when the ratio becomes 80:20, with 3.1% protein (Kung et al., 2018). Most babies are on a whey-based formula initially, but this is substituted with non-whey formula before the age of one year. The key reason given is that infants were hungry for the former. The use of whey formula is 62.4% at two months, 40.4% at six months, and 12.8% at twelve months. More studies are needed on the benefits of whey formula (Smith et al., 2016).

One of the advantages of whey-based formula is that it helps to prevent infant and life-long obesity. Marketing on formula tins influences mothers' choice of brand, implying that better advertising strategies are needed for whey products against their competitors. Mothers felt there was insufficient postnatal guidance on the feeding of the infant and tended to rely on informal, possibly uninformed sources. A stigma is attached to selecting bottle-feeding over breastfeeding (Appleton et al., 2018).

Although breastfeeding has many benefits over formula, and it is recommended by the World Health Organization (WHO) exclusively for the first six months of life, it is not always possible. The Academy of Nutrition and Dietetics also recommends this, with complementary foods being introduced from the age of six months, and the American Academy of Pediatrics supports breastfeeding for twelve months. Across the globe, 38% of infants are exclusively fed breastmilk; at three months, 67% are on formula, either partially or entirely (Martin, Ling and Blackburn, 2016).

Either soy milk or cow's milk is used in infant formula with the addition of substances to match breast milk more closely. This includes iron, nucleotides, fatty acids of arachidonic acid (AA), and docosahexaenoic acid (DHA) and probiotics. It is anticipated that the formula market will grow by 7-9% per annum from $50 billion,

making it the fastest-growing category of packaged food. Regulations specify the amount of water, carbohydrate, protein, fat, vitamins, and minerals that infant formula must contain. These exist in higher amounts in bovine formulas, which must be diluted and skimmed. Protein, sodium, and potassium are in excess, and additional Vitamin E, iron, and essential fatty acids must be added (Martin, Ling and Blackburn, 2016).

SINGLE DROPLET DRYING

The single droplet drying (SDD) approach involves a single droplet suspended on the tip of a glass filament/glass capillary tube (Charlesworth and Marshall, 1960, Lin and Chen, 2002, Cheong et al., 1986), where changes in droplet diameter, mass, and temperature can be measured during drying (Adhikari et al., 2000). Drying an isolated droplet under controlled conditions are analogous to spray drying (Charlesworth and Marshall, 1960, Walton and Mumford, 1999), as the moisture is being removed by convection at elevated air temperature for both processes. The drying kinetics data generated using this technique have been used to verify a number of drying models (Chen and Lin, 2005, Lin and Chen, 2007, Mezhericher et al., 2007, Mezhericher et al., 2008), and can be incorporated into CFD modeling of spray drying operations (Woo et al., 2008, Woo et al., 2012). One of the drying models, the Reaction Engineering Approach (REA), has been found to produce more accurate drying predictions and better correlation with experimental data during the investigation of physical and biochemical characteristics of food powders (Patel and Chen, 2005). The model treats evaporation as an activation process with zero-order kinetics and offers the advantage of a simplified ordinary differential equation without spatial distribution during the modeling of moisture

and temperature profiles for small droplets. The REA model, when coupled with the SDD data, can be used to produce an activation curve unique to a material at a certain solid content, providing accurate drying kinetics data necessary for the simulation of the spray drying process. The parameters from the activation energy curve are used for dryer wide predictions of particle moisture and temperature profiles for different initial solids concentration of a material in an industrial spray dryer. The REA model has demonstrated good agreements between predicted and experimental results under the assumption of uniform droplet temperature (Patel and Chen, 2008; Mezhericher et al., 2010).

Building on the comprehensive research on drying kinetics via the single droplet drying approach that this Monash University group has previously conducted (Lin and Chen, 2004, Fu et al., 2011b, Fu et al., 2012b), the same technique can be used to study drying effects on the surface formation on droplets. This is important particularly for heat-sensitive materials such as proteins, enzymes, or probiotic bacteria where denaturation adversely affects their functionality (i.e., solubility, bioavailability). A comprehensive laboratory set-up can be used to measure size, droplet/particle temperature, and mass changes during drying of a single droplet via the glass filament method (Lin and Chen, 2004), and analysis through the Reaction Engineering Approach to model dryer-wide behavior (Fu et al., 2011a). This protocol is used to obtain drying kinetics data for high solids milk (Figure 1) (Fu et al., 2012b, Chew et al., 2013) that could be combined with other kinetics data, for example, on the insoluble material formation (Rogers et al., 2012), to predict the dryer behavior to minimize insoluble material formation. Recently, we used the protocol to investigate dissolution behavior in

situ (Fu et al., 2011b), inactivation of bacterial cells (Fu et al., 2013a), and surface crystallization of lactose and amino acids in real-time (Fu et al., 2012a, Lin et al., 2013).

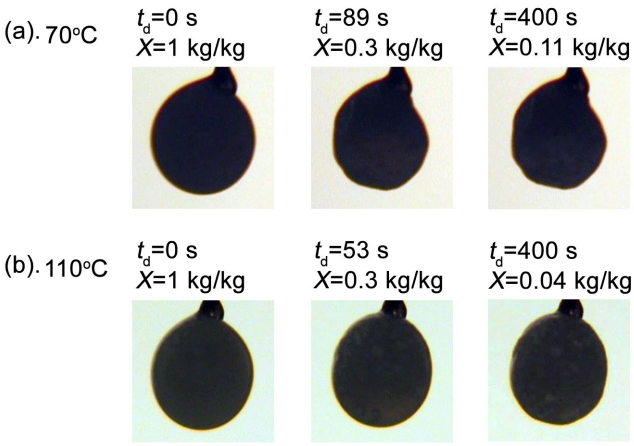

Figure 10 – (a & b). single droplet drying of 50 wt.% skim milk (td: drying time; X: moisture content) demonstrating an earlier crust formation (less shrinkage) for droplet dried at 110 °C (Fu et al., 2012b, Fu et al., 2013b); (c) heat damage on L. cremoris cells dried with 10 wt.% skim milk at 110 °C as indicated by the existence of fine holes on cell walls (Fu et al., 2013a).

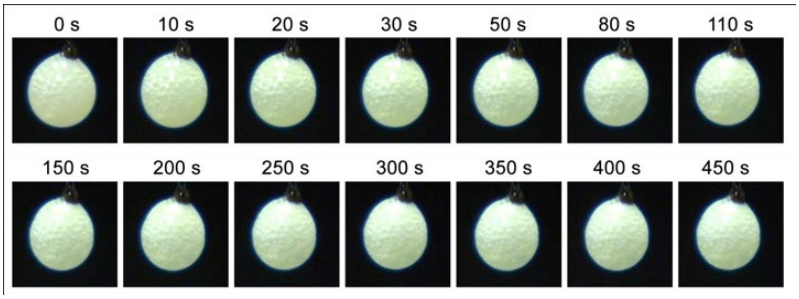

Figure 11. – (i) Time-lapsed images of a 50 wt.% skim milk particle dried at 90°C; (ii) Difference in shrinkage behavior observed for 50 wt.% skim milk particles dried at 110°C.

Recently published works (Lin et al., 2013) reported the use of this technique to investigate the crystallization of amino acids (taurine), docosahexaenoic acid (DHA) microencapsulation (Wang et al., 2014), and high solids drying of dairy liquids (Chew et al., 2013). For bioactive materials, single droplet drying can provide information on inactivation kinetics as a function of droplet temperature due to thermal stresses and evaporation (Ghandi et al., 2012, Chen and Patel, 2007), microstructural changes, including the onset of crust formation and the role of protective carriers (e.g., skim milk or starch), which can be translated into the understanding on optimum drying conditions and matrix formulation to prevent excessive heat damage during spray drying (Schutyser et al., 2012).

OBJECTIVES AND HYPOTHESIS OF THE CURRENT RESEARCH

Objectives of the current study are:

1. To install a Single Droplet Dryer and build Single Droplet Drying capabilities at SDSU.
2. Study the effect of different solids concentration on the drying kinetics of whey protein concentrate by a single droplet drying technique.
3. Comparison of drying kinetics of Micellar Casein Concentrate (MCC) vs Modified (CO_2 induced) MCC on SDD.
4. Dissolution behavior of Infant Milk formula and its effect on the properties of dried particle.

A detailed hypothesis for each study conducted on SDD is mentioned below.

STUDY 1: Study the effect of different solid concentration on the drying kinetics of Whey Protein Concentrate.

HYPOTHESIS 1:

Due to differences in the solid concentration of Whey Protein Concentrate (viz., 10%, 20%, and 30%), we may observe differences in the drying kinetics because at the higher solid concentration level, it is difficult to achieve equilibrium temperatures due to the faster formation crust on the outer surface versus at the lower solid concentration.

STUDY 2:

Comparison of drying kinetics of Micellar Casein Concentrate (MCC) vs Modified (CO_2 induced) MCC.

HYPOTHEIS 2:

Due to the differences between MCC and Modified MCC in the pH and mineral balance and the presence of the higher amount of de-aggregated casein micelle in the modified MCC, we hypothesize that we will observe differences in the drying properties (like change in moisture removal pattern, mass change of the particle, etc.) of both the materials as mentioned below.

- Moisture removal will be faster in the case of modified MCC as compared to MCC. This is due to the de-aggregation and change in pH from 6.7 to 5.7.
- The mass change should be rapid for Modified MCC as compared to MCC.

- Modified MCC will reach the equilibrium temperature faster as compared to MCC.
- Both will have unique drying kinetics and hence unique activation energy equations at each level (10% and 20%) of total solids been dried.

(As there are changes in the molecular weight and protein composition of WPC and MCC, this study was conducted after WPC. WPC has a molecular weight of approx. 2 – 8 $x10^4$ KD as compared to MCC, which has a molecular weight of approximately $2.5X10^8$ KD. WPC comprises of α-lactalbumin, β-lactoglobulin, BSA, IG's, lactoferrin, lactoperoxidase, glacomacropeptides, proteose-peptones while MCC contains an entirely different set of proteins viz. αs1-casein, β-casein, k-casein, and gamma-casein. Also, whey proteins remain in solution at the isoelectric pH (4.6) of milk while casein precipitates out from the solution).

STUDY 3:

Dissolution behavior of Infant Milk formula and its effect on the properties of dried particle.

HYPOTHESIS 3:

We hypothesize that we will observe better rehydration/ higher solubility of the powder particle of Infant Milk formula dried at 70°C temperature as compared to those dried at 110°C.

- This is predicting that the outlet temperatures of the dryer have some effect on the rehydration properties of dried powder. Since rehydration properties of powder is

one of the very important criteria for infant milk formula it would be interesting to study the dissolution behavior.

- Due to higher temperatures of drying, there will be a faster formation of crust on the surface of the particle, which may lead to slower rehydration or absorption of the attached water droplet to the dried particle in case of 110°C followed by 70°C.
- Since there may be fat in the material which tends to rise to the surface of the dried particle may also impact the rehydration time, and hence we may observe that there may be incomplete rehydration of the particle for some of the temperatures of drying used in the study.

REFERENCES

Appleton, J., Laws, R., Russell, C., Fowler, C., Campbell, K., and Denney-Wilson, E. 2018. Infant formula feeding practices and the role of advice and support: An exploratory qualitative study. BMC Pediatrics, 18(1).

ADPI2020.www.adpi.org/DairyProducts/Whey/WheyProteinConcentrate/tabid/94/Default.aspx

ADPI. 2020. Concentrated Milk Protein Standard. American Dairy Products Institute. 50-52.

Adhikari, B., Howes, T., Bhandari, B. R. and Truong, V. 2000. Experimental studies and kinetics of single drop drying and their relevance in drying of sugar-rich foods: a review. Int J Food Prop. 3, 323-351.

Bagalman, E., et al. 2014. "Prescription Drug Abuse" Journal of Drug Addiction, Education, and Eradication, Nova Science Publishers, Inc. 10 (4), 459.

Barton, R. 2000. The effect of nutrition intervention, using the Balance of Good Health Model, on the composition of the packed lunches of 10–11-year-old schoolchildren. Journal of Human Nutrition and Dietetics, 13: 363-371.

Burrington, K.J., Agrawal, S. 2012. Technical Report: Whey Protein Heat Stability. Arlington, VA: US Dairy Export Council.

Bylund, G. 2005. Dairy Processing Handbook. Lund, Sweden: Tetra Pak Processing Systems AB, Print: 1995. Dairy Processing Handbook by Tetrapak. Reprint. Chapter 15.

Charlesworth, D. H. and Marshall, W. R. J. 1960. Evaporation from drops containing dissolved solids. AIChE J. 6, 9-23.

Chen, X. D. and Lin, S. X. Q. 2005. Air drying of milk droplet under constant and time-dependent conditions. AIChE Journal. 51, 1790-1799.

Chen, X. D. and Patel, K. C. 2007. Micro-organism inactivation during drying of small droplets or thin-layer slabs ‚Äì A critical review of existing kinetics models and an appraisal of the drying rate dependent model. Journal of Food Engineering. 82, 1-10.

Cheong, H. W., Jeffreys, G. V. and Mumford, C. J. 1986. A receding interface model for the drying of slurry droplets. AIChE Journal. 32, 1334-1346.

Chew, J. H., Fu, N., Woo, M. W., Patel, K., Selomulya, C. and Chen, X. D. 2013. Capturing the effect of initial concentrations on the drying kinetics of high solids milk using reaction engineering approach. Dairy Science and Technology. 93, 415-430.

Dalgleish, D. G., and M. Corredig. 2012. The structure of the casein micelle of milk and its changes during processing. Ann. Review Food Sci. Technol. 3:449-467.

de Kruif, C. G. 1999. Casein micelle interactions. Int. Dairy J. 9:183-188.

de Kruif, C.G., Holt, C. 2003. Casein Micelle Structure, Functions and Interactions. In: Fox PF, McSweeney PLH, eds. Advanced Dairy Chemistry, Volume 1: Proteins. 3rd ed. New York, NY: Kluwer Academic/Plenum Publishers; 2003:233-276.

de Kruif, C. G., T. Huppertz, V. S. Urban, and A. V. Petukhov. 2012. Casein micelles and their internal structure. Adv. Colloid Interface Sci. 171–172:36–52.

de Wit, J.N. 1984. Functional properties of whey proteins in food systems. Neth Milk Dairy J.;38:71-89.

de Wit, J.N. 1989. The use of whey protein products. A review. Ede, Neth: NIZO.

de Wit, J.N. 1990. Thermal Stability and Functionality of Whey Proteins. J Dairy Sci.; 73(12):3602-3612.

DiRienzo, D. 2016. Research Gaps in the Use of Dairy Ingredients in Food Aid Products. Food and Nutrition Bulletin, 37(1_suppl), S51–S57.

Donovan, M., Mulvihill, D.M. 1987. Thermal Denaturation and Aggregation of Whey Proteins. Ir J Food Sci Tech.;11(1):87-100.

Fox, P.F. 1982. Heat-induced coagulation of milk. In: Fox PF, ed. Developments in Dairy Chemistry, Volume 1: Proteins. London, England: Applied Science Publishers; 189-228.

Fu, N., Wai Woo, M., Qi Lin, S. X., Zhou, Z. and Dong Chen, X. 2011a. Reaction Engineering Approach (REA) to model the drying kinetics of droplets with different initial sizes‚Äîexperiments and analyses. Chemical Engineering Science. 66, 1738-1747.

Fu, N., Woo, M. W. and Chen, X. D. 2011b. Colloidal transport phenomena of milk components during convective droplet drying. Colloids and Surfaces B: Biointerfaces. 87, 255-266.

Fu, N., Woo, M. W., Moo, F. T. and Chen, X. D. 2012. Microcrystallization of lactose during droplet drying and its effect on the property of the dried particle. Chemical Engineering Research and Design. 90, 138-149.

Fu, N., Woo, M. W., Selomulya, C. and Chen, X. D. 2013a. Inactivation of Lactococcus lactis ssp. cremoris cells in a droplet during convective drying. Biochemical Engineering Journal. 79, 46-56.

Fu, N., Woo, M. W., Selomulya, C. and Chen, X. D. 2013b. Shrinkage behaviour of skim milk droplets during air drying. Journal of Food Engineering. 116, 37-44.

Fu, N., Woo, M. W., Selomulya, C., Chen, X. D., Patel, K., Schuck, P. and Jeantet, R. 2012b. Drying kinetics of skim milk with 50 wt.% initial solids. Journal of Food Engineering. 109, 701-711.

Fox, P.F. 2003. Milk Proteins: General and Historical Aspects. In: Fox PF, McSweeney PLH, eds. Advanced Dairy Chemistry, Volume 1: Proteins. 3rd ed. New York, NY: Kluwer Academic/Plenum Publishers; 1-48.

Ghandi, A., Powell, I., Chen, X. D. and Adhikari, B. 2012. Drying kinetics and survival studies of dairy fermentation bacteria in convective air drying environment using single droplet drying. Journal of Food Engineering. 110, 405-417.

Holt, C. 1992. Structure and stability of bovine casein micelles. Adv. Protein Chem. 43:64–151.

Horne, D. S. 2003. Casein micelles as hard spheres: limitations of the model in acidified gel formation. Colloids and Surfaces A: Physicochemical and Engineering Aspects. 213: 255‑263.

Horne, D. S. 2006. Casein micelle structure: models and muddles. Current opinion in colloid and interface science. 11:148-153.

Huffman, L.M. 1996. Processing of whey for use as a food ingredient. Food Technol.; 50(2):49-52.

Huppertz, T. 2013. Chemistry of caseins. In: McSweeney PLH, Fox PF, eds. Advanced Dairy Chemistry, Volume 1A: Proteins: Basic Aspects. 4th ed. New York, NY: Springer Science and Business Media; 135-160.

Huppertz, T., Smiddy, M.A., de Kruif, C.G. Biocompatible Micro-Gel Particles from Cross-Linked Casein Micelles. Biomacromolecules. 2007; 8(4):1300-1305.

IDF. 2019. Manufacture of milk protein concentrates and isolates y membrane filtration. International Dairy Federation. IDF Factsheet 009/ 2019-12.

Jelen, P., Rattray, W. 1995. Thermal denaturation of whey proteins. In: Fox PF, ed. Heat-induced changes in milk. 2nd ed. Brussels, Belgium: International Dairy Federation :66-85.

Kung, B., Anderson, G., Paré, S., Tucker, A., Vien, S., Wright, A., and Goff, H. 2018. Effect of milk protein intake and casein-to-whey ratio in breakfast meals on postprandial glucose, satiety ratings, and subsequent meal intake. Journal of Dairy Science. 101(10), 8688-8701

Lin, R., Woo, M. W., Fu, N., Selomulya, C. and Chen, X. D. 2013. In Situ Observation of Taurine Crystallization via Single Droplet Drying. Drying Technology. 31, 1553-1561.

Lin, S. X. Q. and Chen, X. D. 2002. Improving the glass-filament method for accurate measurement of drying kinetics of liquid droplets. Chemical Engineering Research and Design. 80, 401-410.

Lin, S. X. Q. and Chen, X. D. 2004. Changes in Milk Droplet Diameter During Drying Under Constant Drying Conditions Investigated Using The Glass-Filament Method. Food and Bioproducts Processing. 82, 213-218.

Lin, S. X. Q. and Chen, X. D. 2007. The reaction engineering approach to modelling the cream and whey protein concentrate droplet drying. Chemical Engineering and Processing. 46, 437-443.

Marella, C., P. Salunke, A. C. Biswas, A. Kommineni, and L. E. Metzger. 2015. Manufacture of modified milk protein concentrate utilizing injection of carbon dioxide. J. Dairy Sci. 98:3577–3589.

Martin, C., Ling, P., and Blackburn, G. 2016. Review of Infant Feeding: Key Features of Breast Milk and Infant Formula. Nutrients. 8(5), 279.

Metzger, L. E. 2007. Manufacture and application of casein concentrate. J. Dairy Sci. 90 (Suppl. 1):183-184 (abstr.).

Metzger, L. E., C. Marella, and P. Salunke. 2012. Micellar Casein Concentrate – Performance of Spiral Wound Process and Characterization of MCC. J. Dairy Sci. 95: Suppl. 2 (Abstr).

Metzger, L. E, and Vora, H. N. 2018. Single Droplet Drying—A New Technology for Optimization of Drying Conditions for Dairy Ingredients., Dairy Science Publication Database.

Mezhericher, M., Levy, A. and Borde, I. 2007. Theoretical drying model of single droplet containing insoluble or dissolved solids. Drying Technology, 25**,** 1025-1032.

Mezhericher, M., Levy, A. and Borde, I. 2008. Modelling of particle breakage during drying. Chemical Engineering and Processing. 47, 1404-1411.

Mezhericher, M., Levy, A. and Borde, I. 2010. Theoretical models of single droplet drying kinetics: A review. Drying Technology. 28, 278-293.

Mulvihill, D.M., Donovan, M. 1987. Whey Proteins and Their Thermal Denaturation - A Review. Ir J Food Sci Technol.;11:43-47.

Mulvihill, D.M. 1992. Production, functional properties and utilization of milk protein products. In: Fox PF, ed. Advanced Dairy Chemistry, Volume 1, Proteins. London, England: Elsevier Applied Science; 1992:369-404.

Morr, C.V., Foegeding, E.A. 1990. Composition and functionality of commercial whey and milk protein concentrates and isolates: a status report. Food Technol. ; 44(8):100-112.

Patel, K. and Chen, X. D. 2005. Prediction of spray-dried product quality using two simple drying kinetics models. J Food Process Eng. 28, 567-594.

Patel, K. and Chen, X. D. 2008. Surface-centre temperature differences within milk droplets during convective drying and drying-based Biot number analysis. AIChE Journal, 54**,** 3273-3290.

Patel, H., Patel, S., Beausire, R. Agrawal, S. 2015. Technical Report: Understanding the Role of Dairy Proteins in Ingredient and Product Performance. US Dairy Export Council.

Pearce, R. J. Thermal denaturation of whey protein. International Dairy Fed Bulletin. 1989; 238:17-23.

Rogers, S., Fang, Y., Lin, S. X. Q., Selomulya, C. and Chen, X. D. 2012. A monodisperse spray dryer for milk powder: Modelling the formation of insoluble material. Chemical Engineering Science, 71, 75-84.

Ross, A. C., Taylor, C.L., Yaktine, A.L., et al., editors. 2011. Institute of Medicine (US) Committee to Review Dietary Reference Intakes for Vitamin D and Calcium; Dietary Reference Intakes for Calcium and Vitamin D. Washington (DC): National Academies Press (US); 2011. 2, Overview of Calcium. Available from: https://www.ncbi.nlm.nih.gov/books/NBK56060/

Rozenberg, S., Body, J., Bruyère, O. et al. 2016. Effects of Dairy Products Consumption on Health: Benefits and Beliefs—A Commentary from the Belgian Bone Club and the European Society for Clinical and Economic Aspects of Osteoporosis, Osteoarthritis and Musculoskeletal Diseases. Calcif Tissue Int 98, 1–17.

Sawyer, L. 2003. β-Lactoglobulin. In: Fox PF, McSweeney PLH, eds. Advanced Dairy Chemistry, Volume 1: Proteins. 3rd ed. New York, NY: Kluwer Academic/Plenum Publishers; 319-386.

Schmidt, D. G. 1982. Association of caseins and casein micelle structure. Developments in dairy chemistry. 1, 61-86.

Schmidt, D. G. 1986. Association of casein and casein micelle structure. In Developments in Dairy Chemistry. Vol 1, Ed by Fox PF, Elsevier Applied Science, London. 61-86.

Schutyser, M. A. I., Perdana, J. and Boom, R. M. 2012. Single droplet drying for optimal spray drying of enzymes and probiotics. Trends in Food Science and Technology. 27, 73-82.

Shahbandeh, M. 2019. A report on Milk Market in the United States. U.S. Milk Market - Statistics and Facts. Extracted from www.statista.com.

Shahbandeh, M. 2020. U.S. per capita consumption of skim milk 2000-2017. Extracted from www.statista.com

Singh, H., Creamer, L.K. 1992. Heat stability of milk. In: Fox PF, ed. Advanced Dairy Chemistry—1 Proteins. 2nd ed. London, England: Elsevier Applied Science Publishers; 621-656.

Singh H. 1995. Heat-induced changes in casein, including interactions with whey proteins. In: Fox PF, ed. Heat-induced Changes in Milk, 2nd ed. Brussels, Belgium: International Dairy Federation; 86-104.

Singh, H., and Havea, P. 2003. Thermal Denaturation, Aggregation and Gelation of Whey Proteins. In: Fox PF, McSweeney PFH, eds. Advanced Dairy Chemistry, Volume 1: Proteins. 3rd ed. New York, NY: Kluwer Academic/Plenum Publishers; 1257-1283.

Smith, H., Hourihane, J., Kenny, L., Kiely, M., Leahy-Warren, P., and Murray, D. 2016. Infant formula feeding practices in a prospective population-based study. BMC Pediatrics, 16(1).

Swaisgood, H.E. 2003. Chemistry of the caseins. In: Fox PF, McSweeney PLH, eds. Advanced Dairy Chemistry, Volume 1: Proteins. 3rd ed. New York, NY: Kluwer Academic/ Plenum Publishers; 2003:139-201.

USDA (2019). www.choosemyplate.gov/eathealthy/dairy/dairy-nutrients-health

Vora, H. 2008. Studies on the formulation of cow milk dairy whitener using ultrafiltration process. Thesis submitted to National Dairy Research Institute towards M.Tech degree. 20-25.

Walstra P, and Jenness. R. Dairy Chemistry and Physics. John Wiley and Sons, New York; 1984.

Walton, D. E. and Mumford, C. J. 1999. The morphology of spray-dried particles: the effect of process variables upon the morphology of spray-dried particles. Trans IChemE. 77, 442-460.

Wang, Y., Che, L., Selomulya, C. and Chen, X. D. 2014. Droplet drying behaviour of docosahexaenoic acid (DHA)-containing emulsion. Chemical Engineering Science. 106, 181-189.

Woo, M. W., Daud, W. R. W., Mujumdar, A. S., Talib, M. Z. M., Hua, W. Z. and Tasirin, S. M. 2008. Comparative study of droplet drying models for CFD modelling. Chemical Engineering Research and Design. 86, 1038-1048.

Woo, M. W., Rogers, S., Selomulya, C. and Chen, X. D. 2012. Particle drying and crystallization characteristics in a low velocity concurrent pilot scale spray drying tower. Powder Technology. 223, 39-45.

CHAPTER 2

STUDY THE EFFECT OF DIFFERENT SOLIDS CONCENTRATION ON THE DRYING KINETICS OF WHEY PROTEIN CONCENTRATE BY SINGLE DROPLET DRYING TECHNIQUE

INTRODUCTION

In the dairy and food industry, the drying of materials – whether liquids or slurries is one of the oldest and most used unit operations to improve storage life or reduce transportation costs. Drying of whey protein is also done in a similar way as the drying of milk. Whey is currently commonly dried using the Spray drying process. (Dairy Processing Handbook, 1998). In addition to milk powder, many US manufacturers are now focusing on specialty products such as whey powders and milk protein concentrates as ingredients for higher-value dairy products (e.g., ice cream, yogurt, infant formula, and clinical formulas for the elderly). In spray drying, the WPC is first concentrated by evaporation and then dried in a spray tower. Throughout the first stage of drying processes, the additional water in free form is removed, while in the final stage of drying, the water in the bound form is removed from pores and capillaries. The main stage is generally quick, while the final stage requires more time and energy. The retentates obtained from the ultrafiltration of whey are dried to produce Whey protein concentrates (WPC) powders. These powders are termed based on their protein content, e.g., 35% to 85% (% protein on dry matter basis).

Single droplet drying is a newer technology and can also optimize processing conditions and their commercial operations. The predictive model generated using SDD can be used as a tool to optimize the drying conditions and will help them to reduce

costly plant trials when developing new ingredients with new functionalities. This knowledge base helps the dairy industry improves ingredient quality to better meet the needs of consumers. The single droplet drying (SDD) approach involves a single droplet suspended on the tip of a glass filament/glass capillary tube (Charlesworth and Marshall, 1960; Lin and Chen, 2002; Cheong et al., 1986), where changes in droplet diameter, mass, and temperature can be measured during drying (Adhikari et al., 2000). Drying an isolated droplet under controlled conditions are analogous to spray drying (Charlesworth and Marshall, 1960; Walton and Mumford, 1999), as the moisture is being removed by convection at elevated air temperature for both processes. The drying kinetics data generated using this technique have been used to verify a number of drying models (Chen and Lin, 2005; Lin and Chen, 2007; Mezhericher et al., 2007; Mezhericher et al., 2008), and can be incorporated into CFD modeling of spray drying operations (Woo et al., 2008; Woo et al., 2012). One of the drying models, the Reaction Engineering Approach (REA), has been found to produce more accurate drying predictions and better correlation with experimental data during the investigation of physical and biochemical characteristics of food powders (Patel and Chen, 2005). The model considers evaporation as an activation process with zero-order kinetics and offers the advantage of a simplified ordinary differential equation without spatial distribution during the modeling of moisture and temperature profiles for small droplets. The REA model, when coupled with the SDD data, can be used to produce an activation curve unique to a material at a certain solid content, providing accurate drying kinetics data necessary for the simulation of the spray drying process. The parameters from the activation energy curve are used for dryer wide predictions of particle moisture and temperature profiles for different initial solids

concentration of a material in an industrial spray dryer. The REA model has demonstrated good agreements between predicted and experimental results under the assumption of uniform droplet temperature (Patel and Chen, 2008; Mezhericher et al., 2010).

It is important to know that the REA modelings are independent of the changes in temperature or droplet size (Chew et al., 2013; Fu et al., 2012).

MATERIAL AND METHODS

General Procedures

Sample procurement

WPC80 (in liquid form) was procured from Valley Queen Cheese Factory (Milbank, SD) for the experiment. WPC80 was manufactured at Valley Queen Cheese factory by ultrafiltration of cheese whey and subsequent diafiltration/ reverse osmosis. This process is similar to that applied by most WPC processors. Approximately 80 lbs. of WPC80 was procured for each trial run. The total solids ranged from 32 – 35%.

Standardization of WPC80 and experimental design/ statistics

WPC80 was standardized to three different total solids level viz. 10%, 20%, and 30% using glass distilled water at room temperature. The average composition analyzed for the standardized WPC is mentioned in Table 1. Triplicate samples were analyzed for each trial run. Average values and Standard Error of Mean (SEM) were calculated from three trial runs of WPC80. The R^2 values were calculated for the actual and projected curves, and P values at 0.01 significance were calculated between each of the solids levels for each of the diameter, temperature, and mass measurements.

These standardized solutions were dried both in the SDD as well as spray-dried using a single-stage pilot-scale spray dryer (NIRO) in the Davis Dairy Plant. The inlet and outlet temperatures were maintained at 200° and 90°C, respectively, for the pilot-scale spray dryer. The powders were collected and packed in airtight containers and stored at room temperature for further analysis.

Chemical Analysis

The standardized WPC samples were analyzed for Total Solids, Fat, pH, and Minerals, which were determined using the standard wet chemistry procedures as described by Hooi et al. (2004), while Protein content was determined by using the micro-Kjeldahl method again by Hooi et al. (2004).

Single Droplet Drying System

SDD device is used to measure droplet drying kinetics, including diameter change history, weight change history, and temperature history. The data can be interpreted using a drying rate model, which may then be used in spray drying simulation. The device can also be used for the minimal scale product development and to look at the morphological development during drying.

The glass filament single droplet dryer used in this work is a newly built equipment. The working principles of this equipment and the procedures of droplet drying experiments are that described in past research work (Che and Chen, 2010; Chen and Lin, 2005; Lin and Chen, 2002; Fu, 2012; Chew et al., 2013). The details are included here for completeness.

Most parts of the procedure for Single Droplet Dryer operations are adopted from Fu, Nan (2012), with changes relevant to the current equipment and experiments.

Set-up of the equipment

A pictorial representation of the Single Droplet Dryer is shown in Figure 1. Briefly, compressed air was firstly filtered and dehumidified. The resultant dry air with a moisture content around 0.0001kg/kg was passed through a valve and a flow meter to achieve precise control of the airflow velocity prior to entering the heating tower. A schematic figure of the glass filament dryer set-up is shown in Figure. 2. The dry air stream was then heated by a set of electric elements and was passed through a steel mesh setting at the entrance of the drying chamber in order to achieve an evenly distributed laminar flow within the drying chamber. The dry air used in the experiment was set at 90°C temperature with a velocity of 0.8 m/s. Prior to any experimental runs, the drying chamber was preheated to the desired temperature. The desired temperature is achieved in approximately 20 minutes, depending on the temperature.

Droplet generation and transfer

When generating and transferring a droplet into the drying chamber, a bypass barrier plate was used to divert the conditioned hot air stream away, thus minimizing droplet evaporation before monitoring is started (Figure 3). Single droplets were generated using a 5 mL microsyringe (Part#001450, SGE Analytical Science, Australia). The initial droplet size was 2 ± 0.05 μL was used in this study; the errors were taken as half of the minimal graduation (0.1 μL) of the micro-syringe. The actual size of each droplet was experimentally determined, as described below. The generated droplet was

transferred and hung to the suspending glass filament inside the drying chamber with a separate transferring glass filament.

Monitoring droplet drying kinetics during drying

The diameter, temperature, and mass data of the droplet during drying were obtained in separate runs with identical drying conditions. Figure. 4 shows the schematic figures for the experimental set-up of each measurement. The measurement of the three parameters was carried out in separate runs with identical drying conditions, using three separate droplet suspension modules. The working principles of each droplet suspension module are described in the following sections.

For the diameter and temperature measurements, the droplet was suspended by a static glass filament. In contrast, for the measurement of droplet mass, a flexible long glass filament with a bend horizontal section was used.

Three replicates were performed for each trial for each type of measurement viz. diameter, temperature, mass. Three trials were conducted for each set of experiments/ studies. The data were averaged to give a single value for each time-lapse and plotted into charts/ graphs.

Diameter Measurements

The suspension of a single droplet (Figure 5 a) for diameter measurement employed a static glass filament fixed onto the supporting iron wire on the removable holder (Figure 5 b). The diameter of the diameter measuring glass filament was approximately 200 μm to 30 μm from the thick end to the fine end. The tip of the fine end was burned into a knob with a diameter of approximately 200-300 μm for hanging the

single droplet. The glass filament was also coated with Teflon to make it hydrophobic, to prevent the droplet from climbing up the glass filament during drying. The knob at the tip was made hydrophilic by coating with reconstituted whole milk and then baking on the Bunsen burner. The final coating procedure was to blacken the glass filament using a permanent marker (The Original Texta Stubby Black Marker, Jasco 0003537, Jasco Pty. Ltd., Australia). The black color of the glass filament facilitated the video capture and the subsequent image analysis compared to the original transparent color. This glass filaments with a knob to hang a droplet and transfer glass filaments were provided to us by Dr. Nan Fu (Soochow University, China) throughout the experiments at no cost.

The principle of the diameter measurement experiment is illustrated in Figure 4 (a). The drying process of the single droplet under a given condition was continuously monitored by the video camera, and the changes in the droplet size, along with the progress of drying, were reflected by the changes in the projected area in the video. The illumination used for the video recording during diameter measurement was backlighting produced by a lamp with natural white color. The purpose was to produce a clear contrast between the outer contour of the droplet and the background, as shown in Figure 5 (a), which would facilitate the extraction of quantitative data from the video. The diameter was estimated by monitoring the area change of the droplet from video-recording throughout the drying process (Sony DCR-HC36 Camcorder, Sony Corporation, Japan). The detailed data analysis steps will be described in the next section.

Temperature Measurements

Temperature data was obtained by inserting a fine wire thermocouple (Type K, Part# CHAL-001, Omega Engineering Inc., USA) in the center of the droplet and

collecting the temperature data from the thermocouple connected to a computer via a Picometer TC-08 (Pico Technology, UK). The working principle is shown in Figure 4 (b).

A new removable holder made of plexiglass was constructed to implement this working principle. As shown in Figure 6 (c) and Figure 6 (d), the plexiglass holder for temperature measurement was constructed to make three grooves in the front, where three aluminum pieces were glued. The front of each aluminum piece was grooved into a long and narrow channel. In the channels of the two aluminum pieces at the outer side, two fine glass capillary tubes were fixed, which was used to support and protect the thermocouples. In the channel of the middle aluminum piece, flexible copper wire with a diameter of approximately 1 mm was fixed to hold the suspending glass filament. The three aluminum pieces were aligned so that the glass filament and the capillary tubes were placed on the same plane. The conjunction of the thermocouples was roughly placed underneath the tip of the glass filament without touching it. Such a design could minimize the adjustment of the droplet position required during actual drying trials. In addition, the use of the flexible copper wire made it easier to align the tip of the glass filament and the conjunction of the thermocouples in the drying chamber. Instead, to adjust the position of the delicate thermocouples, the glass filament could be moved in a small area to find the conjunction knot. Such alignment is shown in Figure 6 (a) and Figure 6 (b), both with and without a droplet.

Mass Measurements

Mass data was obtained from the change of displacement of the mass-measuring filament during drying. A schematic figure of such displacement measurement is shown

in Figure 4 (c). When there is mass hanging at the tip, the glass filament will deflect, leading to displacement from its original location. Throughout the drying process, this deflection will continuously reduce as moisture gets evaporated. The displacement history was then captured by the camcorder. From calibration, such displacement is in a linear relationship to the mass of the weight and hence can be converted to the actual mass value with a standard curve, as shown in Figure 7. Weight standards were prepared by suspending known amounts of petroleum jelly (viz. Vaseline) coated fine glass beads (0.1–0.2 mg each) under the same drying conditions and recording the corresponding displacement of the glass filament. The actual mass of the standards was obtained by a five-decimal analytical balance (Nevada Weighing, USA).

The diameter of the flexible glass filament used in the current research was approximately 500-150 μm from the fixed end to the free end. At the lower part of the vertical part (free end), the diameter was made to finer, at approximately 50 μm. The end of the vertical part was burnt into a fine knob with a diameter of approximately 200-300 μm to better support the generated single droplet. Therefore, the vertical part of the flexible glass filament was very similar to the glass filament used in the diameter measurement. The vertical part was also subjected to the same coating procedure, as described in the section above for the diameter measurements. For mass measurement, the holder to fix the diameter-measuring glass was removed from the rig. The mass-measuring glass filament was moved forward until the vertical body entered the drying chamber via the small gap on the inner wall of the drying chamber. The gap was sealed using an aluminum part during diameter and temperature measurements. The vertical body of the glass filament was adjusted to be placed at approximately the center of the

drying chamber for starting the drying trials. To facilitate the image analysis, in actual drying trials, the displacement of the glass filament was indicated by a mark on the glass filament. Approaching the end of the glass filament above the knob, a small section of the glass filament that was painted black during coating was marked with white correction fluid (Corporate Express Australia Pty. Limited, Australia). For drying measurement, the back window of the drying chamber opposite to the camcorder was sealed with black paper to produce a black ground in the video. As such, the displacement of the glass filament was indicated by the movement of the white mark on a totally black screen. The illumination source was placed above the drying chamber to increase the contrast between the white mark and the black ground.

Image analysis to extract quantitative drying kinetics data

Droplet diameter and mass change data, which were video recorded, were processed using Adobe After Effects 7.0 (Adobe Systems, USA) to enable the extraction of images. Droplet diameter and glass filament images were extracted at a frame rate of 1 frame per second. An equivalent droplet diameter was calculated from the projected droplet area based on the perfect circle assumption and compared to the glass knob with a known diameter for actual size estimation. The knob on the tip of the glass filament was observed under a microscope with a standard calibration slide to measure its diameter. For droplet mass image analysis, extraction was conducted at the rate of 5 frames per second and later averaged at 1 frame per second of the time interval for improved accuracy.

(This method was adopted from Chew et al., 2013 with the changes relevant to the current experiment).

Image analysis for diameter measurement

The temperature data of the droplet being dried could be directly obtained from the computer; only the diameter and mass measurements required image analysis to generate quantitative data. A flow diagram depicting the diameter image analysis process is shown in Figure 8.

The video which recorded the diameter measurement process was firstly processed with Adobe After Effects 7.0 (Adobe Systems Incorporated, USA) to convert the video into a sequence of images portraying the drying events at a rate of one frame per second.

Then Time 0 of the drying trial was determined by detecting the disappearance of the standing mark attached to the bypass barrier plate. The images starting from Time 0 were further processed with ImageJ 1.5b (National Institute of Health, USA) to estimate the projection area of the droplet on each image. The resultant projected area, which was in a unit of pixel^2, was considered as a perfect circle, and the equivalent diameter was calculated (in a unit of a pixel). Then the droplet diameter in pixel was compared to the diameter of the knob at the tip of the suspending glass filament to estimate the actual droplet size. The projected diameter of the knob was obtained by analyzing blank glass filament with no droplet (blank) during the same drying trial. For each drying trial, at least 50 images before suspending the single droplet were analyzed with ImageJ, using the same image analysis procedure described above.

The average result of these images was used as the final projected diameter of the knob. The actual diameter of the knob was determined using a standard calibration slide of 200 μm (Motic®, Motic Group Co. Ltd., China) under a microscope. Following this

procedure, the actual diameter of the droplet being dried in correspondence to each second of drying can be obtained.

Image analysis for mass measurement

From the recorded video, images were extracted at the rate of five frames per second using Adobe After Effects 7.0. A flow diagram depicting the mass image analysis process is shown in Figure 9.

Time 0 of each drying trial was determined by the disappearance of the standing mark. Images following Time 0 were then processed using ImageJ 1.5b in order to determine the position of the white mark on each image, which corresponded to a 0.2 s time interval of the drying process. For the calculation of the movement of the white mark during drying, the zero position with no weight was firstly measured by analyzing at least 300 images before the bypass barrier plate was inserted. The final zero position was the average of the white mark position on these 300 images. The standard deviation of the results from these 300 images was around ~2.0-3.0 pixels, whereas the coefficient of variation was in the range of 1.0-2.0% for various experiments.

After drying was started, the white mark on the screen dropped down due to the suspended droplet and then gradually moved up as the moisture was removed. The position of the white mark on each image was determined using ImageJ, and then the displacement was calculated by subtracting the zero position from the white mark position on each image. The results from consecutive five images (with a time interval of 0.2 s) were averaged to yield the displacement of the glass filament at each second of drying, to minimize the effects of the fluctuation of the flexible glass filament in the upwards air flow. The image analysis procedure to establish a standard curve associated

with a specific set of mass measurement is also shown in Figure 9. For each weight standard, the position of the white mark was calculated by averaging the results of at least 300 images. Since the weight standard used in the current research was agglomerated fine glass beads, during drying, it was possible that the residual petroleum jelly (viz. Vaseline) on the tip of the glass filament could alter the zero position. Hence for each weight standard, the zero position was separately recorded prior to hanging the weight. The corresponding zero position of each weight standard was also the average of at least 300 images. The difference between the zero position of the white mark and the position with the weight thus indicated the displacement of the glass filament due to the mass of each weight standard. The mass of each standard was measured using the analytical balance (measuring weight up to 5 decimal places) to establish the standard curve for the drying conditions used. Then the measured displacement at each second of a mass measurement drying trial can be converted to the actual mass data of the droplet. Since the commencement of drying was taken as the point when the bypass barrier plate was withdrawn from the drying chamber, the sudden contact to the upwards hot air flow would lead to a significant fluctuation of the glass filament, which usually lasted for 2-3 s. This phenomenon added to the difficulty of determination of the initial mass of the droplet, even though Time 0 can be accurately determined. In the current research, the initial mass of each drying run was estimated by extrapolating the measured droplet mass at the initial 30 s of drying.

A brief about the Reaction Engineering Approach (REA) modeling

The Reaction Engineering Approach was established on the idea that evaporation is an activation process that must overcome an energy barrier for the removal of moisture to occur (Chen and Putranto, 2013). Mass transfer rate (i.e., drying rate) from a droplet during the drying process can be expressed using the following equation:

$$dm/dt = -h_m A (\rho_{v,s} - \rho_{v,b}) \quad (1)$$

where, dm/t refers to drying rate(kg/s), h_m refers to the mass transfer coefficient (m/s), A is the surface area of the droplet (m^2), and $\rho_{v,s}$ and $\rho_{v,b}$ represent the vapor density (kg/m^3) at the droplet surface and at the bulk air, respectively. A fractionality coefficient Ψ is used to correlate the actual vapor density at the droplet surface, $\rho_{v,s}$, to the saturated vapor density at the droplet surface, $\rho_{v,sat}$, as described below:

$$\rho_{v,s} = \Psi \rho_{v,sat} (T_s) \quad (2)$$

where, Ts refers to the surface temperature(K) and approximately equals the average droplet temperature Td (K) when temperature gradient can be neglected at sufficiently small Biot number. The fractionality coefficient Ψ, in effect, represents the relative humidity at the interface of the droplet to the bulk air. The main premise of the REA activation energy approach correlates the fractionality coefficient, Ψ, to the activation energy of evaporation, ΔEv, using a simple Arrhenius type equation:

$$\Psi = \exp (- \Delta E_v / RT_d) \quad (3)$$

where, ΔE_v is termed as the apparent activation energy(J/kmol), which is essentially a ‘‘correction factor’’, representing the increase in difficulty to remove moisture at low moisture content levels, R is the gas constant (8314J/(kmolK)), and Td refers to the average temperature of the droplet or particle (K). Equation (1) can hence be rewritten in the following form:

$$dm/dt = -h_m A [\rho_{v,sat} \exp(-\Delta E_v / RT_d) - \rho_{v,b}] \quad (4)$$

Since dm/dt, Td, and A can be experimentally determined, the history of the activation energy barrier for achieving moisture removal for a droplet under a given condition can be established using an alternative form of equation (4):

$$\Delta E_v = -RT_d \ln [(-(dm/dt) (1/h_m A) + \rho_{v,b}) / \rho_{v,sat}] \quad (5)$$

Extensive experimental work has shown that different activation energy curves obtained from varying drying conditions, for the same initial size and solid content, can be reduced (normalized) to a master characteristic curve of normalized activation energy in the following form (Chen, 2008):

$$\Delta E_v / \Delta E_{v,b} = g (X-X_b) \quad (6)$$

Where, X represents the particle moisture on a dry basis (kg/kg). In equation (6), the particle moisture is normalized with X_b, which is the equilibrium moisture content on a dry basis (kg/kg) for a specific drying condition. The activation energy is normalized with the ‘‘equilibrium’’ activation energy $\Delta E_{v,b}$. When the material to be dried reaches the equilibrium moisture content, $\rho_{v,s}$ equals $\rho_{v,b}$, and there is no removal of moisture, so

dm/dt decreases to 0, and T_d reaches the bulk air temperature T_b. The ‘‘equilibrium’’ activation energy is calculated based on the environmental condition:

$$\Delta E_{v,b} = -R\, T_b \ln (\rho_{v,b} / \rho_{v,sat}) \quad (7)$$

Observation by Scanning Electron Microscopy

The particles of WPC80 dried on the Single Droplet Dryer at three different levels of total solids viz. 10%, 20%, and 30% were mounted on an aluminum stub using conducting carbon tape. Also the individual particles were cut and mounted on the stub to reveal the cross-section. Samples were sputter-coated with ~10nm gold (approx. 99%) to produce a conductive surface for SEM observation. SEM images were obtained using a scanning electron microscope (Hitachi S-3400N, Hitachi America Ltd., Tarrytown, NY), located in the Daktronics Engineering Hall, South Dakota State University, which was operated at 10 kV voltage.

Bulk Density of the powder obtained from Spray Dryer

The loose bulk density and the tapped bulk density of the WPC80 powder dried in a spray drier were measured by filling WPC80 powder loosely in a 100mL plastic volumetric cylinder and recording the initial weight. The tapped bulk density was measured by tapping on a bench surface 100 times and recording the final weight, which was divided by the initial weight to calculate the tapped bulk density. Triplicate measurements were conducted for each sample.

Viscosity

The viscosity of WPC80 (10%, 20%, and 30% total solids) was measured at 20°C with a Viscoanalyzer (Reologica Instruments AB, ATS Rheosystems, Rheometric Scientific Inc., Piscataway, NJ) using bob-and-cup geometry. The samples were conditioned at 20°C for 60 s before analysis. About 13 mL of each concentrate at 20°C was transferred into the cup of the rheometer, and the bob was lowered until the whole bob surface was covered. An equilibrium time of 50.0s and a pre-shear rate of 10 s^{-1} for 20.0 s was applied. The viscosity of the solution was measured at a shear rate of 100 s^{-1} with a delay time of 10 s. (This method was adopted from Marella et al., 2015 with slight modifications). Duplicate measurements were conducted for each sample.

RESULTS AND DISCUSSION

Effect of the total solids content of WPC80 on the drying kinetics

Comparison of droplet diameter measurement profiles

At temperatures above 90°C affect the functional, textural, and nutritive qualities of whey proteins, which also corresponds to the outlet temperature of the commercial spray dryers. The outlet temperature of the air, leaving the drying tower is used for control and provides a measure of the severity and rate of drying in a commercial spray dryer (Mermelstein, 2001). Considering the use of this temperature in the previous studies (Chew et al., 2013 and Fu et al., 2011), 90°C temperature was considered for the single droplet drying experiments using the glass filament method. The velocity of drying air was set at 0.8 m/s, and the droplet size used in the experiment was 2µL. For general understanding, the average diameter of a 2µL water droplet is obtained as 1.5634 mm at 20°C.

The change in diameter followed a similar pattern for all three total solids levels, i.e., a drop in the initial diameter (falling rate drying period) followed by a linear change for the remaining moisture content during the constant rate drying period. Here, the falling rate drying period time can be utilized to design the cylindrical portion of the spray dryer, while constant rate period can be useful for designing the second stage timing in the dryer/ cone size of the dryer. Differences in the time taken for drying / diameter change for each of the solids level can be used to design the process conditions like the flow rate of the feed to the dryer, residence time of the particle in the dryer, and atomization speed/ spray nozzle size for the dryer.

Since the moisture to solid mass ratio is different for different total solids levels, the time required to remove all the internal moisture under the same drying conditions is different. The higher the total solids level, it takes longer time for the removal of moisture (Figure 10). This is also affected by the viscosity of the WPC80 at different solids levels. Also, the drying commenced slowly for 30% solids level followed by 20% and 10% solids level, respectively, mainly due to the possibility of earlier outer crust formation, and hence lower migration of the moisture to the surface of the particle. The value of the coefficient of determination (R^2) for 10%, 20%, and 30% total solids level was 1.00, 0.99, and 1.00, respectively. There was a significant difference ($P < 0.01$) in the diameter change between all three solids level.

Comparison of droplet mass measurement profiles

Droplet mass change and temperature profiles were experimentally obtained for 2 µL WPC80 droplets at 10%, 20%, and 30% total solids level at 90° C with an air velocity of 0.8 m/s as shown in Figure 11. It also can be noted from the graph that as the total solids level increases, the drying time increases. The value of the coefficient of determination for 10%, 20%, and 30% total solids level was 1.00, 1.00, and 0.99, respectively. There was a significant difference ($P < 0.01$) in the mass change between all three solids level. A rapid formation of a dry layer at the droplet surface of the particle was due to skinning over or casehardening of the droplets and subsequent slower moisture migration to the surface of the particle at the higher solid's concentration. A similar phenomenon can also be observed if the inlet air temperature increases, but since here, the inlet temperature of the air is constant, this is only due to an increase in the total solids level.

The remaining mass of the droplet at the end of drying can be used to decide the time required for dryer in the fluidized bed dryer. Mass change of the individual particle formed can be used to study the change in density over the entire drying process. This information along with the volume change of the particle can be used to decide whether the agglomeration is needed or not for the final powder been dried.

Comparison of the droplet temperature profiles

As a thumb rule, in a spray drying system, the feed water content controls the residual moisture in the powder. Lower moisture content can be reached by higher feed solids contents for fixed values of the other process conditions (Goula and Adamopoulos, 2004). Results from the analysis of moisture content and particle size of the dried product both suggest that higher feed concentrations result in a stronger crust (Ananddharmakrishnan, 2007). Combined interactions of dry solids flow rate, inlet air temperature, and atomization speed describes well changes in the residual powder moisture content (Birchal et al., 2005).

Since the air temperature and the droplet size suspended is constant (2 μL) in the SDD experiments here, the total solids affect the time required to reach an equilibrium temperature (Figure 12). The time required for 10% solids to reach equilibrium temperature is 187 seconds (3 min and 7 sec), 282 seconds (4 min and 42 sec) for 20% total solids, and 312 seconds (5 min and 12sec) for 30% total solids respectively. Hence, as the total solids increase, the time required to reach equilibrium moisture also increases. There was a significant difference ($P < 0.01$) in the temperature change between all three solids level.

Equations to describe the activation energy of WPC80 at each different total solid level

The relative activation energy equations obtained from REA modeling can be directly used by the industry in predicting the drying histories of whey protein concentrate without using longer dryer runs. The activation energy is the amount of energy required to overcome the energy barrier and initiate the evaporation/ drying process. These activation curves are independent of the initial droplet sizes and different drying conditions but dependent on the initial total solids' concentration, hence calculated separately for each level of total solids.

The relative activation energy of 10% WPC

$$\frac{\Delta E_v}{\Delta E_{v,b}} = 0.172(X - X_b)^6 - 1.4796(X - X_b)^5 + 4.956(X - X_b)^4 - 8.213(X - X_b)^3 + 7.1946(X - X_b)^2 - 3.4907(X - X_b) + 0.9775$$

The relative activation energy of 20% WPC

$$\frac{\Delta E_v}{\Delta E_{v,b}} = -0.0003(X - X_b)^6 + 0.0048(X - X_b)^5 - 0.0291(X - X_b)^4 + 0.0717(X - X_b)^3 - 0.0212(X - X_b)^2 - 3.4907(X - X_b) + 0.9775$$

The relative activation energy of 30% WPC

$$\frac{\Delta E_v}{\Delta E_{v,b}} = 17.56(X - X_b)^6 - 53.582(X - X_b)^5 + 64.048(X - X_b)^4 - 39.314(X - X_b)^3 - 13.5(X - X_b)^2 - 3.1861(X - X_b) + 0.9583$$

This activation energy curves can be directly used for predicting the activation energy required for dying the WPC80 at 10%, 20%, and 30% total solids level in a commercial spray dryer. All the abbreviations in the equations can be found in the material and methods section.

Viscosity

There was a significant ($P < 0.01$) increase in the viscosity of WPC80 with an increase in the total solids' concentration from 10% to 30% (Figure 13). This is obvious with the fact that as the total solids increase, the viscosity of the solution also increases (Table 2). As there is an exponential rise in viscosity with change in total solids in the WPC80 solution, it is interesting to observe this fact.

Droplet size usually increases as the feed concentration or the viscosity increases and the energy available for atomization (i.e., rotary atomizer speed, nozzle pressure, air-liquid flow ratio in a pneumatic atomizer) decreases in a commercial spray dryer. Thus, the effect of feed solids concentration and increase in viscosity on dried particles size is due to its effect on spray droplets size (Keiviet and Kerkhof, 1995; Taylor, 1994; Staiger et al., 2002; Chegini et al., 2013). Since in the experiments, we are keeping the droplet size constant (i.e., 2 μL), the viscosity should have minimum effects on droplet comparison at different total solids level but has a definite combined effect with total solids on the removal of moisture from the droplet. At higher concentrations, the presence of viscosity threshold leads to significant deviation in the shrinkage behavior and influence in the droplet drying rate.

Bulk Density and Particle size

The bulk density values of the powders obtained from the spray dryer were used in the modeling process. It can be observed in Table 3 that as the total solids level increases, the bulk density (loose as well as packed) increases correspondingly. The mean particle size of the particles dried in a pilot-scale single-stage spray dryer was observed to

be 36.57 µm, 41.27 µm, and 44.56 µm for WPC80 at 10%, 20%, and 30% total solids, respectively.

When 2µL droplet was dried on a single droplet dryer, the mean particle sizes obtained at the end of the run were observed to be 1103.5 µm, 1312.3 µm, and 1407.0 µm for WPC80 at 10%, 20%, and 30% total solids, respectively. Since the initial droplet sizes of the semi-commercial spray dryer were 0.5 – 0.7 µL while in the case of SDD was 2µL. Hence the values obtained from the single droplet dryer were converted to 0.5 – 0.7 µL values for ease in the comparison (Table 3). The converted values obtained for SDD were 33.12 µm, 39.37 µm, and 42.21 µm respectively for WPC80 at 10%, 20%, and 30% total solids. Hence the values obtained by SDD were comparable to that of the semi-commercial single-stage spray dryer.

Also, the bulk density of the particles increases correspondingly with the particle size. Droplet size usually increases as the feed concentration or viscosity increases. Hence, the effect of feed solids concentration on dried particle size is due to its effect on spray droplets size. (Chegini et al., 2013).

Scanning Electron Microscopy images

The major difference that was observed in the morphology of WPC80 particles amongst the three different levels of total solids was is the appearance of the porosity and density of the structure. The WPC80 with 10% total solids showed a very thin porous structure (Figure 14 a, b). The particle cracked up easily when it was cut to place on the aluminum stub. The wall of the particles, as seen in the images, was quite thin. The cross-sectional structure was less dense than the other two levels of total solids. Some air

vacuoles were also observed. Kalab (1993) mentioned that when whey is observed under a scanning electron microscope, fat globules and a serum portion are distinctively observed, with fat globules lying on the surface. But since the WPC80 was standardized and had a negligible amount of fat (Table 1), no free particles of fat were observed on the surface. But a uniform particle of WPC was observed at different solids level with some entrapped air. Although from the diameter change and temperature change curves it can be determined that the 10% total solids level dried much faster, but as we can see in the scanning electron microscopy images the particles formed were very fluffy/ lighter in comparison to the other two solids level. These lighter particles will be easily removed at the cyclone separators. To prevent these losses, drying at higher solids is recommended. This is a well-known fact, but SDD offers studying various level of total solids, along with density and viscosity of the particle, which helps to decide what kind of particle can be obtained/ customized. This is also helpful information in deciding the size of agglomerates in the final powder. E.g., each particle is at the size of 50 – 80 μm, the agglomerates will be in the size of 500 – 800 μm, considering average of 10 particles per agglomerate.

The WPC80 with 20% total solids level had intermediate porousness and denseness in comparison to the other two levels of total solids (Figure 15 a, b). The WPC80 with 30% total solids showed a very dense structure (Figure 16 a, b), which was difficult to cut while placing on an aluminum stub and was less porous in comparison to the other two levels of total solids. These differences also come from the fact that WPC80 liquid with 30% total solids had very high viscosity in comparison to the other two levels, as mentioned earlier in Table 2.

This is the most interesting method that can be applied to single droplet particles. It totally avoids commercial spray drying run to observe a particle under a scanning electron microscope and study the morphology of newer materials. SDD turns out to be a very useful tool in viewing images of particles.

LIMITATIONS OF USING SINGLE DROPLET DRYING

1. Since one droplet is formed at a time, most testing methods/ techniques used for milk powder analysis cannot be applied to the droplets generated from this Single droplet drying technology. Hence, the comparison of traditional methods of milk powder analysis and SDD is not feasible.
2. Foaming may occur in some products like WPC, but if the foaming is not visible in videos for diameter measurements by the naked eye, it may cause erroneous data/ difficulty in data to be discarded.
3. The operation of SDD is simple, but the generation and transfer of the droplets, along with data analysis, requires a lot of practice and skills.
4. Also, the SDD temperatures of drying correspond to the outlet temperatures of the traditional spray dryers. Hence any minor changes that may happen due to higher inlet temperatures are not considered.

CONCLUSIONS

SDD can provide controlled drying conditions by an established method to study the drying kinetics and morphological changes. The diameter, temperature, and mass measurements can be successfully performed on SDD. The diameter, temperature, and mass measurements on SDD can be used as input for modeling studies. Each level of total solids represents unique behavior, so modeling must be done considering each different level. Different total solids/ composition has a direct influence on the drying behavior and particle formation of any liquid dairy material intended for drying. There was a significant difference ($P < 0.01$) between 10%, 20%, and 30% solids level for each of the diameter, mass, and temperature measurements performed for WPC80. The viscosity of the WPC80 solution significantly ($P < 0.01$) increases with an increase in the total solids level. There is a correlation between the particles obtained from the semi-commercial spray dryer and the particle generated on the SDD. Despite all the limitations, morphological changes of any powder particle can be well studied using SDD and can be viewed using scanning electron microscopy.

REFERENCES

Anandharamakrishnan, C., C.D. Rielly and A.G.F. Stapley. 2007. Effects of process variables on the denaturation of whey proteins during spray- drying. Journal of Drying Technology, 25(5): 799-807.

Birchal,V.S., M.L. Passos, G.R.S. Wildhagen and A.S. Mujumdar. 2005. Effect of spray-dryer operating variables on the whole milk powder quality. Journal of Drying Technology, 23: 611-636.

Chen, X., and Putranto, A. 2013. Reaction engineering approach II. In Modelling Drying Processes: A Reaction Engineering Approach. Cambridge: Cambridge University Press. 121-168.

Chew, J. H., N. Fu, M. W. Woo, K. Patel, C. Selomulya, and X. D. Chen. 2013. Capturing the effect of initial concentrations on the drying kinetics of high solids milk using reaction engineering approach. Dairy Sci. Technol. 93(4-5):415-430.

Chegini, G.R. & Taheri, M. 2013. Whey powder: Process technology and physical properties: A review. Middle East Journal of Scientific Research. 13. 1377-1387.

Fu, N., M. W. Woo, S. X. Q. Lin, Z. Zhou, and X. D. Chen. 2011. Reaction Engineering Approach (REA) to model the drying kinetics of droplets with different initial sizes—experiments and analyses. Chem. Eng. Sci. 66(8):1738-1747.

Fu, N., M. W. Woo, F. T. Moo, and X. D. Chen. 2012. Microcrystallization of lactose during droplet drying and its effect on the property of the dried particle. Chem. Eng. Res. Des. 90(1):138-149.

Gosta, B. 2012. Dairy Processing Handbook. Tetrapak Processing Systems AB. Whey Processing. 331-352.

Goula, A.M. and K.G. Adamopoulos. 2004. Spray- Drying of tomato pulp: effect of feed concentration. Journal of Drying Technology, 22(10): 2309-2330.

Hooi, R., D. M. Barbano, R. L. Bradley, D. Budde, M. Bulthaus, M. Chettiar, J. Lynch, and R. Reddy. 2004. (E. A. Arnold, Tech. Comm.) Chapter 15 Chemical and Physical Methods. Standard Methods for the examination of dairy products (17th Edition). Eds H. M. Wehr and J. F. Frank. American Public Health Association, Washington DC, USA. 480-510.

Kaláb, M. 1993. Practical aspects of electron microscopy in dairy research. Food Structure 12(1), 95-114.

Kieviet, F.G. and P.J.A.M. Kerkhof. 1995. Measurements of particle residence time distributions in a co-current spray dryer. Drying Technology, 13(5-7): 1241-1248.

Kim, E. H.-J., X. D. Chen, and D. Pearce. 2003. On the mechanisms of surface formation and the surface compositions of industrial milk powders. Drying Technol. 21(2):265-278.

Lin, S. X. Q. and X. D. Chen. 2007. The reaction engineering approach to modelling the cream and whey protein concentrate droplet drying. Chem. Eng. Process. 46(5):437-443.

Marella, C., P. Salunke, A. C. Biswas, A. Kommineni, and L. E. Metzger. 2015. Manufacture of modified milk protein concentrate utilizing injection of carbon dioxide. J. Dairy Sci. 98:3577–3589.

Mermelstein, N.H., 2001. Spray Drying. Food Technol., 55(4): 92-95.

Staiger, M., P. Bowen, J. Ketterer and J. Bohonek. 2002. Particle Size Distribution Measurement and Assessment of Agglomeration of Commercial Nanosized

Ceramic Particles. Journal of Dispersion Science and Technology, 23(5): 619-630.

Taylor, T., 1994. Powder and Air Residence Time Distributions in Countercurrent Spray Driers, In Proceedings of the 9th International Drying Symposium, Bebington.

Vora, H.N.; Metzger, L.E.; Selomulya, C.; Woo, M.W.; and Putranto, A. 2017. The effect of different solids concentration on the drying kinetics of whey protein concentrate. Dairy Science Publication Database. 1859.

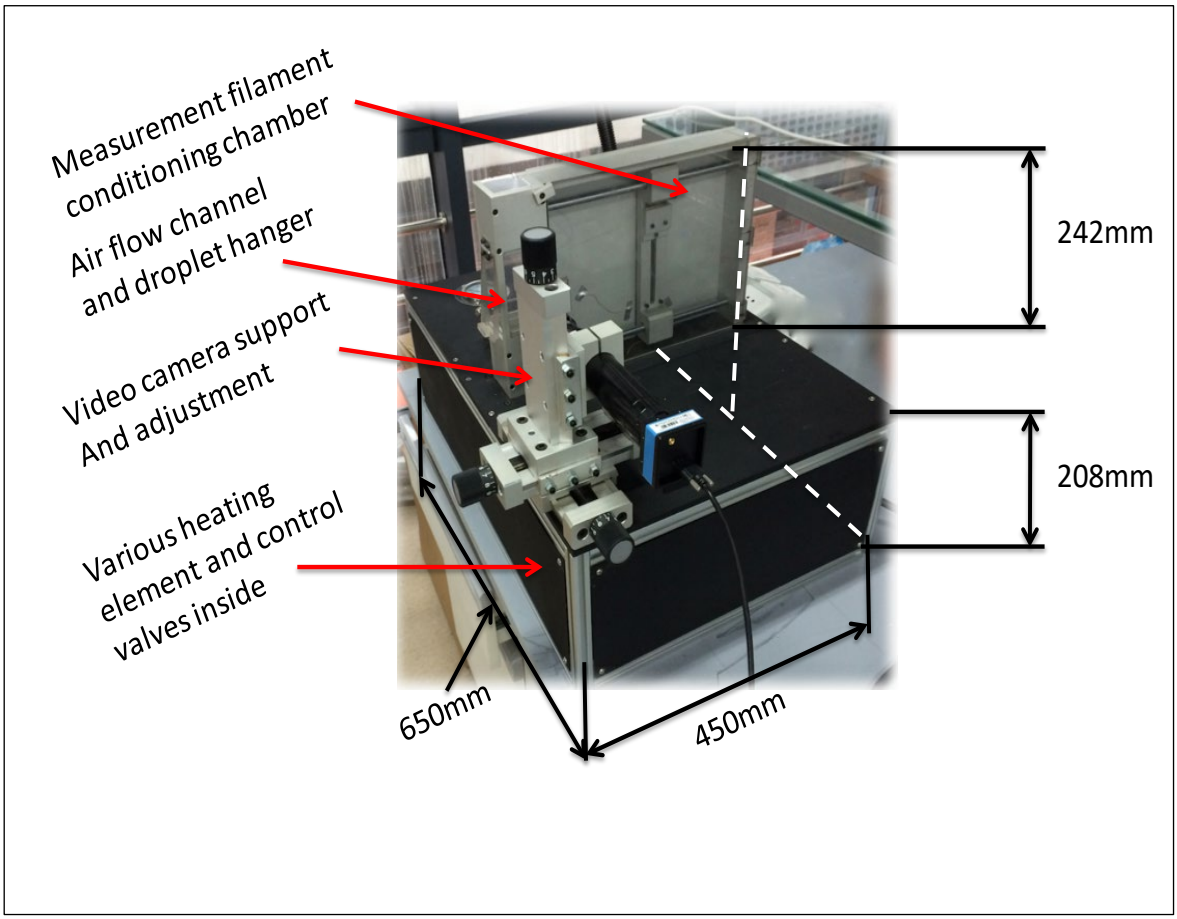

Figure 1. Pictorial representation of the Single Droplet Dryer.

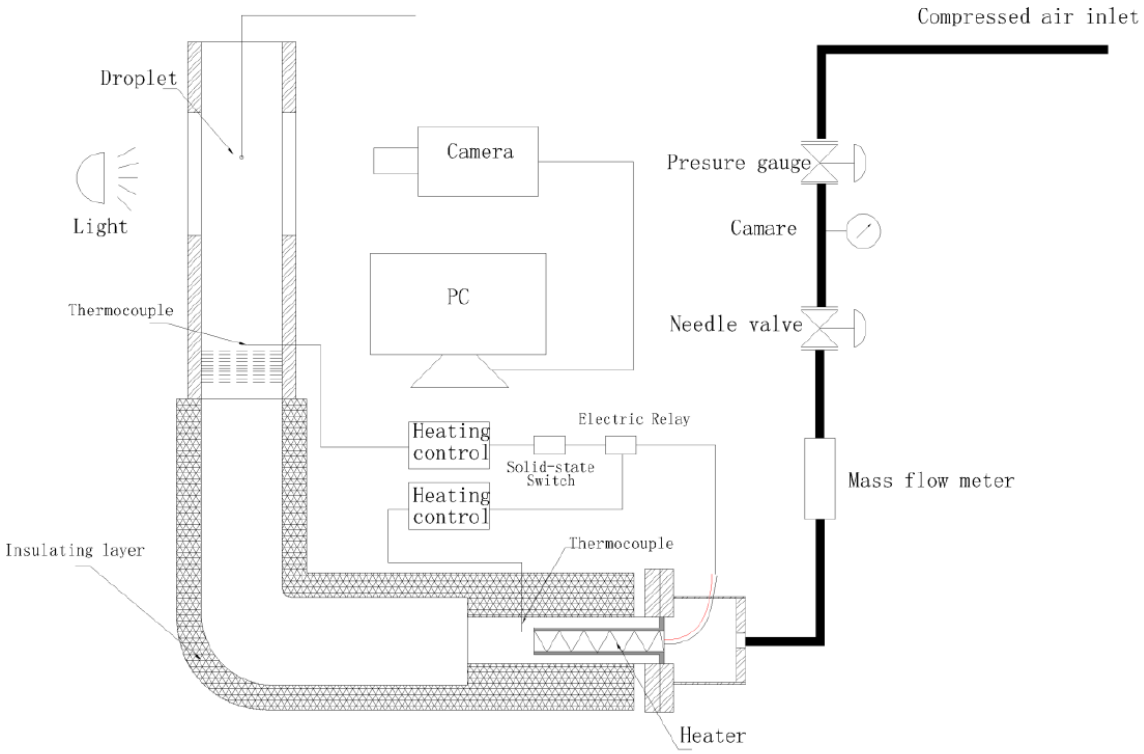

Figure 2. A schematic figure of the air supply and drying set-up of the Single Droplet Dryer used in the current study.

Open the door of the drying chamber.

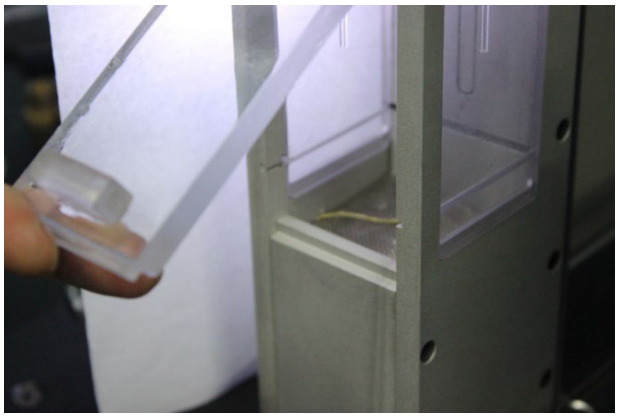

Insert the baffle.

Generate a droplet using a micro syringe.

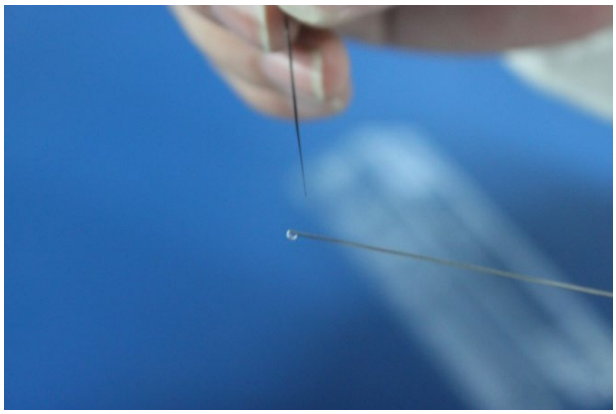

Continued on the next page...

Transfer the droplet using a transferring glass filament.

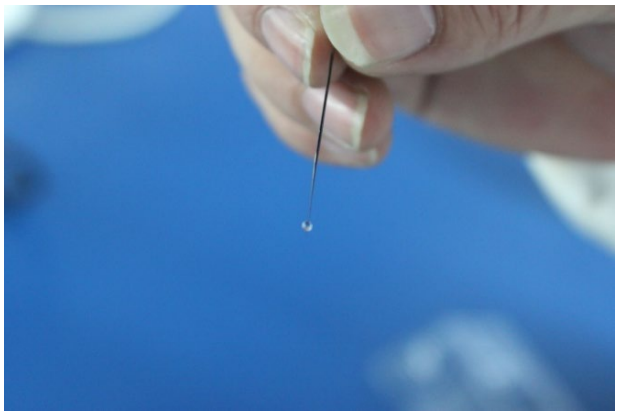

Attach the droplet to the temperature measuring glass filament.

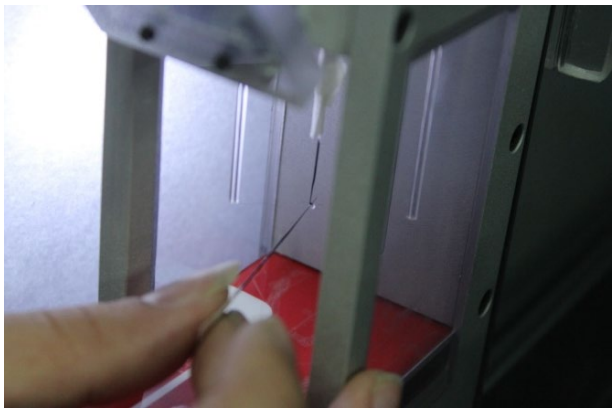

Gently pull away the baffle and close the door.

Figure 3. Pictorial representation of generation and transfer of a droplet in SDD.

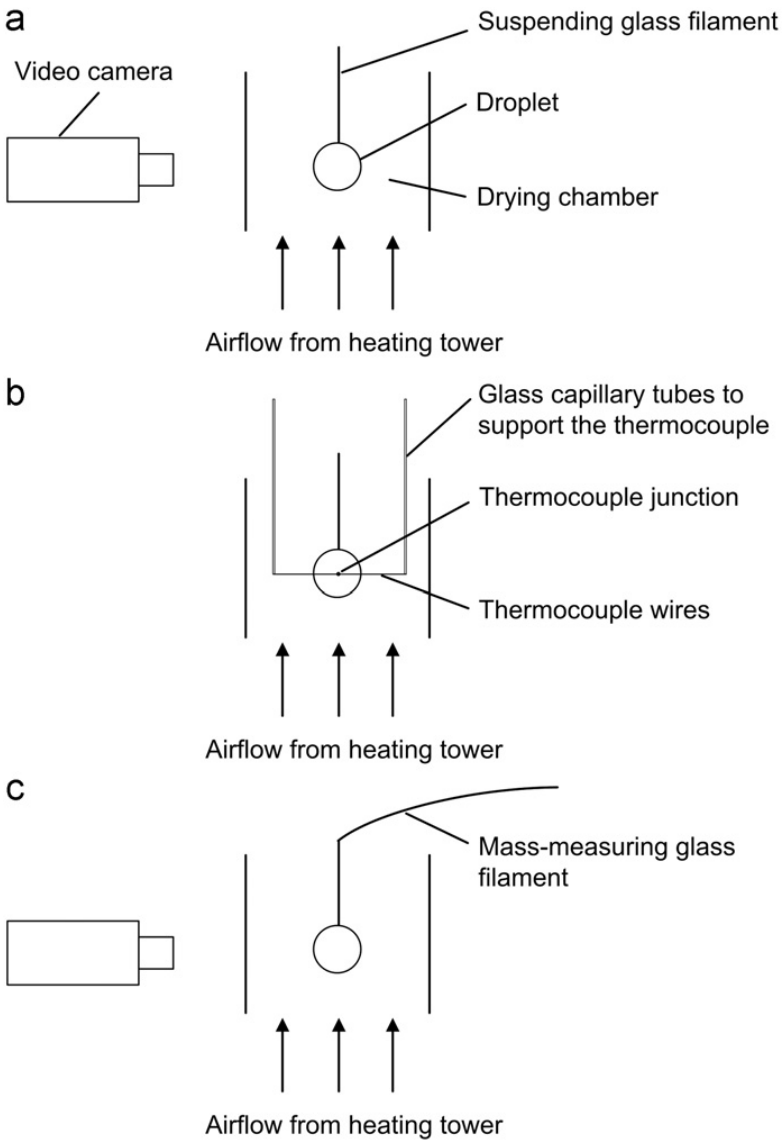

Figure 4. Schematic figures for the experimental set-up of (a) diameter measurement, (b) temperature measurement and (c) mass measurement in the glass filament rig.

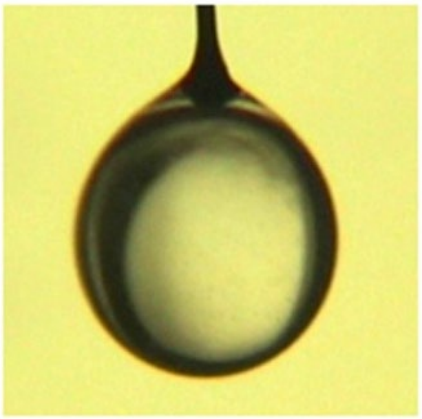

(a)

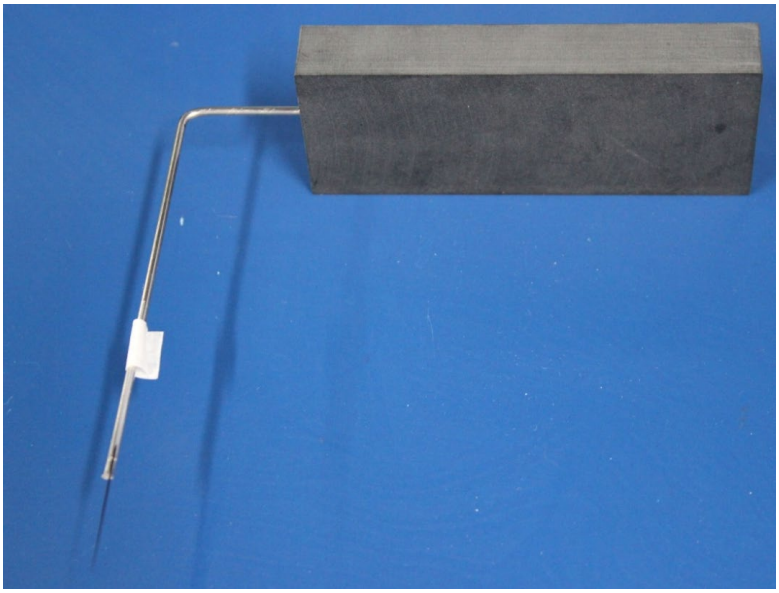

(b)

Figure 5 (a). A picture showing the actual droplet suspension during diameter measurement.

(b). Diameter/ morphology measuring module suspended with glass filament with knob.

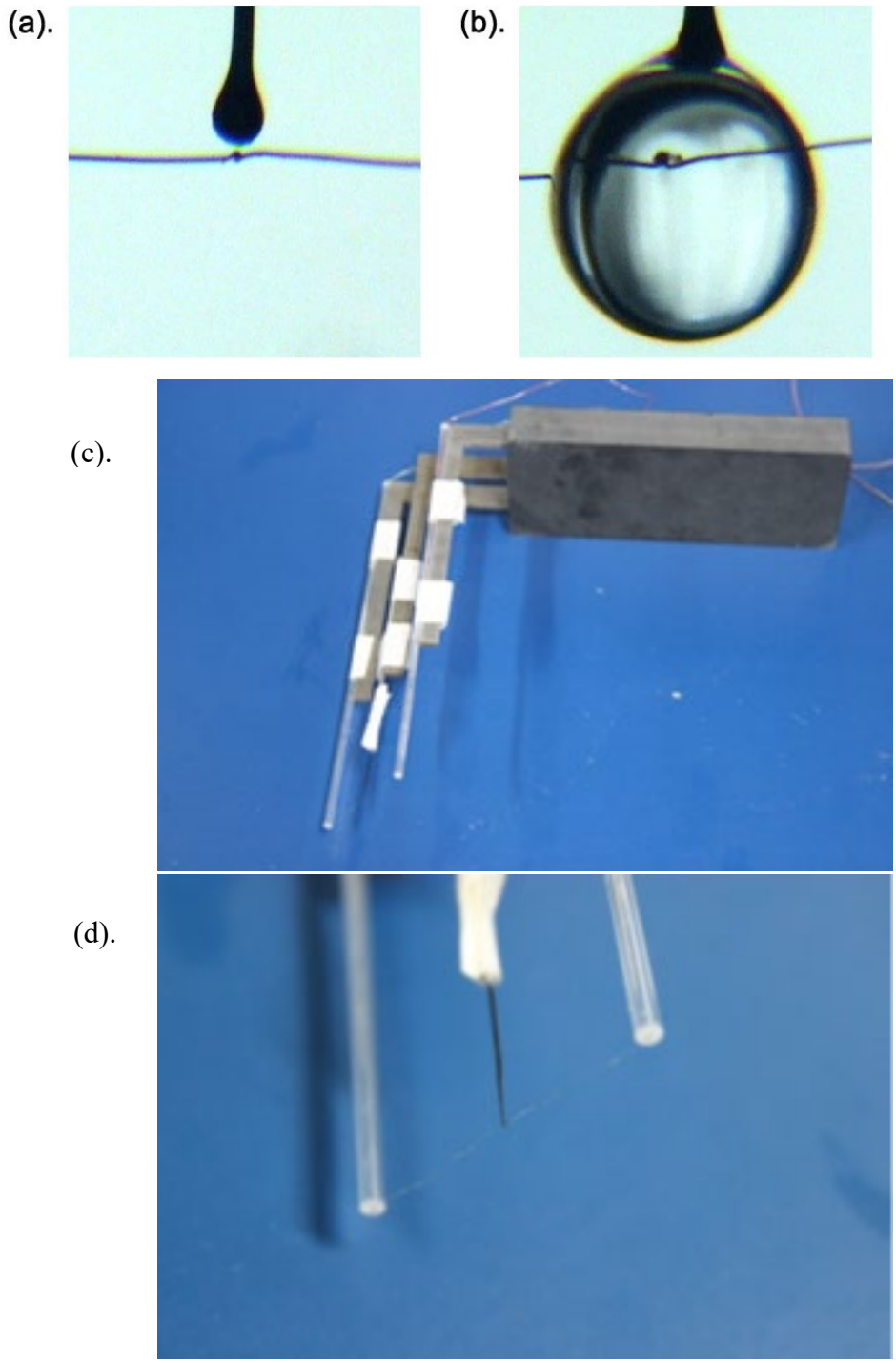

Figure 6. The alignment of the glass filament and the conjunction of thermocouples during temperature measurement. (a) Normal location; (b) during temperature measurement of a water droplet. (c) and (d) Actual temperature measuring module suspended with glass filament with knob and a thermocouple wire.

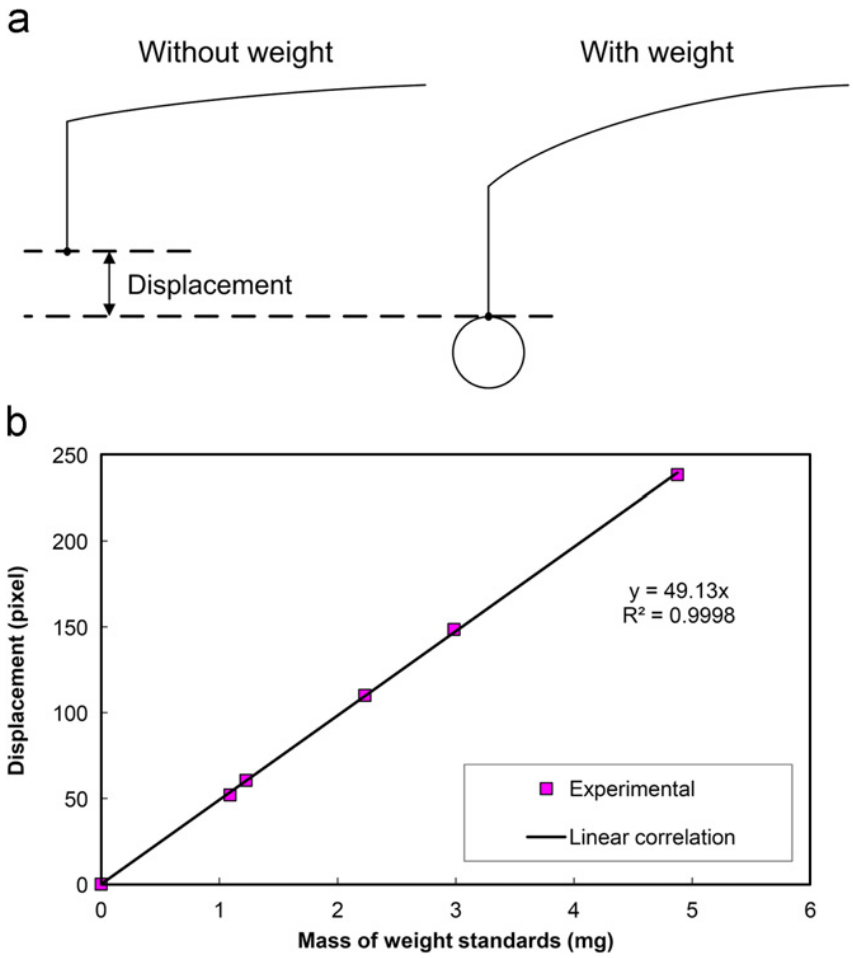

Figure 7. The mass measurement of the droplet during drying. (a) Schematic figure of the displacement of mass-measuring glass filament; (b) a typical standard curve obtained by suspending standards with known mass and recording the resultant displacement of glass filament.

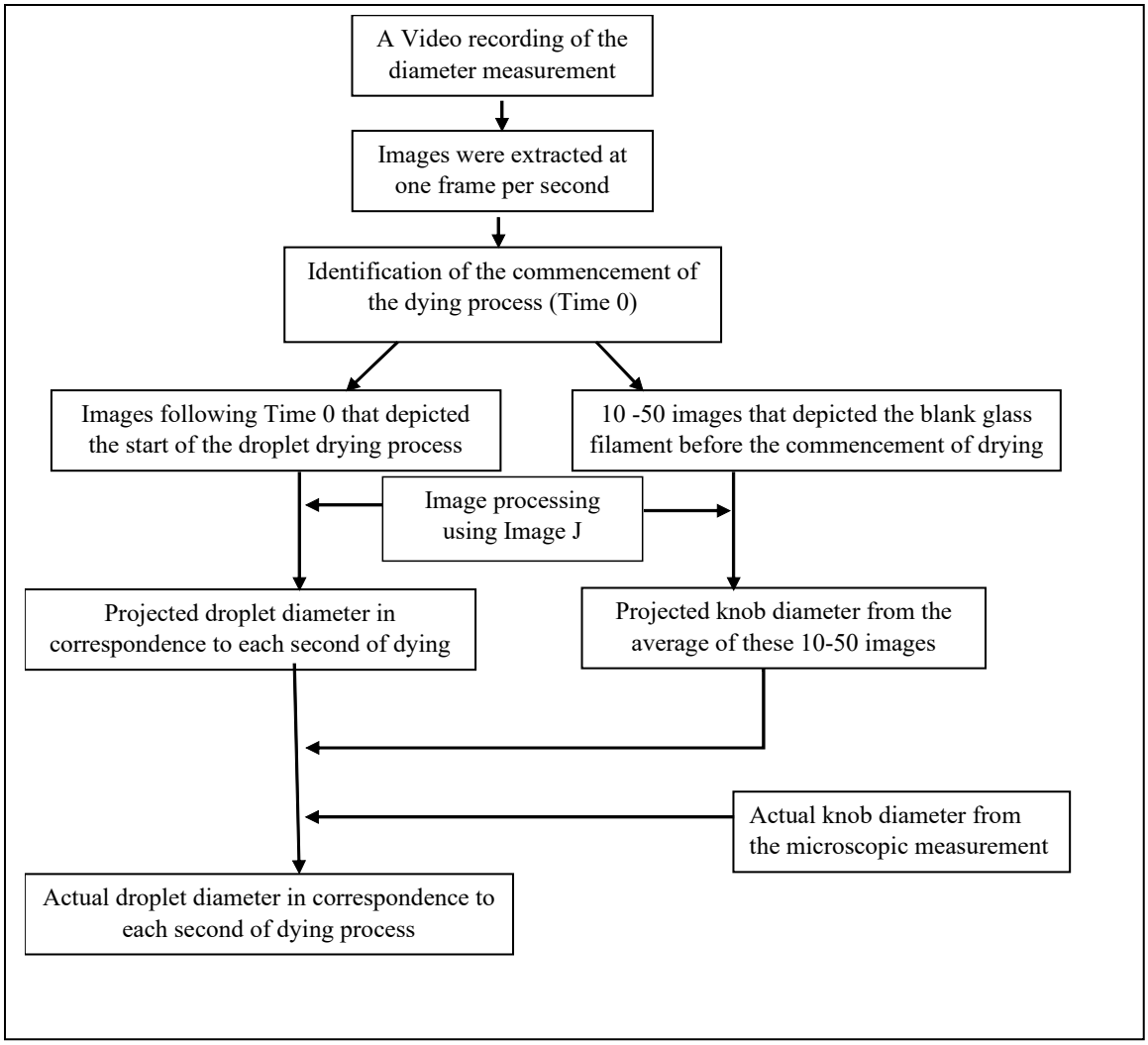

Figure 8. Image analysis process for the diameter measurement.

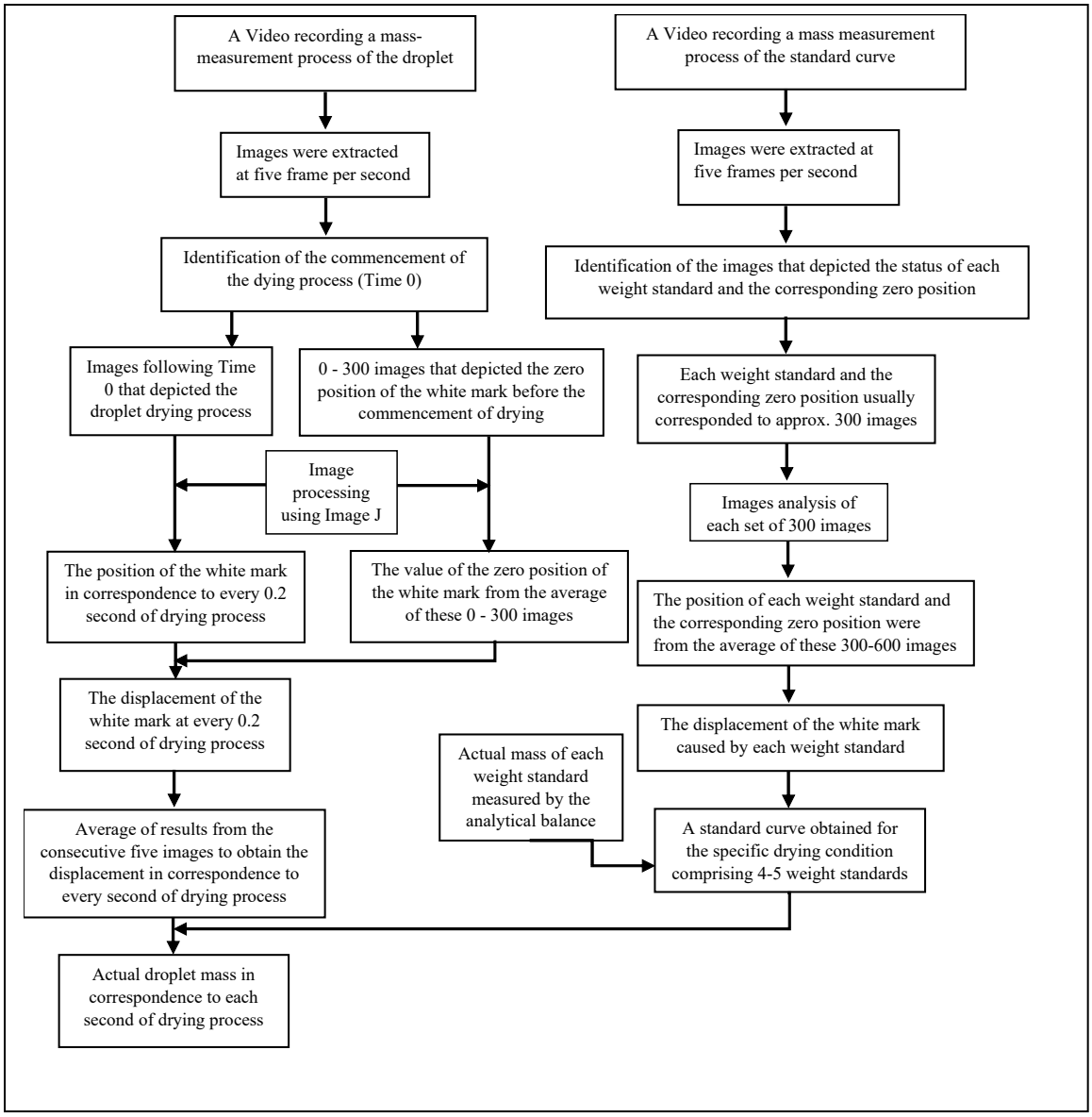

Figure 9. Image analysis process for the mass measurement.

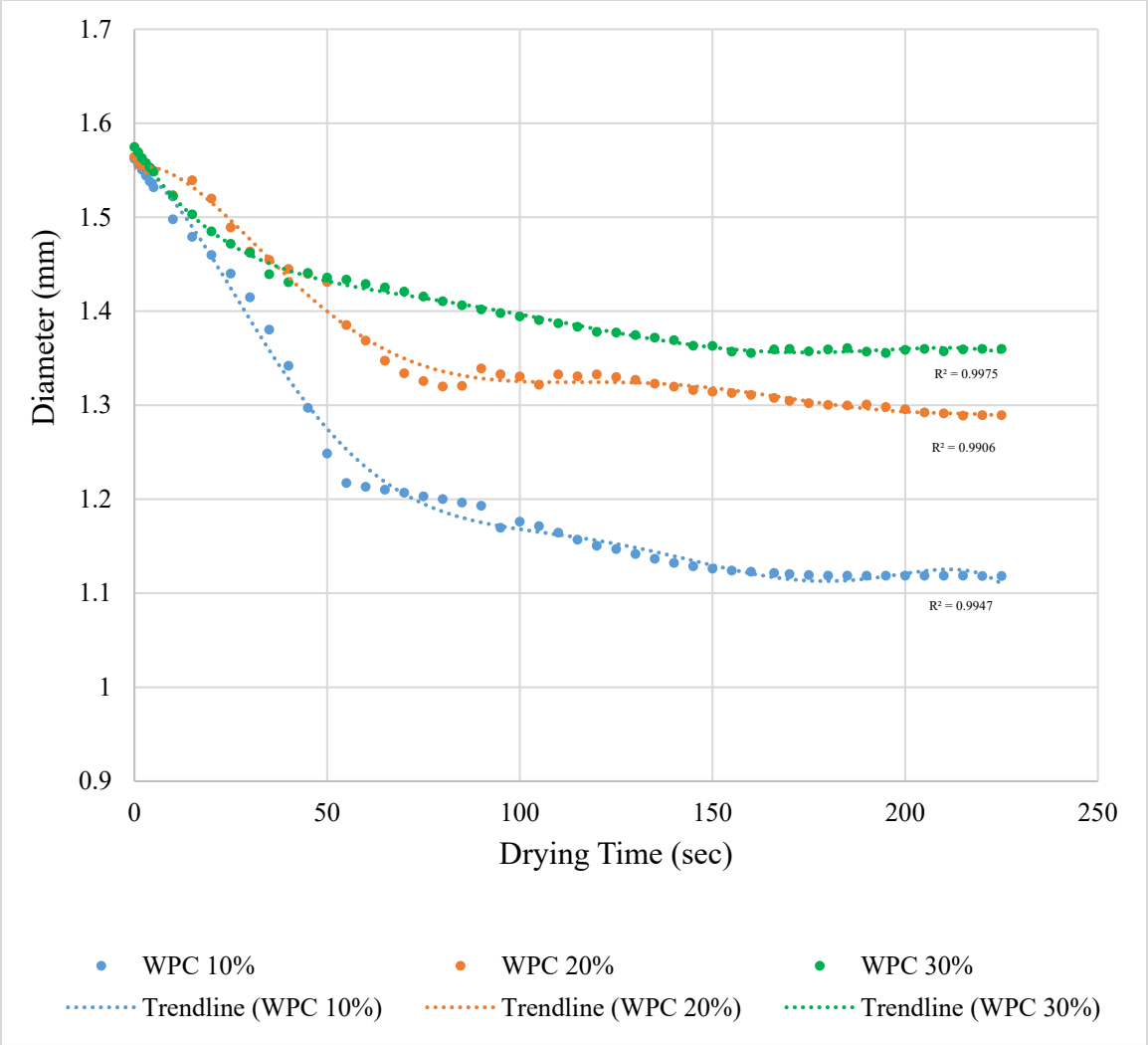

Figure. 10. Effect of total solids on the diameter change for 2 µL WPC80 droplet at 10%, 20%, and 30% total solids level at 90° C with an air velocity of 0.8 m/s.

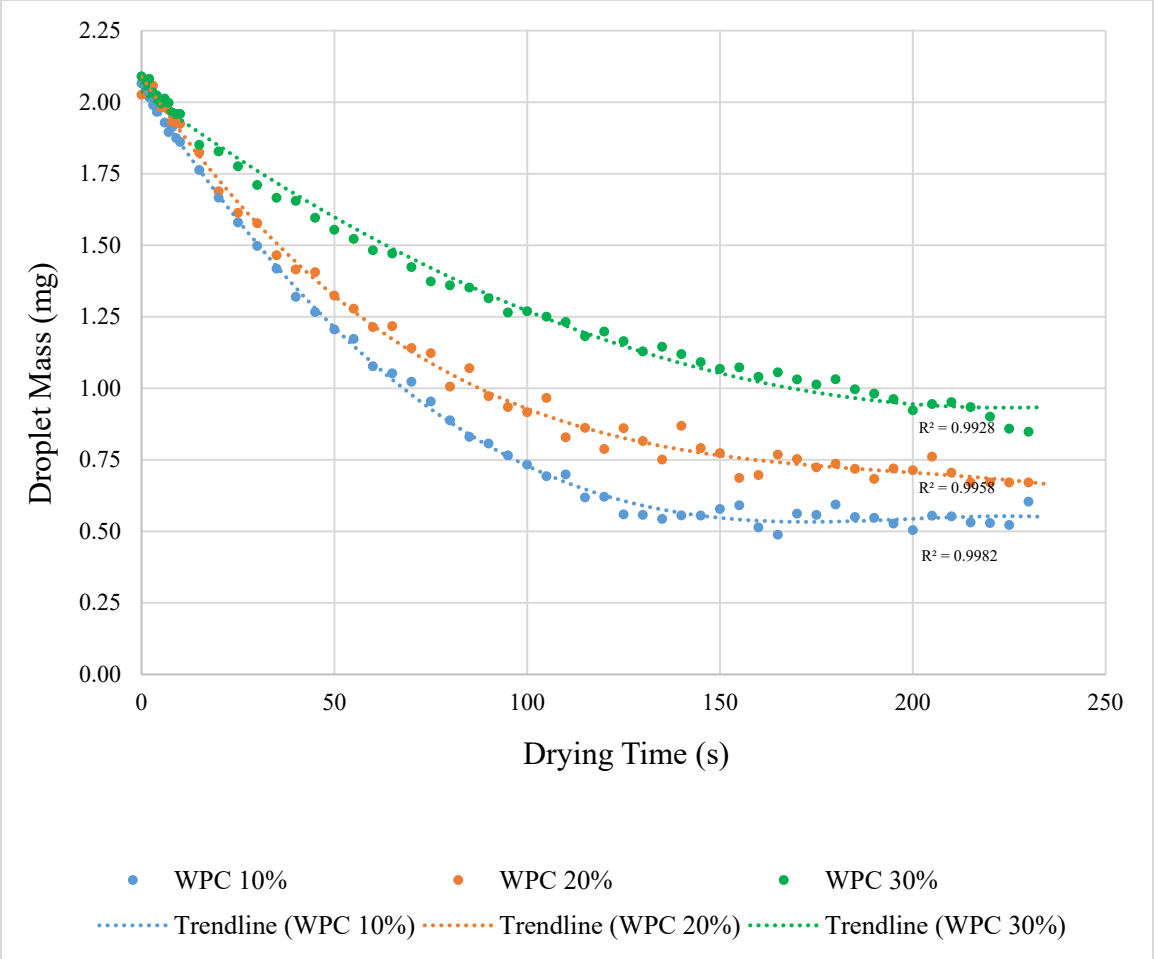

Figure 11. Experimentally obtained droplet mass change (mg) vs. Drying time (s) for 2 µL WPC80 droplet at 10%, 20%, and 30% total solids level at 90° C with an air velocity of 0.8 m/s.

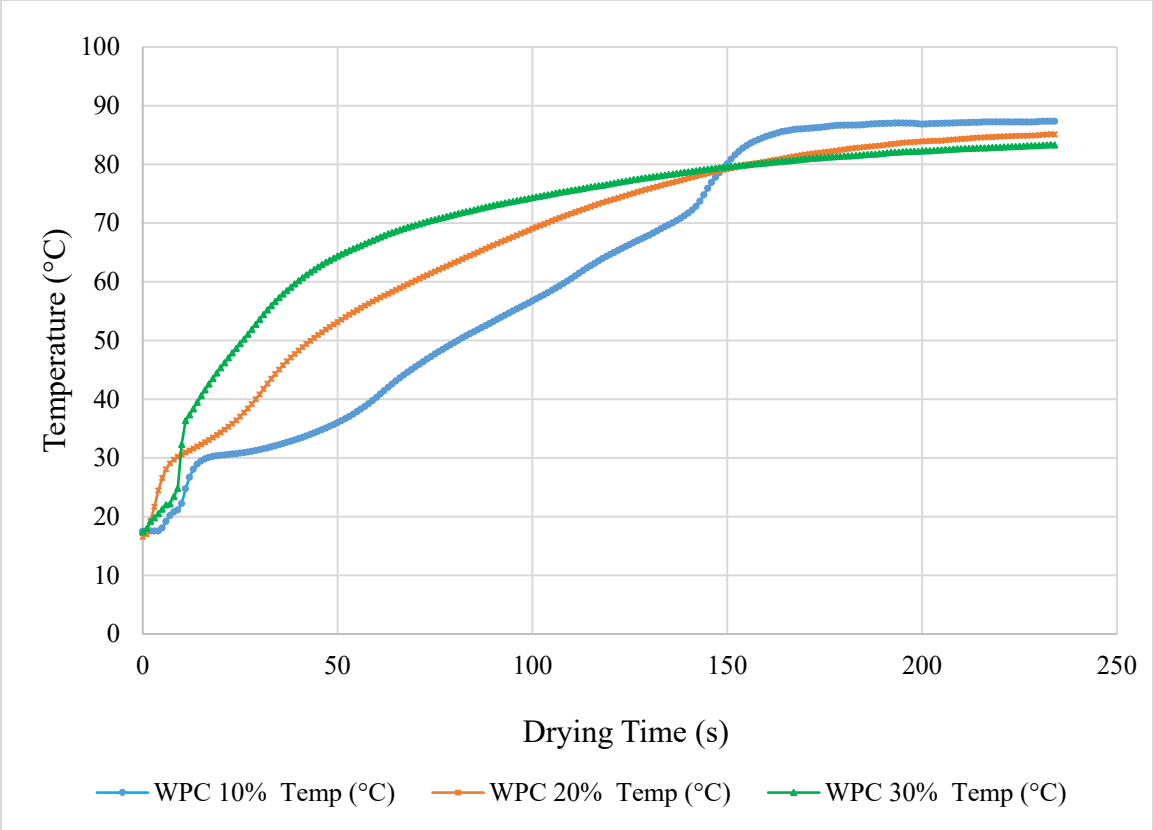

Figure 12. Droplet temperature profile (°C) vs Drying time (s) of WPC80 at three different total solids level viz. 10%, 20%, and 30% total solids level at 90° C with an air velocity of 0.8 m/s.

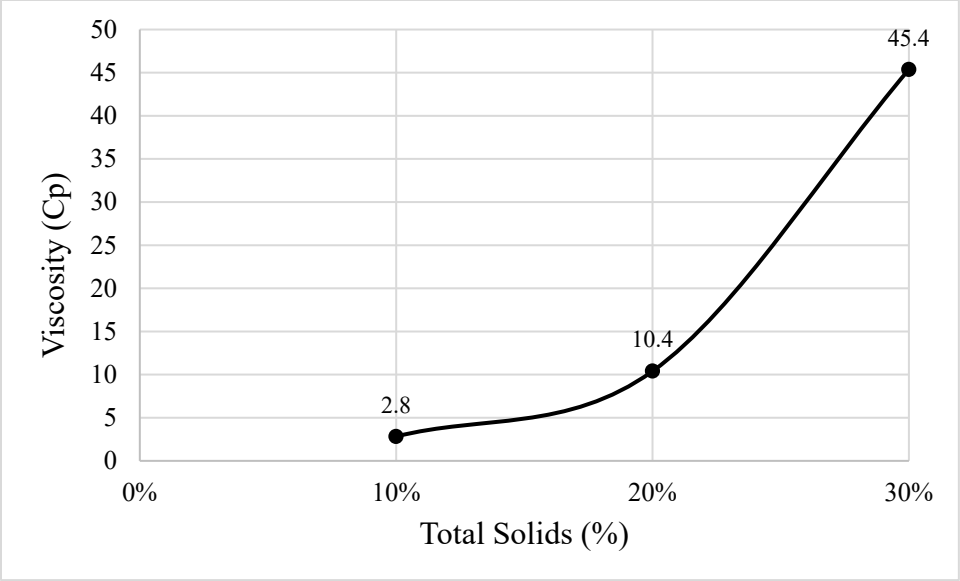

Figure 13. Graph of Viscosity (Cp) vs. Total solids (%) for WPC80 solution standardized at 10%, 20%, and 30% total solids level.

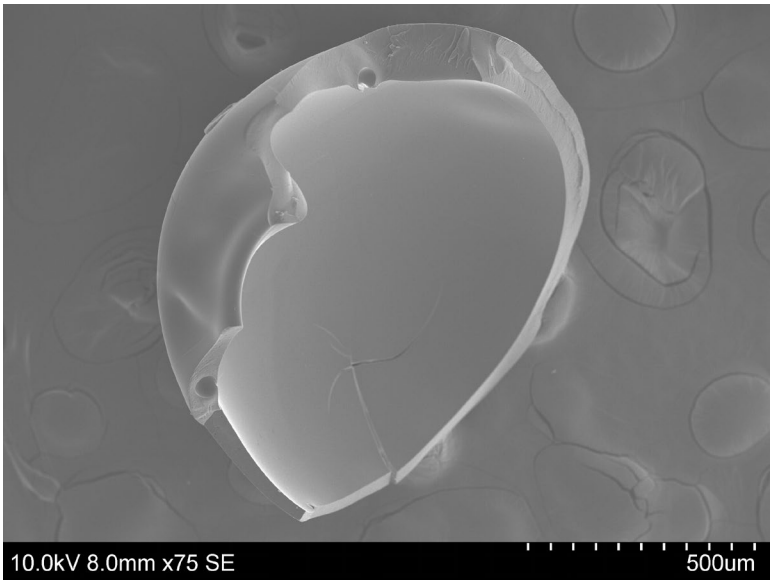

a. Particle of 10% WPC80 dried on SDD

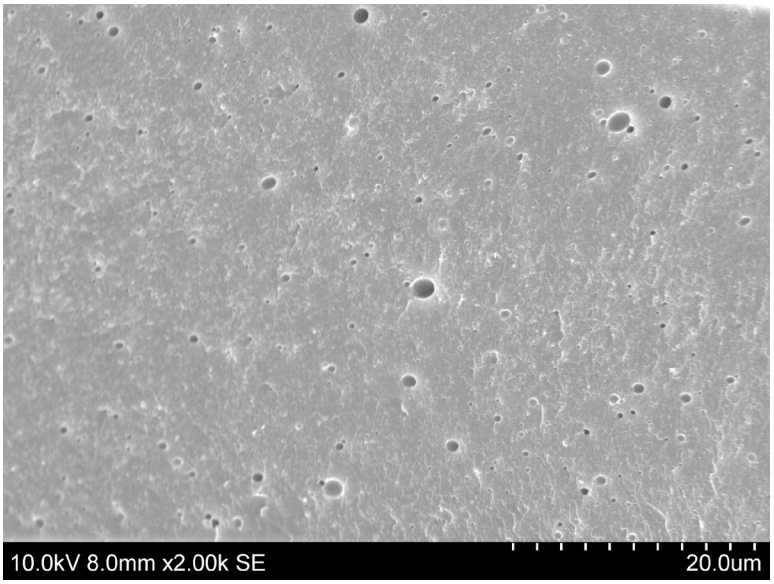

b. Cross-section of 10% WPC80 dried on SDD

Figure 14. Scanning Electron Microscopy images of WPC80 particles at 10% total solids dried at 90°C with drying air velocity of 0.8 m/s.

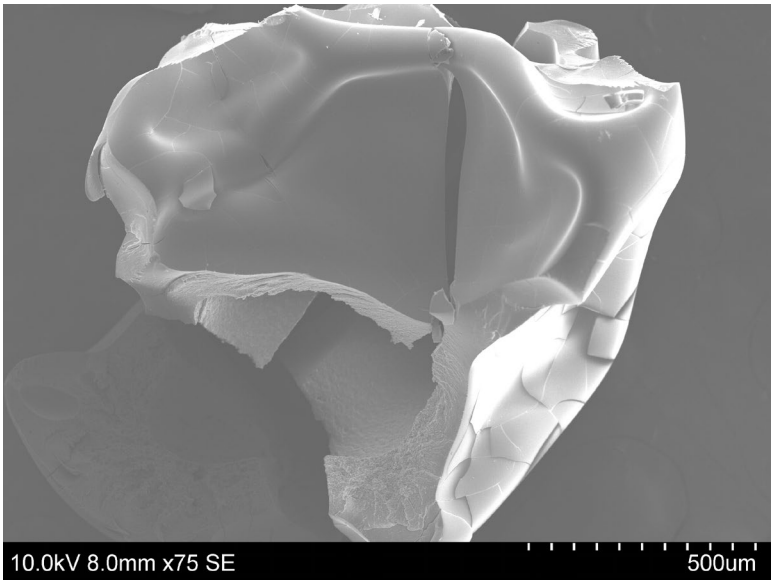

a. Particle of 20% WPC80 dried on SDD

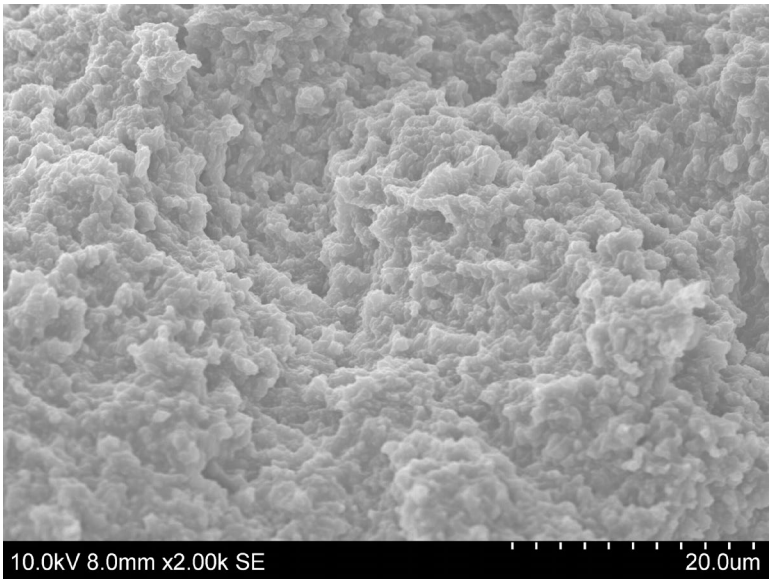

b. Cross-section of 20% WPC80 dried on SDD

Figure 15. Scanning Electron Microscopy images of WPC80 particles at 20% total solids dried at 90°C with drying air velocity of 0.8 m/s.

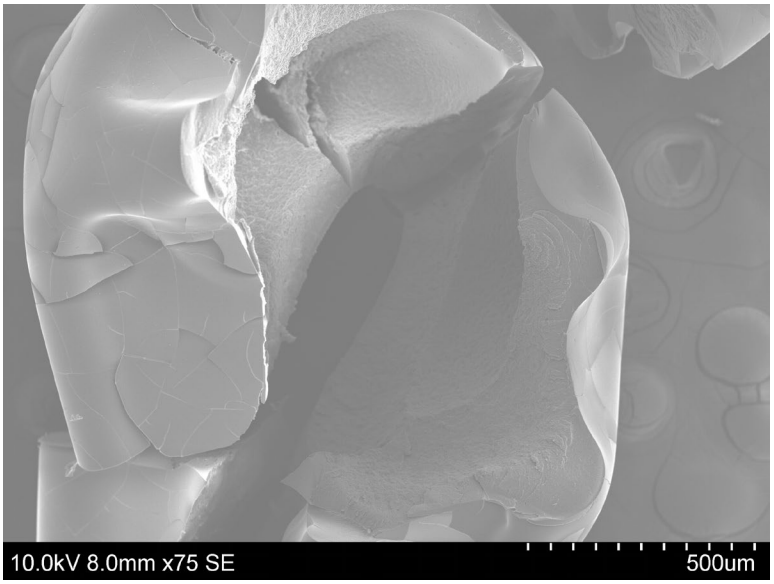

a. Particle of 30% WPC80 dried on SDD

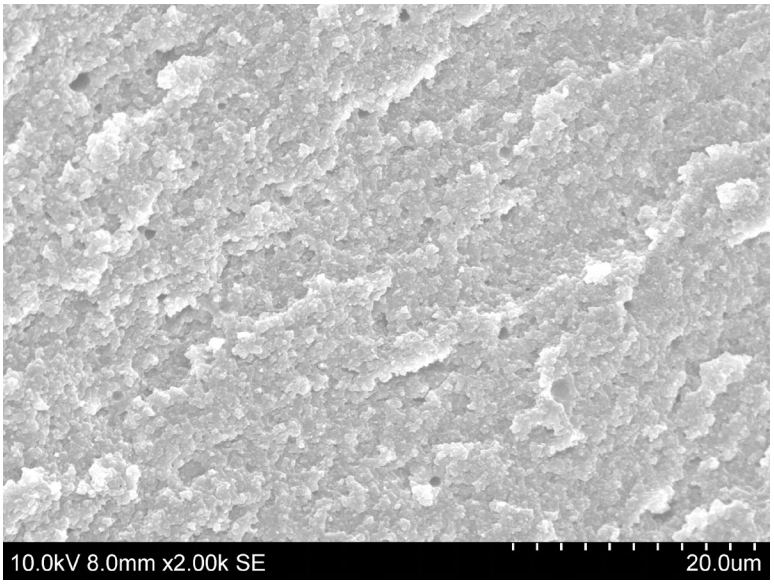

b. Cross-section of 30% WPC80 dried on SDD

Figure 16. Scanning Electron Microscopy images of WPC80 particles at 30% total solids dried at 90°C with drying air velocity of 0.8 m/s.

Table 1. Composition of WPC80 standardized to three different total solids content.

WPC80	Total Solids (%)	SEM	Fat (%)	SEM	Protein (%)	SEM
10	9.67	0.44	0.26	0.01	8.22	0.05
20	19.78	0.11	0.38	0.03	16.53	0.04
30	30.01	0.05	0.42	0.01	24.71	0.12

(All values are average values of three replicates obtained from three different trials.)

Table 2. Showing average viscosity values (Cp) of WPC80 at a three different solids' concentration.

Total Solids	Viscosity (Cp)	SEM
10%	2.8[a]	0.04
20%	10.4[b]	0.15
30%	45.4[c]	0.70

Cp = Centipoise

[a,b,c] Means within the same column not sharing a common superscript are significantly different ($P<0.01$).

(All values are average values of three replicates obtained from three different trials.)

Table 3. Average bulk density and particle size values of WPC80 dried in a pilot-scale spray dryer and particle size of a droplet (2μL) at the end of SDD diameter run.

			Actual Mean Particle Sizes (μm)		Calculated Values (μm) from (B)
Total Solids (%)	Loose Bulk Density (g/ml)	Packed Bulk Density (g/ml)	Pilot-scale Spray Dryer (A) (0.5 – 0.7 μL droplet)	Single Droplet Dryer (B) (2 μL droplet)	Single Droplet Dryer (C) (Converted to 0.5 – 0.7 μL droplet)
10%	0.74	1.32	36.57	1103.5	33.12
20%	0.77	1.33	41.27	1312.3	39.37
30%	0.86	1.34	44.56	1407.0	42.21

(All values are average values of three replicates obtained from three different trials. For each parameter, the calculated value of SEM is < 2%)

CHAPTER 3

EVALUATION OF THE DRYING KINETICS OF MICELLAR CASEIN CONCENTRATE AND MINERAL REDUCED MICELLAR CASEIN CONCENTRATE (REDUCED MINERAL) AT DIFFERENT SOLIDS CONCENTRATIONS

INTRODUCTION

Due to the heterogeneity of milk proteins, it is possible to separate milk proteins. The level of whey protein in MPC can be reduced using microfiltration (MF) to produce MCC. MCC is obtained from MF / DF of skim milk, which removes the whey protein from skim milk and produces MPC that had a reduced level of whey protein (Pouliot et al., 1996; Kelly et al., 2000; Nelson and Barbano, 2005; Metzger et al., 2012) and altered casein-to total nitrogen ratio. The utilization of MF to produce MPC with a higher ratio of casein to whey protein than is present in normal milk had been performed on a variety of membrane systems, including ceramic and spiral wound systems using various processing temperatures ranging from 7 to 50°C. The level of DF and other processing parameters affect the portioning of constituents such as casein, whey protein, minerals, and lactose. From a product and technological point of view, the caseins are the most important and valuable component of milk (de Kruif et al., 2012). The membrane filtration techniques cause selective fractionation and concentrate the casein micelle maintaining their integrity (micellar and native) and soluble nature. Most of the functional properties of the casein micelle depend on its surface properties rather than its interior makeup (de Kruif, 1999; Dalgleish and Corredig, 2012) and are highly related to their molecular structure (Dickinson and McClements, 1995). Microfiltration (MF) is a

membrane process widely used in the dairy industry to separate casein micelles (CN) and serum proteins (SP). Because of the difference in diameter between SP (0.003-0.010 μm, exist as a soluble protein in skim milk) and CN (0.02-0.40 μm, exist in colloidal micelles), this separation is possible (Walstra et al., 1999). Therefore, a 0.1 μm MF separation of skim milk results in retentate fraction (high-CN) and permeate fraction (high-SP).

Membrane fouling (the membrane pores get hindered by foulant) reduces the efficiency of MF, which decreases flux, processing times, and transmission of SP in permeate (Sachdeva and Bucheim, 1997). Crossflow filtration (the fluid is pumped tangentially across the membrane surface) minimizes and overcomes rapid membrane fouling. Decreasing in the concentration polarization layer and increasing solute particles away from the membrane surface because of shear at the membrane surface led to rising flux in crossflow filtration (Belfort et al., 1994).

A drop in the pressure in a crossflow MF will occur along the length of the membrane on the retentate side in the direction of fluid flow; however, the pressure is relatively constant on the permeate side of the membrane. Due to the relationship between pressure drop and a fluid's velocity through the membrane, the increasing crossflow velocity results in high transmembrane pressure (TMP) at the membrane's inlet and a low TMP at the membrane's outlet. As a result, a decreasing flux tendency over the length of the membrane, causing rapid fouling at the inlet and underutilization of the membrane at the outlet (Hurt and Barbano, 2010).

Ceramic membranes are very resistant to high chemical and physical conditions and can endure pH range from 0.5 to 13.5 and temperatures >100°C (Baruah et al., 2006).

The membrane can get cracked if the temperature did not change gradually (<10°C/min). Two varieties of ceramic membranes have been introduced that claim to deliver uniform permeate flux along the length of the membrane without using a permeate recirculation pump (Garcera and Toujas, 2002; Grangeon et al., 2002). The Membralox graded permeability (GP, Pall Corp., Cortland, NY, patented by SCT in 2002) ceramic membrane is designed with a permeability gradient along the exterior surface of the macroporous support structure that increases in mean porosity from inlet to outlet; thereby, GP maintains a constant and uniform flux along with all parts of the membrane. A gradual decrease is provided in hydraulic resistance from inlet to the outlet (Garcera and Toujas, 2002). Papadatos et al. (2003) reported the use of micellar CN concentrate to increase cheese yields or in food ingredients applications, where caseinates are used. More than 60% of the SP from the micellar CN can be removed in a single-stage UTP (Uniform Transmembrane pressure) MF process with a 3x of concentration factor (CF) using 0.1 μm ceramic membranes (Nelson and Barbano, 2005; Zulewska et al., 2009).

Whey proteins are not heat stable, and at 70°C begin denaturation (de Wit and Klarenbeck, 1984), while CN micelles are very heat stable (Holt, 1992). Also, lactose undergoes degradation, including Maillard reactions with proteins that can lead to browning and off-flavors (Walstra et al., 1999). MF uniform transmembrane pressure (UTP) 3x, 3-stage can remove 97% of the SP from pasteurized skim milk, proposed theoretically (Hurt and Barbano, 2010). However, SP removal efficiency considerably varies among different membrane types: 98.3% UTP (Hurt and Barbano, 2010), 96.5% GP (Zulewska et al., 2009), and 70.3% polyvinylidene fluoride spiral-wound (PVDF-SW; Beckman et al., 2010).

MCC production involves unit operations common to US dairy plants. MCC processing involves five basic steps starting with raw milk: cream separation, pasteurization, microfiltration, concentration, and drying. We manufactured MCC by using GP membranes during the production of high solids MCC, with feed and bleed mode in the first 2-stage, 3x GP MF process with diafiltration between stages (DF) and recirculation mode in the 3-stage. Our objective for the first day was to manufacture retentate with 2-stage, 3x, and determine SP removal for each stage in a 2-stage, 3X, feed, and bleed MF system equipped with 0.1 μm GP ceramic membrane when processing pasteurized skim milk at 50°C with one stage of DF. On the second day/ third stage, recirculation mode for retentate has been used to get high solids MCC without adding water (DF) to the retentate from the second stage.

Membrane filtration has been effective at increasing the amount of MCC in a final food product while simultaneously decreasing the amount of lactose in the final food product. However, milk contains many minerals, including but not limited to calcium (Ca), phosphorus (P), potassium (K), magnesium (Mg), sodium (Na), chloride (CI), and other minerals in low concentrations. Therefore, it would be desirable to provide a method and system that cures the deficiencies identified in the manufacture of MCC. In order to change the distribution of minerals and individual proteins between the colloidal and serum phases in milk by altering milk's native environment, including pH, temperature, and/or ionic atmosphere. For example, decreasing milk pH from 6.75 to 6.00 (i.e., acidification) redistributes Ca, P, and casein proteins from the colloidal to the serum phase. The manufacture of modified MMCC utilizes this relationship between pH

and mineral distribution of milk to modify the manufacture of MCC to change its end functionality (Metzger, 2018).

Carbon dioxide injection before and during UF of skim milk significantly affected ash and calcium contents of MPC80; ash content was reduced by 28% and Ca content by 34%. Injection of CO_2 resulted in a 2-fold reduction in the viscosity of the retentate infused with CO_2 compared with control UF retentate. The reduction in viscosity may have a beneficial effect during further concentration of UF retentates before drying. However, a decreased flux rate of ~20% decrease was observed in CO_2 infused retentate compared with the control, primarily due to the solubilization of calcium phosphate. The MPC retentate obtained from the injection of CO_2 retained its solubility when stored at elevated temperature for about 90 days of storage. The results indicated that CO_2 injection could be used to produce MPC80 with reduced calcium and mineral contents and optimal functionality. (Marella et al., 2015). The same was replicated in MMCC by Metzger (2018). A similar principle was used in the manufacture of MMCC here.

The objective of this study was to compare the drying kinetics of Micellar Casein Concentrate (MCC) vs. Modified (CO_2 induced) MCC.

MATERIAL AND METHODS

MCC MANUFACTURE

Experimental Design and Statistical Analysis

One lot of bovine milk (approximately 670 kg) was separated in South Dakota State University dairy plant at 4°C using a model MSE 140-48-177 Airtight cream separator (GEA Co., Oelde, Germany). Raw skim milk was pasteurized at 72°C with a holding time of 16 s in a plate heat exchanger with three sections (regeneration, heating, and cooling: model PR02-SH, AGC Engineering, Bristow, VA). The milk was cooled to 4°C and stored at ≤4°C until processing in the following day. On the first day and before processing, pasteurized skim milk was heated to 50°C with a plate heat exchanger (SABCO Plate-pro Sanitary Chiller (NP925-41)), after that skim milk was microfiltered using a pilot-scale ceramic GP system in constant flux, feed-and-bleed mode to produce a 3× MF retentate and MF permeate continuously (1 kg of retentate : 2 kg of permeate) at 50°C in a feed and bleed mode. The MF retentate was collected and stored. DF has taken place on the same day, and retentate has diluted back to a 3× concentration with soft-water (2 kg of soft-water: 1 kg of retentate) to complete a 3-stage process. It was heated to 50°C with a plate heat exchanger (SABCO Plate-pro Sanitary Chiller (NP925-41)) and filtered with the ceramic GP MF system to produce a 3× retentate. The retentate from the second stage has cooled to≤4°C and stored to the following day. On the second day, the retentate from the first day was microfiltered without DF using a pilot-scale ceramic GP system in a recirculation mode to produce high solids micellar casein concentrate at 62°C by the beginning of the process and 73°C at the end when total solid increased to about 20-22% to minimize denaturation of whey protein early and to increase SP removal. Each

replicate was produced over a 2-day period running on the MF system. This trial was replicated three times using three separate lots of raw milk in different weeks.

Microfiltration Operation

A pilot-scale GP MF system (Tetra Alcross M7, TetraPak Filtration Systems, Aarhus, Denmark) equipped with 0.1-µm pore diameter ceramic Membralox (Model M-7P1940, EP1940GL0.1µA, alumina, Pall Corp., Cortland, NY) membranes (1.68 m^2 surface area and 1.02 m of membrane length), and flow meters were used for permeate. No beads were used to reduce the dead volume on the permeate side of the GP membrane. The membranes had a tubular configuration with 7 tubes, 19 channels each with a 3.3-mm channel diameter, in one stainless steel module that was vertically mounted in the system. The GP MF system consisted only of a feed pump (type LKH 10/110 SSS 1.75 kW) and a retentate recirculation pump (type LKH 20/125 SSS 6.3 kW), all from Alfa Laval (Kansas City, MO). Permeate was removed at the top of the vertical membrane module with back pressure applied. Because of the elevation difference (1.02 m) and weight of the column of liquid, 13.79 kPa bar was added to the permeate pressure at the upper end of the membrane for correction to maintain the target conditions (Rp_i 400, Rp_o 200, and 200 kPa for Pp_o) on the first-day processing. On the second day, the process was started with these conditions, but Pp_o was decreased because of decreasing SP in retentate during recirculation until reaching almost 0 kPa. The permeate removal rate set is 120 L/h and 60 L/h for the retentate removal rate on the first and second day of the process.

Cleaning after production and before new processing

The MF system was cleaned before processing each day. After processing, the milk in the system has been collected. The GP MF system was flushed with soft water to remove any milk inside the membrane. Before washing the system with Alkaline, the clean soft-water flux was determined at 27°C (about 60 kg). The following conditions were applied during the flux measurement: the retentate outlet valve was closed, and the permeate outlet valve was fully open with only the feed pump running. The MF flow system was heated with soft-water to 74°C, then Ultrasil 110 (Ecolab Inc. 370 Wabasha Street N., St Paul, MN) liquid Alkaline membrane cleaner (900 ml) and XY 12 (200 ml; Ecolab Inc. 370 Wabasha Street N., St Paul, MN) was added to the soft-water (about 30 kg soft-water) to reach pH 11. The Alkaline solution was recirculated for 30 min at a permeate removal rate of approximately 350 L/h, and the retentate removal rate of approximately 160 to 180 L/h, with all pumps running. The membrane system was slowly (<10°C per min) cooled to 50°C after cleaning with the tubular heat exchanger in the recirculation loop. The MF system was then flushed with soft water until the pH was neutral. The system has been flushed with soft water to determine the flux again, as described. For washing with acid, the membrane was heated with soft-water to 52°C (30 kg soft-water), then Ultrasil 78 (Ecolab Inc. 370 Wabasha Street N., St Paul, MN) liquid acid membrane cleaner (400 ml) was added to the soft-water (about 30 kg soft-water) to reach pH 2. The acid solution was recirculated for 20 min at a permeate removal rate of approximately 350 L/h with all pumps running. The permeate and retentate outlet valves were closed, and the pumps turned off, and then the nitric acid solution has stored in the membrane for the following day of processing. The holding solution (Ultrasil 78, solution

of nitric acid) was flushed out of the system with soft water at room temperature until the pH was neutral. The flux has been determined one more time after flushing the system from acid at 80°C.

First Stage: Day 1

Before the first day, raw whole milk (approximately 670 kg) was separated at 4 °C and pasteurized in a heat plate exchanger as described 72°C/16 sec, then pasteurized skim milk store at ≤4°C until processing. On the first day of processing, after flushing acid out of the system and rinsing with water, the flux has measured with soft-water, and the system started on the water at 50°C. There was a transition from water to milk with feed and recirculation pumps running. Skim milk was heated to 50°C before processing with a heat plate exchanger. About 670 kg of skim milk was processed to approximately a 3X CF (2 kg of permeate removed from 3 kg of skim milk in a feed and bleed mode) at 50°C using GP ceramic membrane. At the beginning of the process, the water at 50°C has flushed with skim milk about 35 and 13 kg for permeate and retentate respectively, were collected and discarded after recording the weights. The removal rates were 120 L/H (70.58 L/M2/H flux) for permeate and 60 L/H for the retentate. After this start-up, retentate and permeate were collected continuously after recording their weights. The typical pressures (Rpi 400, Rpo 200, and Ppo 200 kPa), temperature (50°C), and flow rates (120 L/h permeate and 60 L/h retentate; collecting permeate and retentate in 15 S to calculate CF) were recorded every 20 min during the processing run duration. To monitor the composition of the retentate and permeate during the MF process, samples of permeate and the retentate were taken for analysis by infrared spectrophotometer (Lactoscope FTIR, Delta Instruments). At the end of the MF run, the collected samples of

retentate and permeate taken each at 20 min were mixed separately and sampled for analysis. The mean time of processing in the first stage was 229 min. After processing, the GP membrane system was cleaned, and flux was measured using the same procedure described above.

Second Stage: Day 1

The second stage was performed on the first day after cleaning the system from the first stage. The retentate from the first stage was diluted by weight: 2 kg of soft-water for every 1 kg of retentate (200 kg of retentate and 400 kg of soft-water); diafiltration factor (DF) of 3 to be the second-stage feed of the 2-stage process. Retentate and water were mixed, heated to 50°C, and processed with the MF GP system using the same operating conditions as described for the first stage. All retentate was collected, cooled to ≤4°C, mixed, and sampled for each stage. Permeate was weighed and sampled every 20 min before discarding. A composite sample of permeate was used for analysis. The average time of processing in the second stage was 194 min.

Third Stage: Day 2

The third stage of the 3-stage process was in a recirculation mode, not feed and bleed mode described for the first and second stage, with the feed being the retentate from the second stage without dilution with water (about 165 kg of retentate). The amount of retentate decreased from stage to stage because of the loss of retentate as the dead volume of the system when ending the previous stage (in the system and holding tank; about 32 kg in stage 1, and 30 in stage 2). The following conditions were applied during the MF: the typical pressures (Rpi 400, Rpo 200, and Ppo 200 kPa), temperature

(63°C), and flow rates (120 L/h permeate and 60 L/h retentate) were recorded every 20 min during the processing. The retentate was recirculated to increase SP removal and increase the total solid in MCC to over 25%. The process was initiated with these conditions, but Pp_o was decreased because of decreasing SP in retentate during recirculation until reaching to almost 0 kPa, and that explained the decreasing the flow rate of permeate to almost 1 L/h. During the process, the solids were monitored with a Brix meter; when the solids increased up to 20%, we increased the process temperature to 74°C. Increasing the temperature at the beginning of the process minimizes separation SP because of the denaturation of whey protein on k-casein. After finishing the third stage process, all retentate (approximately 30 kg) was collected and sampled. Permeate was weighed, sampled, and discarded. A composite sample of permeate was used for analysis. The average time for the third stage was 123 min, and the total time for the whole process on the first and second day was 546 min.

Cleaning after processing

Immediately after processing, the GP membrane system was cleaned using the same procedure described (rinsing, flux, alkaline, rinsing, flux, acid, and holding for the next day processing) before processing in the GP system. During flux determination, the retentate outlet valve was closed, and the permeate outlet valve was fully open with only the feed pump on, and the temperature was maintained at 27°C. After processing milk and flushing the system with 27°C water, the fouled water flux was typically about 35% of the initial clean water flux (94.64 vs. 267.85 kg/m^2 per hour). The post-run clean water fluxes were also close to pre-run clean water flux (i.e., about 287 to 263 L/m^2 per hour).

MMCC MANUFACTURE

The method includes mixing carbon dioxide (CO_2) with at least a portion of the micellar casein concentrate to solubilize one or more components of the micellar casein concentrate. The method includes performing an additional filtration process on the mixture of carbon dioxide and micellar casein concentrate to remove at least a portion of the one or more solubilized components of the micellar casein concentrate to form a modified micellar casein concentrate. The CO_2 supply unit may inject CO_2 into the MCC at a pressure between 10 kPa and 800 kPa to achieve a selected pH range in the MCC between approximately 5.7 and 6.5. More specifically, CO_2 may be injected into flowing MCC in the processing line at a pressure between 30 kPa and 700 kPa (e.g., 0 to 5 L/min). It is noted that decreasing the pH of the MCC via the injection of gaseous CO_2 facilitates the solubilization of one or more minerals in the colloidal phase of the MCC. More specifically, decreasing the pH of the MCC facilitates a transfer of one or more minerals (e.g., micellar calcium phosphate or the like) from a colloidal phase of the MCC to a serum phase of the MCC. The solubilized minerals (e.g., micellar calcium phosphate or the like) in the serum phase of the MCC permeate through the associated ultrafiltration membrane as permeate and leave behind the micellar casein as retentate (Metzger, 2018).

Micellar casein concentrate (MCC) was produced by microfiltration of skim milk in Davis Dairy Plant at SDSU. After microfiltration, the MCC retentate is typically further concentrated by the addition of water and with ultrafiltration and then dried into a powder.

Mineral-reduced micellar casein concentrate (MMCC) was produced by incorporating carbon dioxide (CO_2) during MCC concentration during the ultrafiltration step. Both MCC and MMCC obtained after processing had total solids in the range of 20 – 22%.

Both MCC and MMCC were standardized to two different total solids level viz. 10% and 20% using distilled water at room temperature. The average composition of the standardized MCC and MMCC is mentioned in Table 1.

These standardized solutions were then dried in a Single Droplet Dryer (SDD).

Chemical Analysis

Final Skim milk retentate was analyzed for Fat, Ash, TS, total N (TN), using Mojonnier, furnace (AOAC, 2000; method 945.46; 33.2.10), forced-air oven drying (AOAC, 2000; method 990.20; 33.2.44), Kjeldahl (AOAC, 2000; method 991.20; 33.2.11), respectively. Total protein was calculated by TN and multiplying by 6.38.

Other physico-chemical analysis procedures are the same as those described in Chapter 2.

Single Droplet Drying

All the procedures applied in this study for diameter, temperature, and mass measurements are the same as those mentioned in Chapter 2.

Particle Density

Particle density (g/ml) is defined as the mass of particles having a total volume of 1 ml. Particle density can be calculated from the initial mass measurements from SDD, as the volume of the droplet been dried on SDD is fixed (2 μL).

Scanning Electron Microscopy observation

The particles of MCC and MMCC were dried in SDD at two different levels of total solids viz. 10% and 20% were cracked and mounted on an aluminum stub using conducting carbon tape. Samples were sputter-coated with ~10nm gold (approx. 99%) to produce a conductive surface for Scanning Electron Microscopy observations. Scanning Electron Microscopy images were obtained using a scanning electron microscope (Hitachi S-3400N, Hitachi America Ltd., Tarrytown, NY), located in the Daktronics Engineering Hall, South Dakota State University, which was operated at 10 kV voltage.

RESULTS AND DISCUSSION

Composition of MCC and MMCC

As shown in Table 1, the MCC 10% and MCC 20% had pH values of 6.77 and 6.8, respectively, while MMCC 10% and MMCC 20% had pH values of 5.78 and 5.77, respectively. Due to the addition of CO_2, a ~ 1.0 pH drop was observed in MMCC's. This change was significant ($P < 0.01$). The mineral content of MCC 10% and MCC 20% were observed to be 0.85% and 1.67%, respectively, while for MMCC 10% and MMCC 20%, the mineral content was observed to be 0.73% and 1.43%, respectively. This evidently indicated a significant ($P < 0.01$) decrease in the mineral content by ~ 16 – 17%.

Effect of the total solids content of MCC and MMCC on the drying kinetics

At temperatures above 90°C affect the functional, textural, and nutritive qualities of MCC and MMCC, which also corresponds to the outlet temperature of the commercial spray dryers. Considering the use of this temperature in the previous studies (Chew et al., 2013 and Fu et al., 2011), 90°C temperature was considered for the single droplet drying experiments using the glass filament method. The velocity of drying air was set at 0.8 m/s, and the droplet size used in the experiment was 2µL. The change in diameter followed a similar pattern for all total solids level, i.e., a drop in the initial diameter (falling rate drying period) followed by a linear change for the remaining moisture content during the constant rate drying period. Since the moisture to solid mass ratio is different for different total solids levels, the time required to remove all the internal moisture under the same drying conditions is different. The higher the total solids level

takes longer time for the removal of moisture (Figure 1). The average diameter change showed a significant difference ($P < 0.05$) between MCC and MMCC at both 10% and 20% solid levels. MCC showed a rapid change in average diameter as compared to MMCC. It also concludes that MMCC retains higher moisture as compared to MCC. It can be related to the change in pH and mineral balance (Table 1) of MMCC as compared to MCC and the presence of de-aggregated casein micelle in the MMCC.

Comparison of droplet mass and temperature profiles

Droplet mass change and temperature profiles were experimentally obtained for 2 µL MCC and MMCC droplet at 10%, and 20% total solids level at 90° C with the air velocity of 0.8 m/s as shown in Figure 2. It can be noted from the graph that as the total solids level increases, the drying time increases; this is mainly due to the formation of crust formation on the particle and subsequent slower moisture migration to the surface of the particle with a higher total solids level. A statistically significant difference ($P<0.05$) was observed in the mass and temperature change between MCC and MMCC at both 10% and 20% total solids level. MCC reached the drying temperatures faster as compared to MMCC.

Particle Density

The particle density obtained from mass measurements data, for MCC 10%, MCC 20%, MMCC 10% and MMCC 20% are 1.023 g/ml, 1.043 g/ml, 1.025 g/ml, and, 1.040 g/ml, respectively (Table 2). Although the values obtained for MCC's and MCC's were not significantly different ($P>0.05$), but we can determine the particle density from the data already obtained during the mass measurements.

Viscosity

The values of viscosity obtained for MCC 10% is 5.8 Cp, MCC 20% is 131.16 Cp, MMCC 10% is 4.0 Cp, and MMCC 20% is 45.61 Cp. There is a significant difference ($P<0.01$) in the viscosity values between MCC 10% and MMCC 10% by ~ 35%. The decrease in viscosity observed between MCC 20% and MMC 20% is ~ 65%.

Scanning Electron Microscopy images

The Scanning Electron Microscopy images for MCC and MMCC at 10% total solids level are shown in Figure 4 (a, and c) and their cross-section Figure 4 (b, and d). The images for MCC and MMCC at 20% total solids level are shown in Figure 5 (a, and c) and their cross-section Figure 5 (b, and d).

There was not much difference observed at 10% total solids level, mainly due to the presence of higher moisture available for drying as compared to 20% total solids level. The major difference observed in the morphology of MCC and MMCC particles at 20% levels of total solids was the appearance of the particle in terms of its shape. The MCC particle at 20% total solids level showed a more wrinkled structure. It retained its shape to a greater extent compared to the MCC particle at 20% total solids level, which showed an elongation of the particle and smoother surface due to higher retention of moisture for a more extended period and lower mineral content (Fig. 5). In the cross-sections of the particles, MMCC showed a uniform distribution of air vacuoles compared to MCC, at both 10% and 20% total solids levels.

CONCLUSION

We have observed a significant difference ($P<0.01$) in the diameter change/ moisture removal pattern, mass change, and temperature change between MCC and MMCC. Due to the differences between MCC and Modified MCC in the pH and mineral balance and the presence of the higher amount of de-aggregated casein micelle in the modified MCC. We hypothesize that we will observe differences in the drying properties (like change in moisture removal pattern, mass change of the particle, etc.) of both the materials. Moisture removal was faster in the case of modified MCC as compared to MCC. This is due to the de-aggregation and change in pH from 6.7 to 5.7 (Table 1). The mass change was rapid for Modified MCC as compared to MCC. Modified MCC reached the equilibrium temperature faster as compared to MCC. Hence, our hypothesis stands true. Materials with higher viscosities, higher total protein, and higher total solids can be performed on SDD. Also, differences between the composition of the two materials can be studied on SDD.

REFERENCES

AOAC. 2000. Official Methods of Analysis. 17th ed. AOAC, Gaithersburg, MD.

Baruah, G. L., A. Nayak, and G. Belfort. 2006. Scale-up from laboratory microfiltration to a ceramic pilot plant: Design and performance. J. Membr. Sci. 274:56–63.

Beckman, S. L., J. Zulewska, M. Newbold, and D. M. Barbano. 2010. Production efficiency of micellar casein concentrate using polymeric spiral-wound microfiltration membranes. J. Dairy Sci. 93:4506–4517.

Belfort, G., R. H. Davis, and A. L. Zydney. 1994. The behavior of suspensions and macromolecular solutions in crossflow microfiltration. J. Membr. Sci. 96:1–58.

Chew, J. H., N. Fu, M. W. Woo, K. Patel, C. Selomulya, and X. D. Chen. 2013. Capturing the effect of initial concentrations on the drying kinetics of high solids milk using reaction engineering approach. Dairy Sci. Technol. 93(4-5):415-430.

de Wit, J. N., and G. Klarenbeck. 1984. Effects of various heat treatments on structure and solubility of whey proteins. J. Dairy Sci. 67:2701–2710.

Fu, N., M. W. Woo, S. X. Q. Lin, Z. Zhou, and X. D. Chen. 2011. Reaction Engineering Approach (REA) to model the drying kinetics of droplets with different initial sizes—experiments and analyses. Chem. Eng. Sci. 66(8):1738-1747.

Fu, N., M. W. Woo, F. T. Moo, and X. D. Chen. 2012. Microcrystallization of lactose during droplet drying and its effect on the property of the dried particle. Chem. Eng. Res. Des. 90(1):138-149.

Garcera, D., and E. Toujas, inventors. 2002. Graded permeability macroporous support for crossflow filtration. Societe des Ceramiques Techniques, assignee. US Pat. No. US 6,375,014 B1.

Gosta, B. 2012. Dairy Processing Handbook. Tetrapak Processing Systems AB. Whey Processing. 331-352.

Grangeon, V., P. Lescoche, T. Fleischmann, and B. Ruschel, inventors. 2002. Crossflow filter membrane and method to manufacture it. Technologies Avancees & Membranes Industrialles (Societe Anonyme), assignee. US Pat. No. 6,499,606 B1.

Holt, C. 1992. Structure and stability of bovine casein micelles. Adv. Protein Chem. 43:63–151.

Hurt, E., J. Zulewska, M. Newbold, and D. M. Barbano. 2010. Micellar casein concentrate production with a 3X, 3-stage UTP ceramic membrane process at 50°C. J. Dairy Sci. 93:5588–5600.

Hurt, E., and D. M. Barbano. 2010. Processing factors that influence casein and serum protein separation by microfiltration. J. Dairy Sci. 93:4928–4941.

Kaylegian, K. E., G. E. Houghton, J. M. Lynch, J. R. Fleming, and D. M. Barbano. 2006. Calibration of infrared milk analyzers: Modified milk versus producer milk. J. Dairy Sci. 89:2817–2832.

Kim, E. H.-J., X. D. Chen, and D. Pearce. 2003. On the mechanisms of surface formation and the surface compositions of industrial milk powders. Drying Technol. 21(2):265-278.

Lin, S. X. Q. and X. D. Chen. 2007. The reaction engineering approach to modelling the cream and whey protein concentrate droplet drying. Chem. Eng. Process. 46(5):437-443.

Marella, C., P. Salunke, A. C. Biswas, A. Kommineni, and L. E. Metzger. 2015. Manufacture of modified milk protein concentrate utilizing injection of carbon dioxide. J. Dairy Sci. 98:3577–3589.

Metzger, L. E. 2018. Method and System for Manufacturing Mineral-Reduced Micellar Casein Concentrate. Patent Publication number: 20180343880.

Nelson, B. K., and D. M. Barbano. 2005. A microfiltration process to maximize removal of serum protein from skim milk before cheese making. J. Dairy Sci. 88:1891–1900.

Papadatos, A., M. Neocleous, A. M. Berger, and D. M. Barbano. 2003. Economic feasibility of microfiltration of milk prior to cheesemaking. J. Dairy Sci. 86:1564–1577.

Sachdeva, S., and W. Buchheim. 1997. Separation of native casein and whey proteins during crossflow microfiltration of skim milk. Aust. J. Dairy Technol. 52:92–97.

Vora, H. N, and Metzger, L. E. Evaluation of the Drying Kinetics of Micellar Casein Concentrate and Reduced-mineral Micellar Casein Concentrate at Different Solids Concentrations., 2018, Dairy Science Publication Database.

Walstra, P., T. J. Geurts, A. Noomen, A. Jallema, and M. A. J. S. van Boekel. 1999. Dairy Technology: Principles of Milk Properties and Processes. Marcel Dekker Inc., New York, NY.

Zulewska, J., M. Newbold, and D. M. Barbano. 2009. Efficiency of serum protein removal from skim milk with ceramic and polymeric membranes at 50°C. J. Dairy Sci. 92:1361–1377.

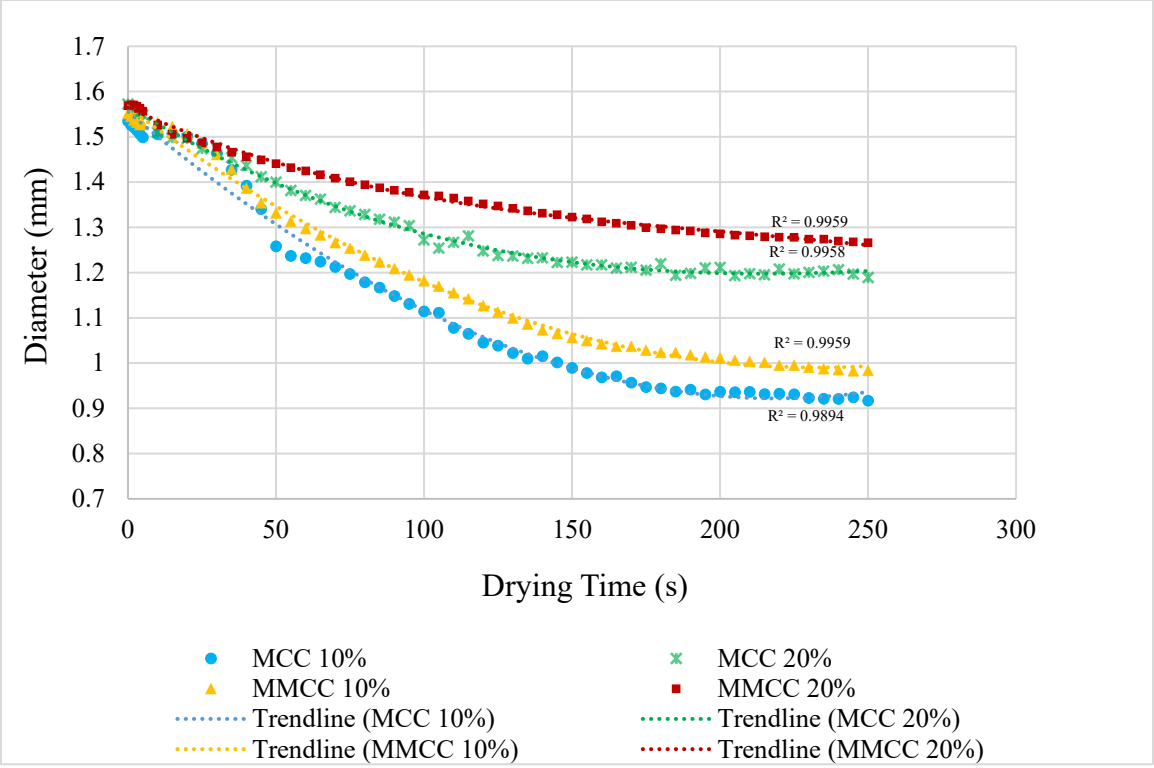

Figure 1. Effect of total solids on the diameter change of MCC and MMCC at two different total solids level.

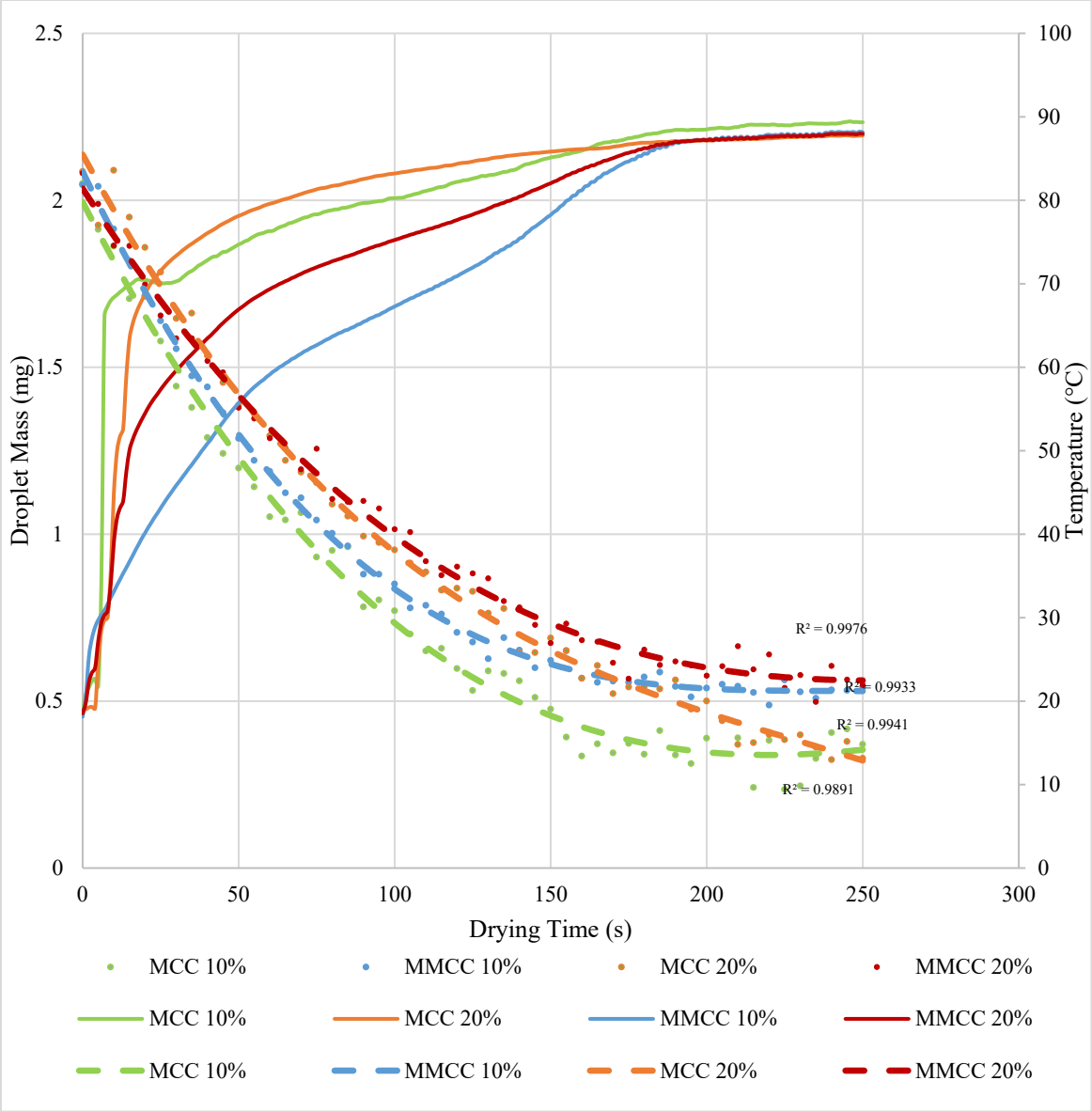

Figure 2. Experimentally obtained droplet mass and temperature profile for 2 µL WPC80 droplet at 10%, and 20% total solids level at 90° C with the air velocity of 0.8 m/s.

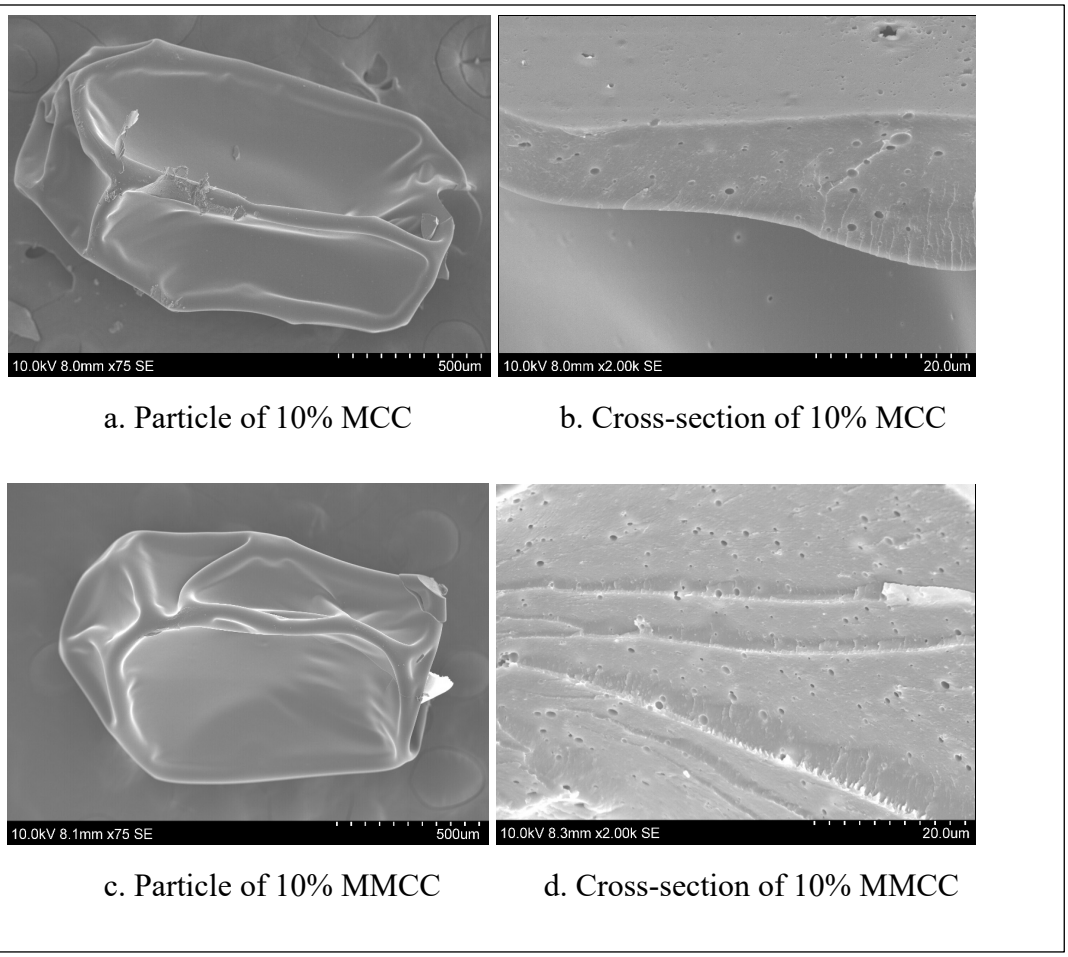

Figure 3. Scanning electron microscopy images of MCC and MMCC particles at 10% total solids level dried at 90°C with drying air velocity of 0.8 m/s.

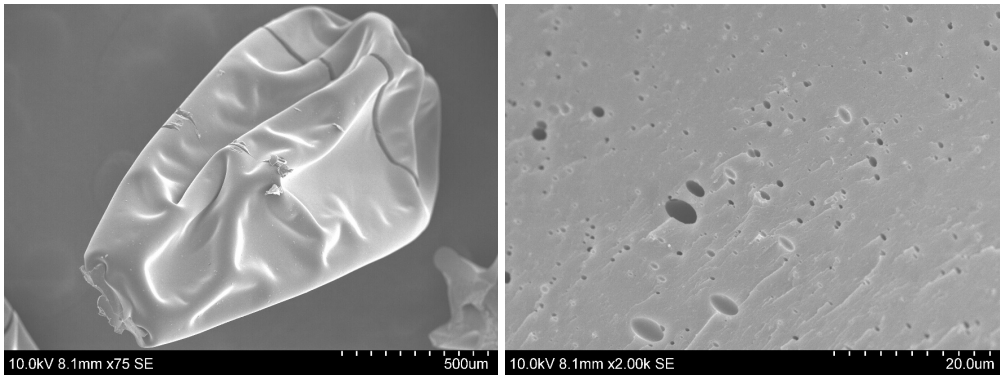

a. Particle of 20% MCC b. Cross-section of 20% MCC

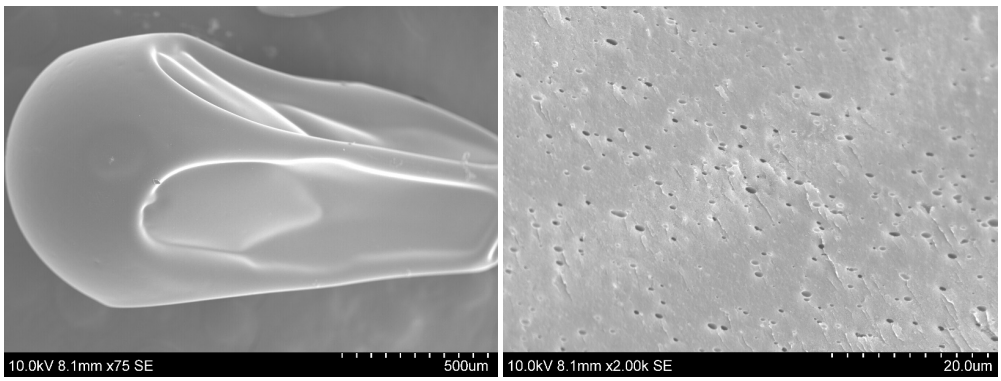

c. Particle of 20% MMCC d. Cross-section of 20% MMCC

Figure 4. Scanning electron microscopy images of MCC and MMCC particles at 20% total solids level dried at 90°C with drying air velocity of 0.8 m/s.

Table 1. The composition of MCC and MMCC standardized to two different total solids content.

Parameters	**MCC 10 %**	**MCC 20 %**	**MMCC 10 %**	**MMCC 20 %**
pH	6.77	6.80	5.78	5.77
Total Solids (%)	10.38	20.30	10.17	20.09
Protein (%)	8.43	16.51	8.11	15.59
Fat (%)	0.28	0.55	0.25	0.45
Minerals (%)	0.85	1.67	0.73	1.43

(All values are average values of three replicates obtained from three different trials. For each parameter, the calculated value of SEM is < 2%)

Table 2. The Particle density of MCC and MMCC standardized at two different solid levels obtained from SDD.

Product	**Particle density (g/ml)**
MCC 10 %	1.023
MCC 20 %	1.043
MMCC 10 %	1.025
MMCC 20 %	1.040

(All values are average values of three replicates obtained from three different trials. For each product, the calculated value of SEM is < 2%)

Table 3. The viscosity of MCC and MMCC standardized at two different solid levels.

Product	**Viscosity (Cp)**
MCC 10 %	5.80[b]
MCC 20 %	131.16[d]
MMCC 10 %	4.00[a]
MMCC 20 %	45.61[c]

Cp = Centipoise

[a,b,c,d] Means within the same column not sharing a common superscript are significantly different ($P<0.01$).

(All values are average values of three replicates obtained from three different trials. For each product, the calculated value of SEM is < 2%)

CHAPTER 4

DISSOLUTION BEHAVIOR OF INFANT FORMULA AND ITS EFFECT ON THE PROPERTIES OF DRIED PARTICLE

INTRODUCTION

Spray drying is the most frequently used technique for the dehydration of dairy products. It is an effective method for preserving biological products as it does not involve severe heat treatment and allows the storage of powders at ambient temperature. Due to the variety and complexity of the concentrates to be dried, a more rigorous understanding of spray drying based on physico-chemical and thermodynamic properties has now become necessary. The only way to determine these parameters is to perform several complicated and expensive experiments with spray dryer pilots (Schuck et al., 2009). Spray drying of mannitol at different outlet temperatures studied to modifying particle surface topography, which, for example, may be useful for tailoring interparticle interactions between the drug and the carrier in interactive mixtures of dry powder (Mass et al., 2011). Dairy powders rehydration: mixing equipment design, operating conditions (stirring, temperature), and chemical composition of powder are the significant parameters that affect the reconstitution process (Richard et al., 2013). It was concluded by Wu et al. (2014) that due to the higher feed solids content (53.5% vs. 32.6%) facilitated the crust formation during the single-stream drying process and subsequently maintained the spherical shape. The shrinkage degree decreased with higher feed solids content. The sample obtained from higher feed solids content had better wettability, possibly due to the larger particle size and more lactose content on the surface. However,

also, lower solubility likely resulted from faster crust formation that may expose surface protein to denaturation upon drying (Wu et al., 2014).

We hypothesize that we will observe better rehydration/ higher solubility of the powder particle of Infant Milk formula dried at 70°C temperature than those dried at 110°C.

- This is predicting that the outlet temperatures of the dryer have some effect on the rehydration properties of dried powder. Since the rehydration properties of the powder are one of the very important criteria for infant milk formula, it would be interesting to study the dissolution behavior.
- Due to higher temperatures of drying, there will be a faster formation of crust on the surface of the particle, which may lead to slower rehydration or absorption of the attached water droplet to the dried particle in the case of 110°C followed by 70°C.

Since there may be fat in the material, which tends to rise to the surface of the dried particle may also impact the rehydration time. Hence, we may observe that there may be incomplete rehydration of the particle for some of the temperatures of drying used in the study.

MATERIAL AND METHODS

Materials

The infant formula used in the study is Similac Pro-Advance™ Infant Formula with Iron. It was procured from a local Walmart store in Brookings, South Dakota.

The following were the ingredients in the formula as listed on the package.

Nonfat Milk, Lactose, Whey Protein Concentrate, High Oleic Safflower Oil, Soy Oil, Coconut Oil. Less than 2% of C. Cohnii Oil, M. Alpina Oil, 2'-Fucosyllactose, Fructooligosaccharides, Beta-Carotene, Lutein, Lycopene, Potassium Citrate, Calcium Carbonate, Ascorbic Acid, Soy Lecithin, Potassium Chloride, Magnesium Chloride, Ferrous Sulfate, Choline Bitartrate, Choline Chloride, Ascorbyl Palmitate, Salt, Taurine, m-Inositol, Zinc Sulfate, Mixed Tocopherols, d-Alpha-Tocopheryl Acetate, Niacinamide, Calcium Pantothenate, L-Carnitine, Vitamin A Palmitate, Copper Sulfate, Thiamine Chloride Hydrochloride, Riboflavin, Pyridoxine Hydrochloride, Folic Acid, Manganese Sulfate, Phylloquinone, Biotin, Sodium Selenate, Vitamin D3, Vitamin B12, Calcium Phosphate, Potassium Phosphate, Potassium Hydroxide, and Nucleotides (Adenosine 5'-Monophosphate, Cytidine 5'-Monophosphate, Disodium Guanosine 5'- Monophosphate, Disodium Uridine 5'-Monophosphate).

The nutritional information of this infant formula is as listed in Table 1 was obtained from the website (see references) listed on the package.

The infant formula is standardized to three different total solids level viz. 15%, 40%, and 50%. 15% total solids were considered for the study as the reconstituted formula was around that total solids level, while 40% and 50% were considered for the study as the normal spray drying operations utilize total solids post evaporation in the range of 40 - 50%.

The temperatures of 70°C and 110°C were considered for drying as these are the minimum and maximum outlet temperatures observed in the spray drying operations in the past studies (Fu et al., 2012).

All methods used in this Chapter are described in Chapter 2. Apart from that, additional methods are listed below.

Dissolution/ Rehydration Experiments

The dissolution experiment employed the same experimental set-up as a diameter measurement for droplet drying (Fu, 2012). The generated single droplet was dried until no more morphological changes were observed, usually for 150-300 s. The drying was then discontinued by inserting the bypass barrier plate into the drying chamber to divert the hot air flow away from the drying chamber. The dissolution of the dried single particle was started by attaching a drop of water (solvent) to the single dried particle. The single water droplet (2 μL) was generated using the micro-syringe; the generation and the transfer procedure followed the same as described in Chapter 2. The camcorder continuously recorded the morphological changes during both drying and dissolution/rehydration. During dissolution experiments, a moisture pad soaked with the water was positioned on the bypass barrier plate below the suspended dry particle to increase the relative humidity of the drying chamber. The moisture evaporation from this moisture pad reduced the temperature of the drying chamber. As a result, this moisture pad could minimize any undesired evaporation from the dry particle with the attached solvent droplet.

Monitoring of droplet morphological changes during the drying process (Infant formula only).

For the visual observation of the droplet morphological changes during drying, the video recorded the drying process was processed with the Adobe After Effects 7.0 to extract the images at one frame per second. Time 0 of each drying process was identified first, and then the drying process was illustrated by a sequence of snapshots corresponding to the time of the drying. The contrast and brightness of each image were adjusted using Adobe Photoshop 21.2.3 (Adobe Creative Cloud 5.2.1.441, @ 2020 Adobe Incorporated, US) to improve the clarity.

Observation of the particle surface formation during drying

The above-described principle of dissolution experiments could also be applied to the semi-dried particles. Spray-dried infant milk powders sometimes had a different surface composition to the bulk composition, and the formation mechanism of this phenomenon was still unclear. Besides, milk is a well-known shell-forming material (Hassan and Mumford, 1993; Walton and Mumford, 1999). It would thus be valuable to understand the composition of the formed shell when the particle is still being dried, to determine an approximate time of occurrence of the material segregation, whether it was at the early stage of drying, later stage of drying, or even post-drying process. As part of efforts to answer this question, the current research attempted to investigate the dissolution/ rehydration properties of the formed surface shell as drying progressed. Each set of drying and dissolution experiment was repeated under identical conditions. The drying was stopped at successively longer drying time frame, i.e., 30 s, 60 s, 90 s, 120 s,

and so on. Therefore, each dissolution experiment corresponded to one separate drying process; particles obtained in the repeated drying process were considered nearly identical due to the same conditions used. By this approach, the dissolution behavior of the outer layer of the semi-dried milk particles formed throughout the entire drying process could be investigated, which provided a clear profile of the dissolution properties of the milk droplet surface at different drying stages. All dissolution experiments in the current research were carried out repeatedly to ensure the reproducibility of the observation. In situ analysis of infant milk, shell development was repeated with different drying conditions viz - 70°C and 110°C. The errors in the timing to stop the drying process were ± 3 s. Since the minimal time interval for analyzing the wetting and dissolution behavior was 15 s, the transition time of surface shell property only represented the drying time frame used in the current research.

RESULTS AND DISCUSSION

Comparison of droplet diameter measurement profiles

The outlet temperature of the air, leaving the drying tower is used for control and provides a measure of the severity and rate of drying in a commercial spray dryer (Mermelstein, 2001). Considering this temperature in the previous studies (Fu, 2012), 70°C and 110°C temperatures were considered minimum and maximum outlet temperatures for the single droplet drying experiments using the glass filament method. The drying air velocity set at 0.8 m/s and the droplet size used in the experiment was 2µL. The change in diameter followed a similar pattern for all three total solids levels at each temperature, i.e., a drop in the initial diameter (falling rate drying period) followed

by a linear change for the remaining moisture content during the constant rate drying period. Since the moisture to solid mass ratio is different for different total solids levels, the time required to remove all the internal moisture under the same drying conditions is different. The higher the total solids level, it takes longer time for the removal of moisture (Figure 1). It is also affected by the viscosity of the Infant formula at different solids levels.

The value of the coefficient of determination (R^2) for 15%, 40%, and 50% total solids level at 70°C was 1.00, 1.00, and 1.00, respectively. There was a significant difference ($P < 0.01$) in the diameter change between all three solids levels at 70°C.

The value of the coefficient of determination for 15%, 40%, and 50% total solids level at 110°C was 1.00, 0.99, and 0.99, respectively. There was a significant difference ($P < 0.01$) in the diameter change between all three solids at 110°C.

There was a significant difference ($P<0.01$) between the change in diameter for 15% total solids level at 70°C and 110°C. Similarly, a significant difference ($P<0.01$) in the diameter change at 40% and 50% total solids level between 70°C and 110°C was noted. The temperature has a significant ($P<0.01$) impact on the diameter change of the particle.

Comparison of droplet mass measurement profiles

The droplet mass change and temperature profiles were experimentally obtained for 2 µL Infant Formula droplets at 15%, 40%, 50% total solids level at 70° C, and 110°C with an air velocity of 0.8 m/s as shown in Figure 2. It also can be noted from the graph that as the total solids level increases, the drying time increases. As the temperature

increases from 70° C to 110°C, the drying time decreases significantly ($P<0.01$) due to the faster removal of the moisture.

The value of the coefficient of determination (R^2) for 15%, 40%, and 50% total solids level at 70°C was 1.00, 0.98, and 0.97, respectively. There was a significant difference ($P < 0.01$) in the mass change between all three solids levels at 70°C.

The value of the coefficient of determination for 15%, 40%, and 50% total solids level at 110°C was 0.99, 0.99, and 0.99, respectively. There was a significant difference ($P < 0.01$) in the mass change between all three solids at 110°C.

There was a significant difference ($P<0.01$) between the change in mass for 15%, 40%, and 50% total solids level at 70°C and 110°C temperatures. The temperature has a significant ($P<0.01$) impact on the mass change of the particle.

Comparison of the droplet temperature profiles

A statistically significant difference ($P<0.01$) was observed in the temperature change between 70°C and 110°C at all the three viz. 15%, 40%, and 50% total solids level (Figure 3). Infant formula droplets dried at 110°C reached the drying temperatures significantly ($P<0.01$) faster as compared to the corresponding droplets dried at 70°C.

Viscosity

There was a significant ($P < 0.01$) increase in the viscosity of Infant Formula with an increase in the total solids' concentration from 15% to 40% to 50% (Table 2). The viscosity of Infant Formula with 15% total solids is 2.66 Cp, 40% total solids is 16.33 Cp, and for 50% total solids is 57.39 Cp. It is evident with the fact that as the total solids

increase, the viscosity of the solution also increases (Table 2). As there is an exponential rise in viscosity with change in total solids in the Infant formula solution, it is interesting to observe this phenomenon. Moreover, the viscosity of any dairy solutions directly impacts the properties and functionalities of the finished powder particles.

Dissolution behavior

In this work, an attempt has been made to understand better the mechanisms of hydration, namely the effect of the composition (total solids) and outlet temperatures of the dryer. The digital images of powder during dissolution were obtained using a camera. Digital image analyses were performed to visualize solvent penetration inside powders and to understand better the associated fragmentation mechanisms (Figures 4, 5, 6, 7, 8, and 9). Kinetics of rehydration was shown to be much more sensitive to temperature ($P<0.01$) than to the total solid's concentration in this 3×2 factorial experiment. Rehydration times, solvent (water) penetration mechanisms, and disintegration are discussed about the rehydration conditions of the infant formula.

Drying times

The drying time for each of the total solids viz. 15%, 40%, and 50% of infant milk formula at each temperature viz. 70°C and 110°C are shown in Figure 10. The drying times observed at 70°C for 15% TS is 198 sec, 40% TS is 190 sec, and 50% TS is 170 sec. The drying times observed at 110°C for 15% TS is 120 sec, 40% TS is 114 sec, and 50% TS is 103 sec. The drying times for each total solid at 70°C are significantly ($P<0.01$) different than those at 110°C for corresponding total solid values.

Dissolution/ Rehydration times

Here, the dissolution/ rehydration time is the time taken for a dried particle of the Infant formula to completely dissolve/ rehydrate by 2µL of water attached to the dried particle. The dissolution time for each of the total solids viz. 15%, 40%, and 50% of infant milk formula at each temperature viz. 70°C and 110°C are shown in Figure 11. The dissolution times observed at 70°C for 15% TS is 220 sec, 40% TS is 335 sec, and 50% TS is 360 sec. The dissolution times observed at 110°C for 15% TS is 570 sec, 40% TS is 670 sec, and 50% TS is 690 sec. The dissolution times for each total solid at 70°C are significantly ($P<0.01$) different than those at 110°C for corresponding total solid values.

Dissolution behavior for each solid level at each temperature can be studied, as shown in Figures 4, 5, 6, 7, 8, and 9. A progressive display of drying and dissolution behavior for each particle can be observed in the pictures. The particles dried at outlet temperatures of 70°C showed a better dissolution rate in comparison to the particles dried at 110°C ($P<0.01$).

Although a more porous structure is observed in the scanning electron microscopy images at 110°C vs. 70°C, the crust formed on the particles dried at higher temperatures is difficult to penetrate solvent (water). Hence, 110°C had significantly ($P<0.01$) longer rehydration/ dissolution times in comparison to 70°C.

We must not forget the fact that these are 2µL particles been dried are much larger (almost ten times) in comparison to much smaller particles dried in the commercial spray dryer. Since the particles are much larger, it takes a longer time to rehydration

versus the commercial particles tested for rehydration test (which is normally a few seconds).

Scanning Electron Microscopy images

The significant difference observed in the morphology of Infant formula particles amongst the three different levels of total solids at each temperature (70°C and 110°C) was is the appearance of the porosity and density of the structure (Figures 12 and 13). It is necessary to point out that the use of different dying conditions also influences the morphology of the final dried particle, apart from the different dissolution behavior.

All the droplets at each solid level (15%, 40%, and 50%) dried at 70°C had a compact structure versus all the corresponding droplets dried at 110°C. This is due to faster drying at 110°C; there is a faster formation of crust and hence the formation of a shape/walls/structure of the droplet. Once the droplet structure is formed, there is moisture removal from the inside, retaining a more porous structure at 110°C (Figure 13). While 70°C is a slower drying process with slow and compact and less porous structure is formed and hence the particle appears smaller (Figure 12 a, c, e) in comparison to those dried at 110°C (Figure 13 a, c, e). More entrapped air is seen in the cross-section of particles dried at 110°C (Figure 13 b, d, f) versus those dried at 70°C (Figure 12 b, d, f). No free fat was seen on any of the particles. On close visual observations of the particles with total solids 40% and 50%, dried at 110°C, it was observed that there was not complete dissolution achieved. Single droplet drying provides an excellent means for viewing morphological changes between the particles with different composition/ treatment/ functionalities.

CONCLUSIONS

We have observed a significant difference ($P<0.01$) in the diameter change/ moisture removal pattern, mass change, and temperature change between 70°C and 110°C, two different temperatures of drying at all the solids level viz., 15%, 40%, and 50%. The extended SDD experiments incorporating the dissolution test combined with post-drying instrumental analysis by scanning electron microscopy can help study the particle behavior at every interval of drying and dissolution. Our hypothesis stands true. We observed better rehydration/ higher solubility ($P<0.01$) of the powder particle of Infant Milk formula dried at 70°C temperature compared to those dried at 110°C. This demonstrates that the outlet temperatures of the dryer have some effect on the rehydration properties of dried powder. Hence, the functionality of dairy powders is affected by the outlet temperatures of the dryer. Also, change in total solids for each temperature had a significant ($P<0.01$) effect on the properties of the dried particle. Since the rehydration properties of the powder are very important criteria for infant milk formula, it was interesting to study the dissolution behavior. The dissolution times for each total solid at 70°C are significantly ($P<0.01$) different than those at 110°C for corresponding total solid values. Due to higher temperatures of drying, there was a faster formation of crust on the surface of the particle, which led to slower rehydration or absorption of the attached water droplet to the dried particle in the case of 110°C followed by 70°C. Since there may be fat in the material, which tends to rise to the surface of the dried particle may also impact the rehydration time. Hence, we may observe that there may be incomplete rehydration of the particle for some of the temperatures of drying used in the study.

REFERENCES

Fu, N. 2012. Single Droplet Drying of food and bacterium containing liquids and particle engineering. Thesis submitted to Monash University. 93-97.

Fu, N., M. W. Woo, F. T. Moo, and X. D. Chen. 2012. Microcrystallization of lactose during droplet drying and its effect on the property of the dried particle. Chem. Eng. Res. Des. 90(1):138-149.

Hassan, H.M., Mumford, C.J. 1993. Mechanisms of drying of skin-forming materials. III. Droplets of natural products. Drying Technology. 11, 1765-1782.

Mass, S. G., G. Schaldach, E. M. Littringer, A. Mescher, U. J. Griesser, D. E. Braun, P. E. Walzel, N. A. Urbanetz. 2011. Powder Technology. J. of Food Engineering. 213. 27–35.

Mermelstein, N.H., 2001. Spray Drying. Food Technol., 55(4): 92-95.

Richard, B., J. F. Le Page, P. Schuck, C. Andre, R. Jeantet, G. Delaplace. 2013. Towards a better control of dairy powder rehydration processes. International Dairy Journal 31. 18 – 28.

Schuck, P., A. Dolivet, S. Méjean, P. Zhu, E. Blanchard, R. Jeantet. 2019. Drying by desorption: A tool to determine spray drying parameters. J. of Food Engineering. 94. 199–204.

Walton, D.E., Mumford, C.J. 1999. The morphology of spray-dried particles: the effect of process variables upon the morphology of spray-dried particles. Transactions of IChemE - Part A. 77, 442-460.

Wu, W. D., W. Liu, T. Gengenbach, M. W. Woo, C. Selomulya, X. D. Chen, M. Weeks. 2014. Towards spray drying of high solids dairy liquid: Effects of feed solid

content on particle structure and functionality. J. of Food Engineering. 123 (2014) 130–135.

www.abbottnutrition.com. 2016. Product Information: Similac Pro-Advance™ Infant Formula with Iron

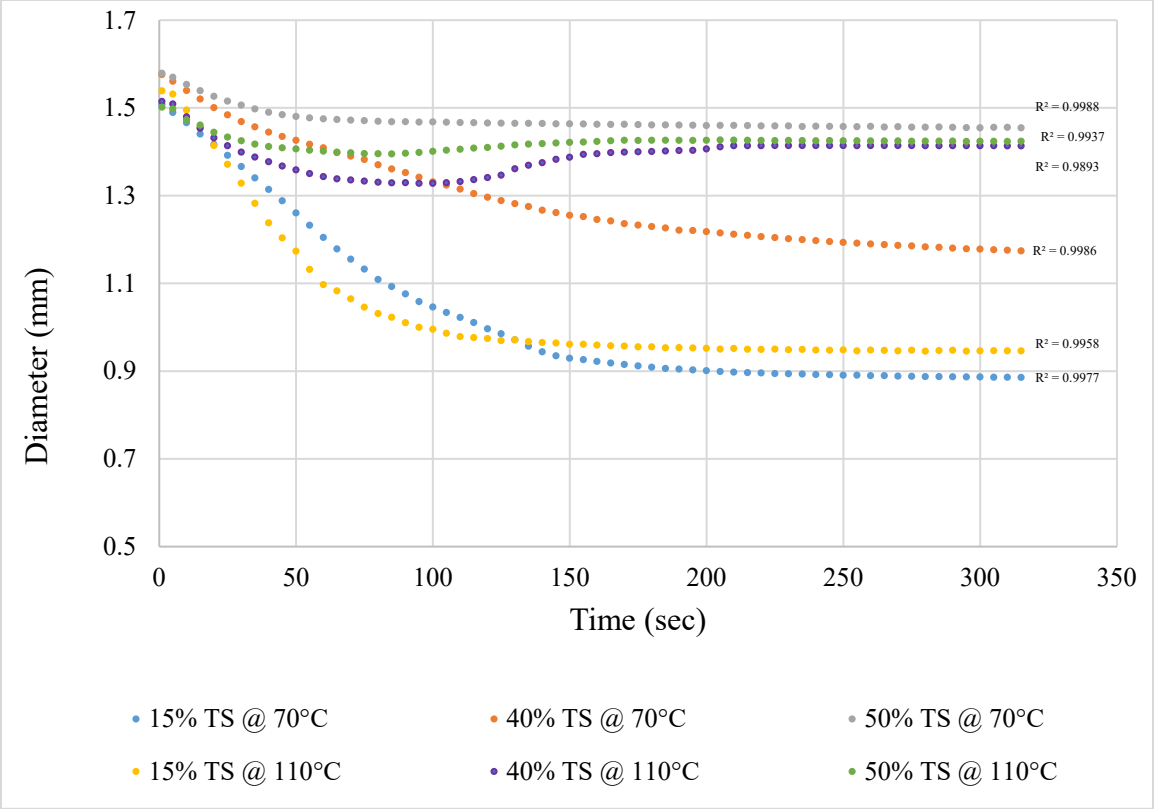

Figure 1. The droplet diameter change (mg) vs. drying time (s) for 2 µL Infant formula droplets at 15%, 40%, and 50% total solids level at 70° C and 110°C, with an air velocity of 0.8 m/s.

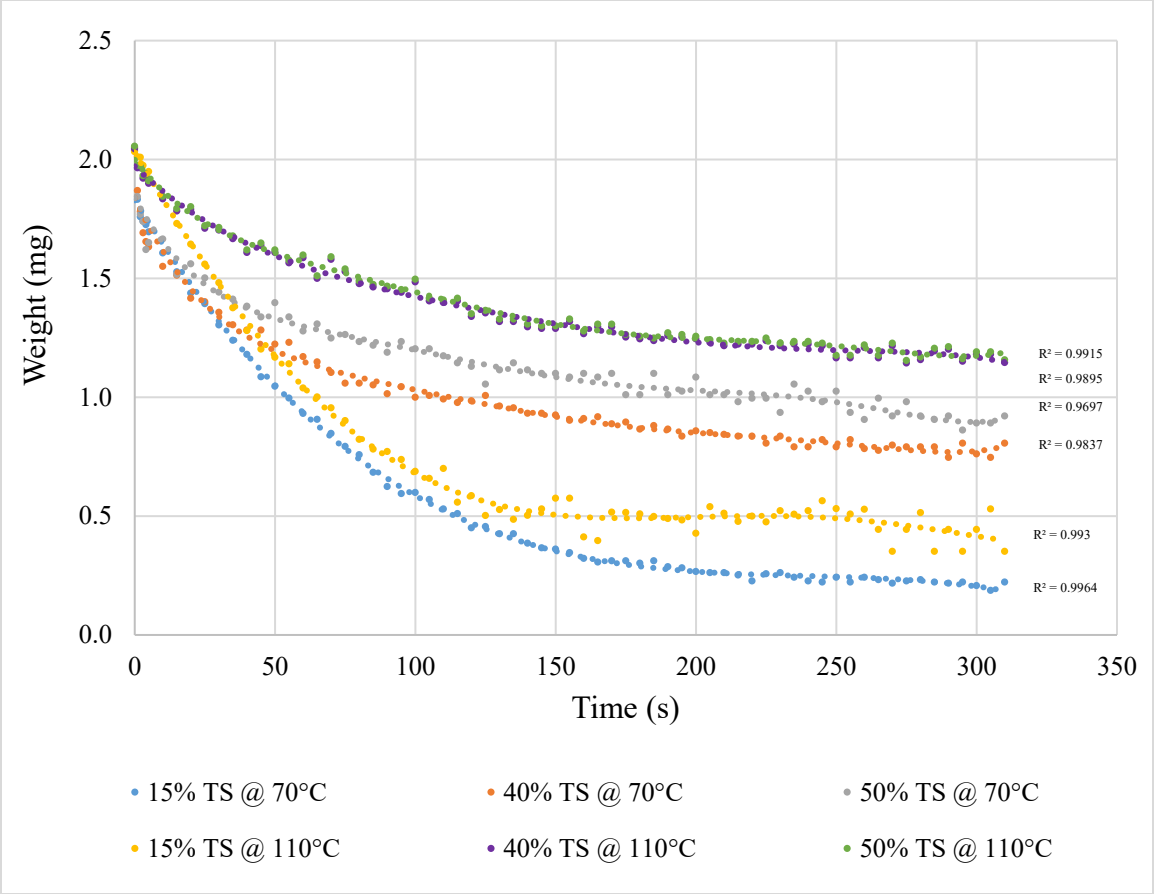

Figure 2. The droplet mass change (mg) vs. drying time (s) for 2 µL Infant formula droplets at 15%, 40%, and 50% total solids level at 70° C and 110°C, with an air velocity of 0.8 m/s.

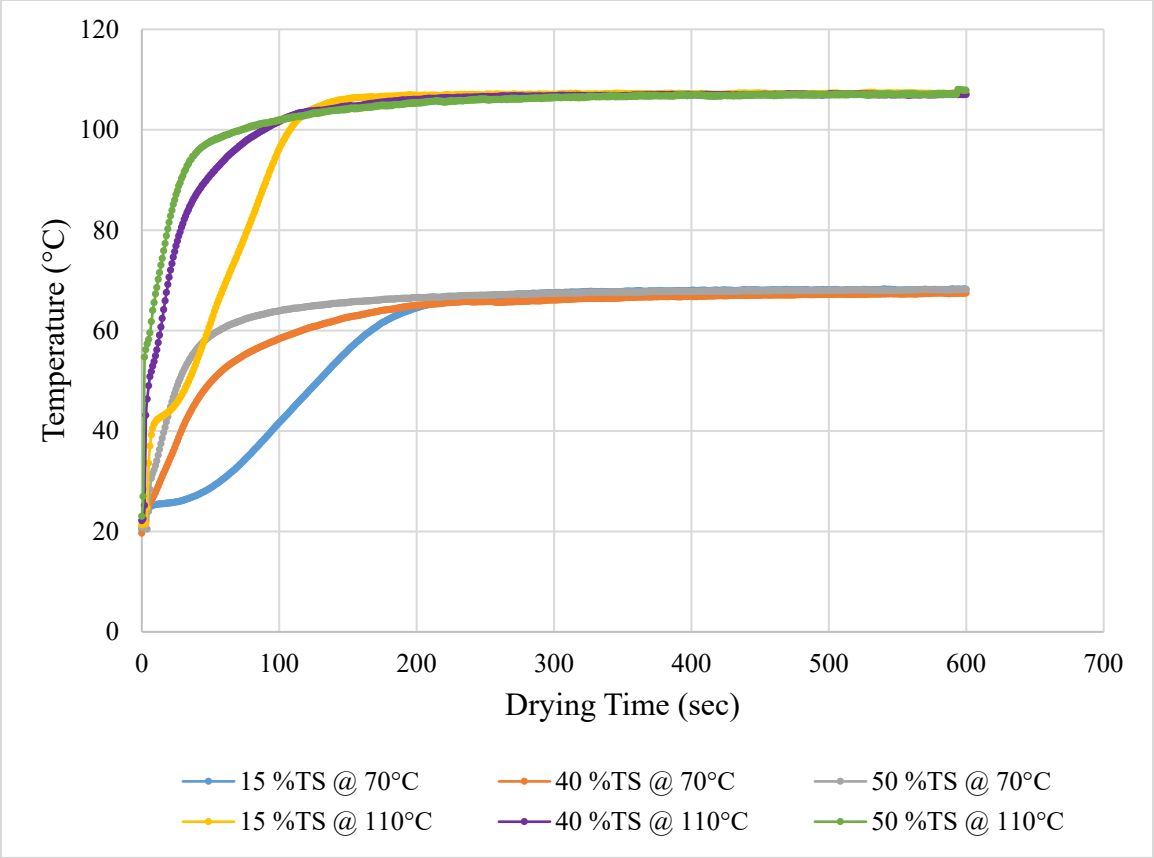

Figure 3. Droplet temperature profile (°C) vs. Drying time (s) of Infant formula at three different total solids level viz. 15%, 40%, and 50% total solids level at 70° C and 110°C with an air velocity of 0.8 m/s.

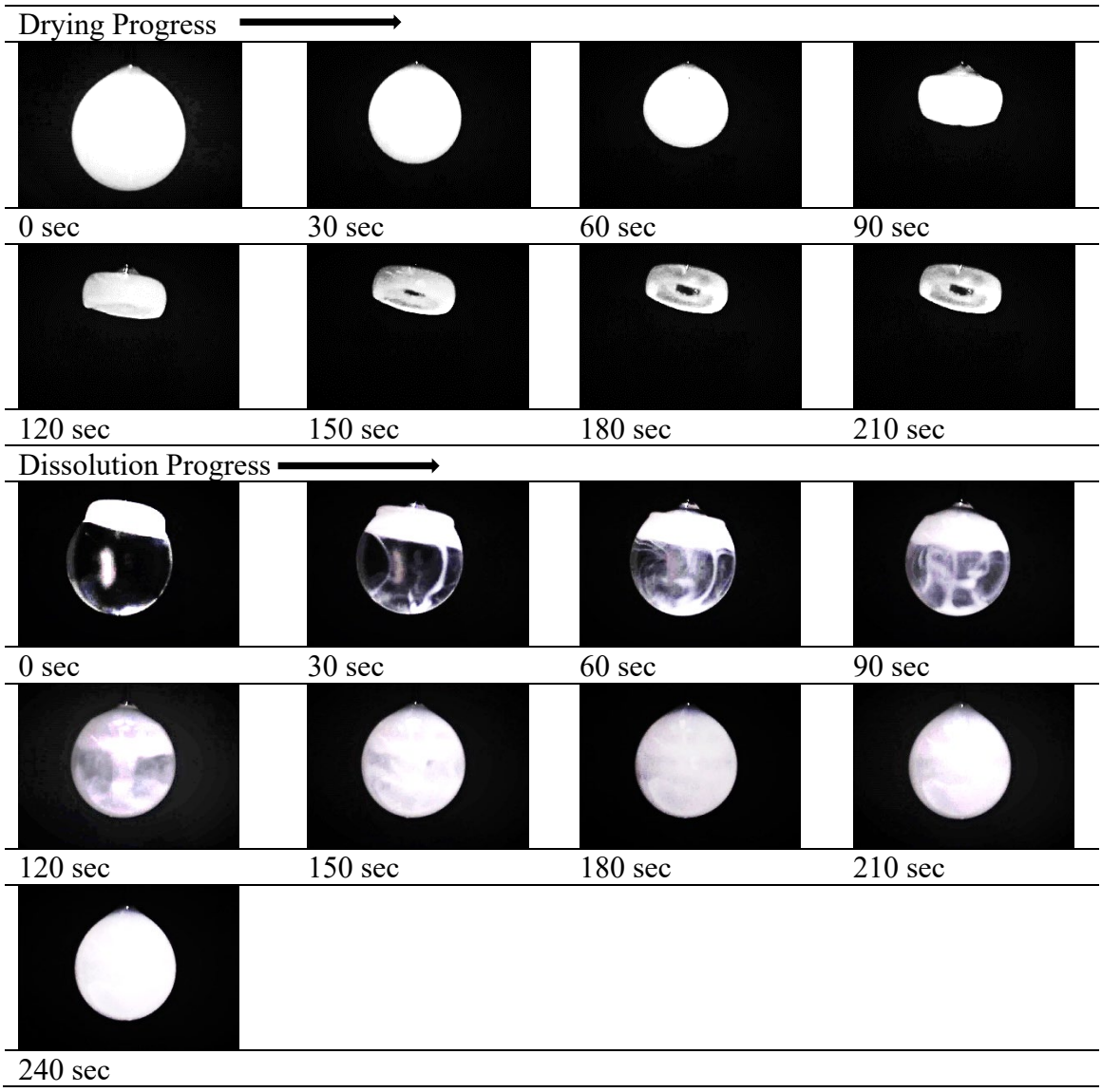

Figure 4. Drying and dissolution/ rehydration behavior of 2µL droplet of 15% Infant formula dried at 70°C/ 0.8 m/s air velocity and rehydrated with a 2µL water droplet.

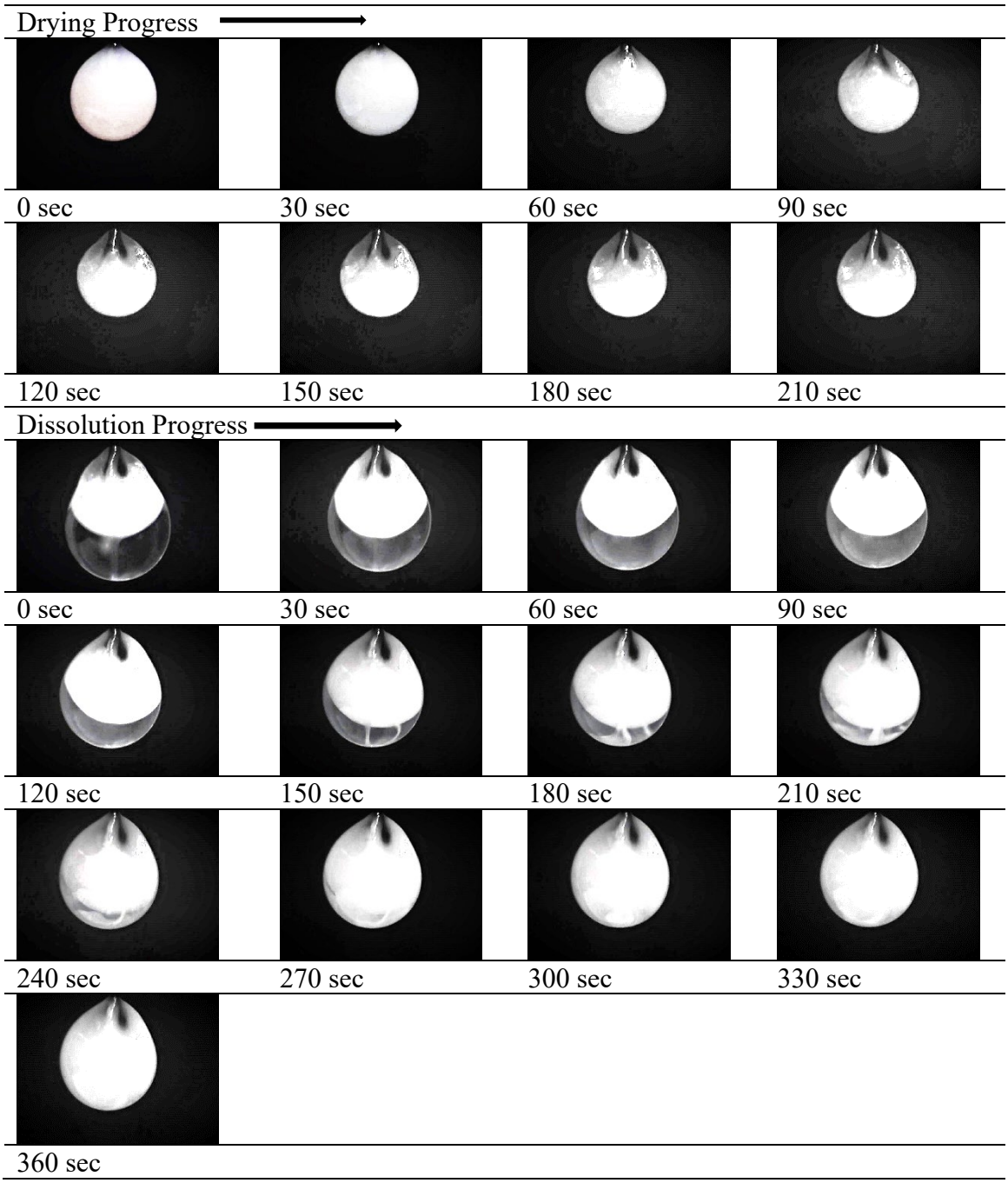

Figure 5. Drying and dissolution/ rehydration behavior of 2µL droplet of 40% Infant formula dried at 70°C/ 0.8 m/s air velocity and rehydrated with a 2µL water droplet.

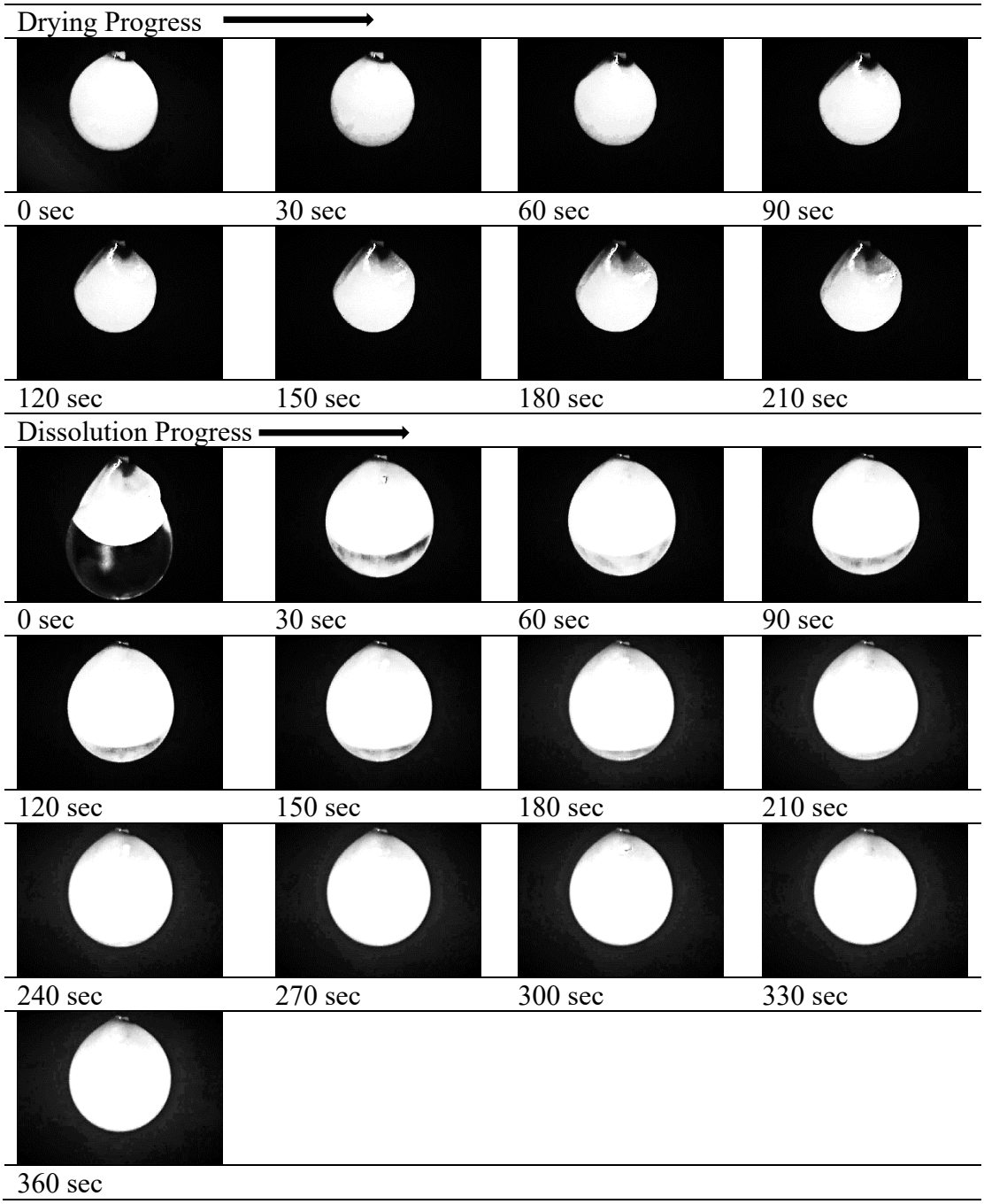

Figure 6. Drying and dissolution/ rehydration behavior of 2µL droplet of 50% Infant formula dried at 70°C/ 0.8 m/s air velocity and rehydrated with a 2µL water droplet.

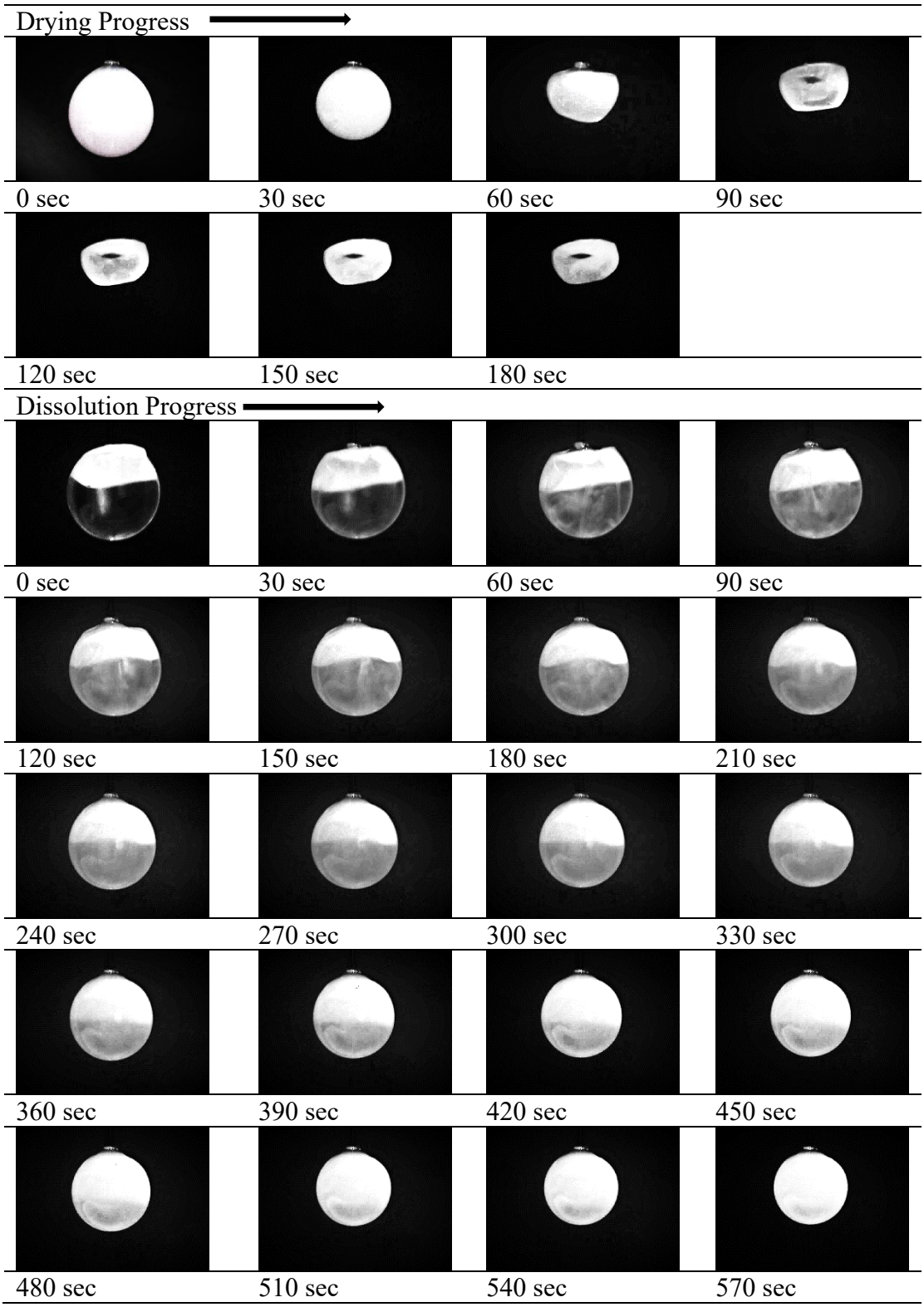

Figure 7. Drying and dissolution/ rehydration behavior of 2µL droplet of 15% Infant formula dried at 110°C/ 0.8 m/s air velocity and rehydrated with a 2µL water droplet.

Drying Progress →			
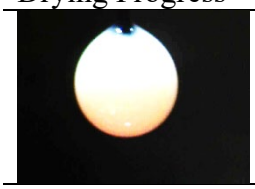		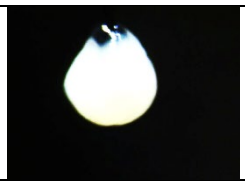	
0 sec	30 sec	60 sec	90 sec
			
120 sec	150 sec	180 sec	
Dissolution Progress →			
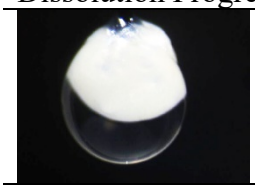	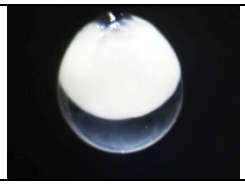	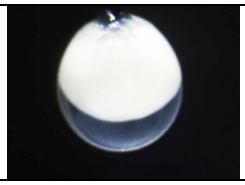	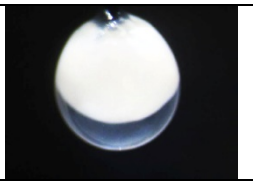
0 sec	30 sec	60 sec	90 sec
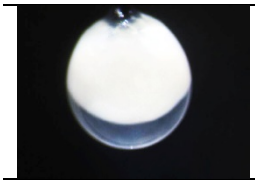	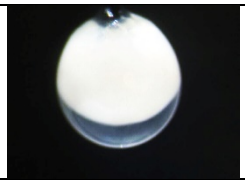	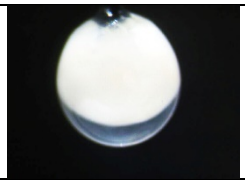	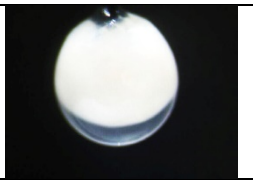
120 sec	150 sec	180 sec	210 sec
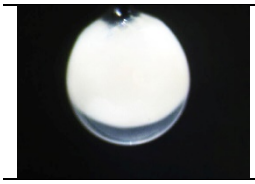	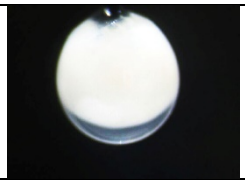	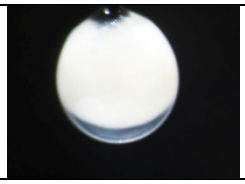	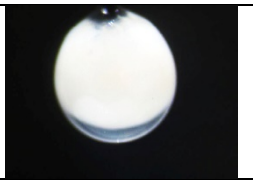
240 sec	270 sec	300 sec	330 sec
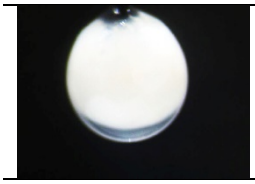	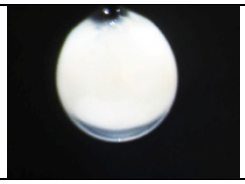	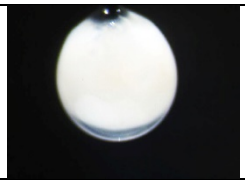	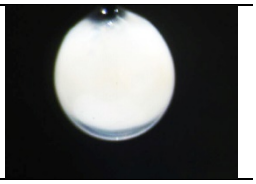
360 sec	390 sec	420 sec	450 sec
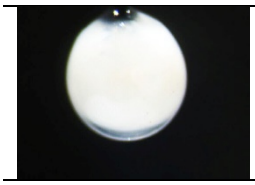	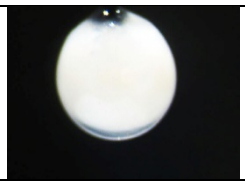	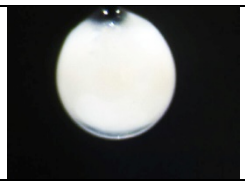	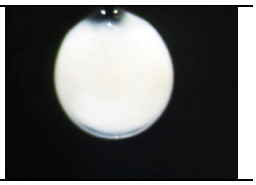
480 sec	510 sec	540 sec	570 sec

Continued on next page…

600 sec	630 sec	660 sec	690 sec

Figure 8. Drying and dissolution/ rehydration behavior of 2µL droplet of 40% Infant formula dried at 110°C/ 0.8 m/s air velocity and rehydrated with a 2µL water droplet.

Drying Progress →

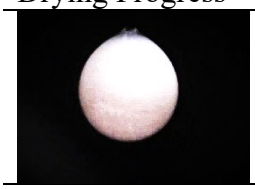
0 sec


30 sec

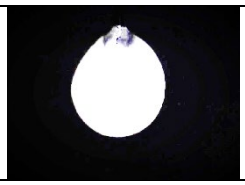
60 sec


90 sec


120 sec

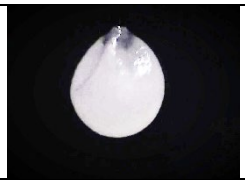
150 sec

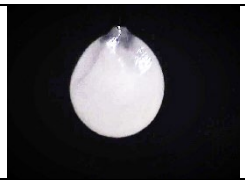
180 sec

Dissolution Progress →


0 sec


30 sec


60 sec


90 sec


120 sec


150 sec

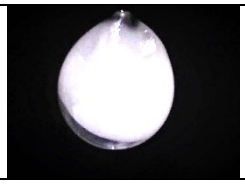
180 sec


210 sec


240 sec


270 sec


300 sec


330 sec


360 sec


390 sec


420 sec


450 sec


480 sec


510 sec


540 sec


570 sec

Continued on next page…

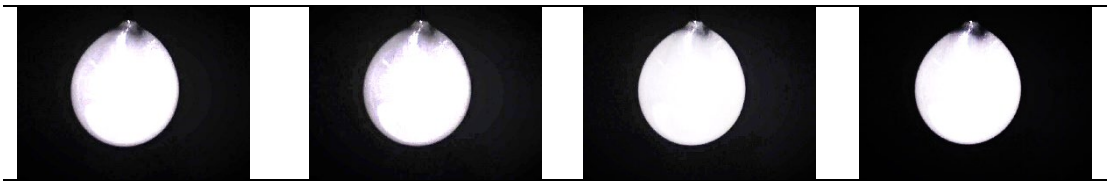

Figure 9. Drying and dissolution/ rehydration behavior of 2µL droplet of 50% Infant formula dried at 110°C/ 0.8 m/s air velocity and rehydrated with a 2µL water droplet.

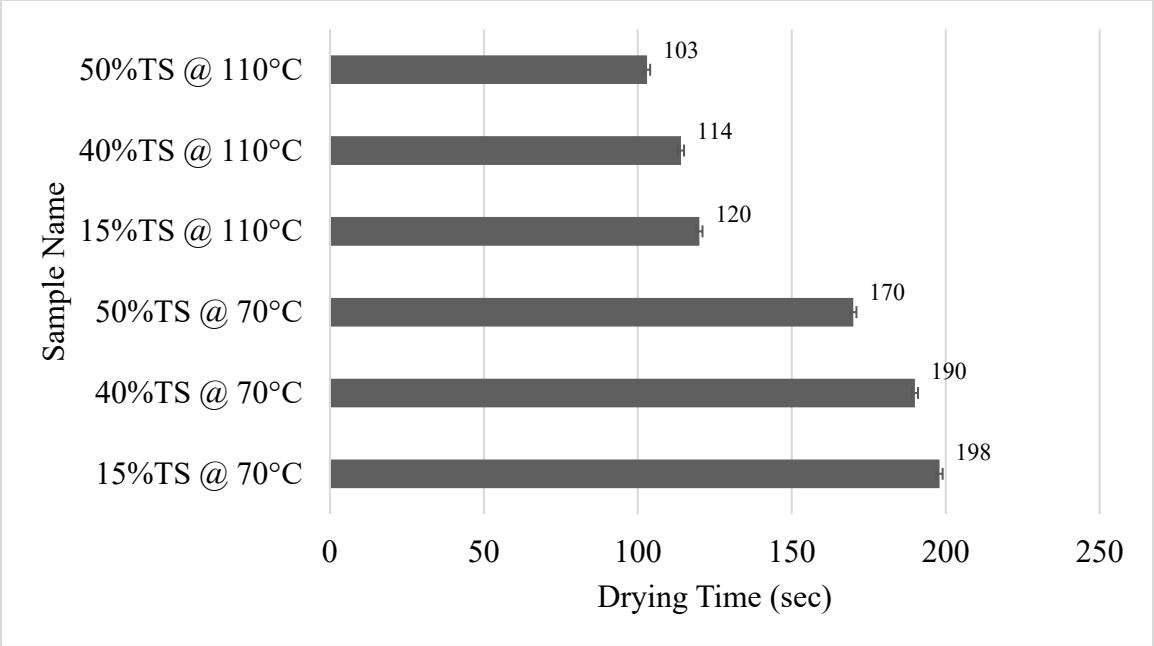

Figure 10. Drying time (sec) for each corresponding sample is shown in this chart. Values are the means of data from triplicate analysis, with the standard deviation indicated by vertical error bars.

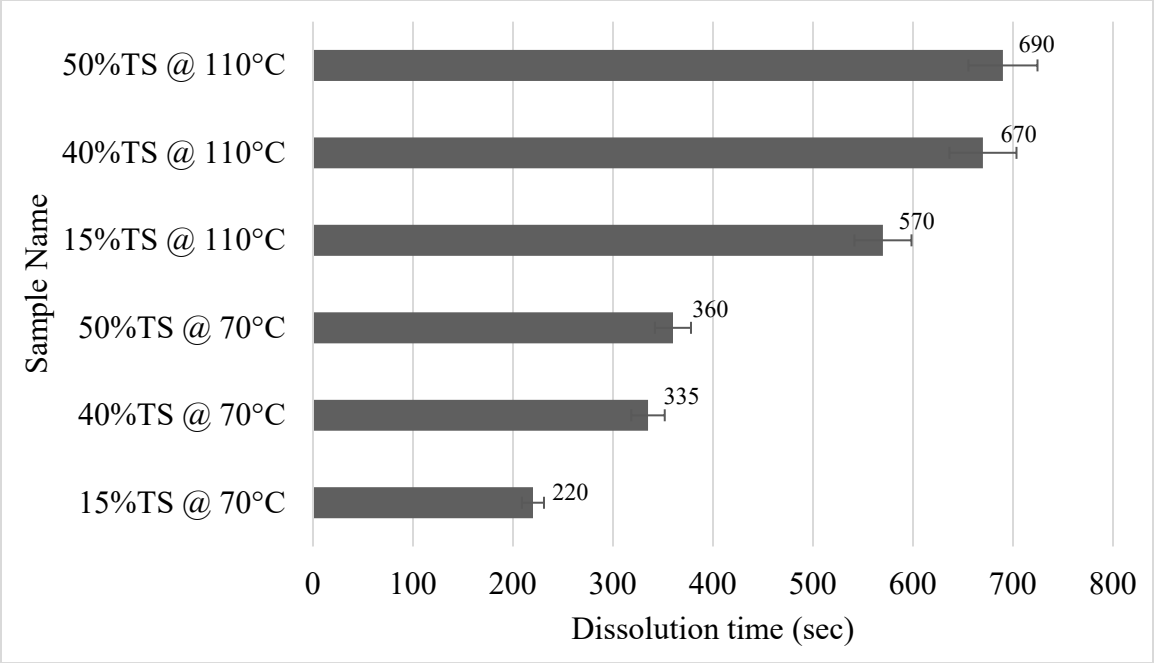

Figure 11. Dissolution time (sec) for each corresponding sample is shown in this chart. Values are the means of data from triplicate analysis, with the standard deviation indicated by vertical error bars.

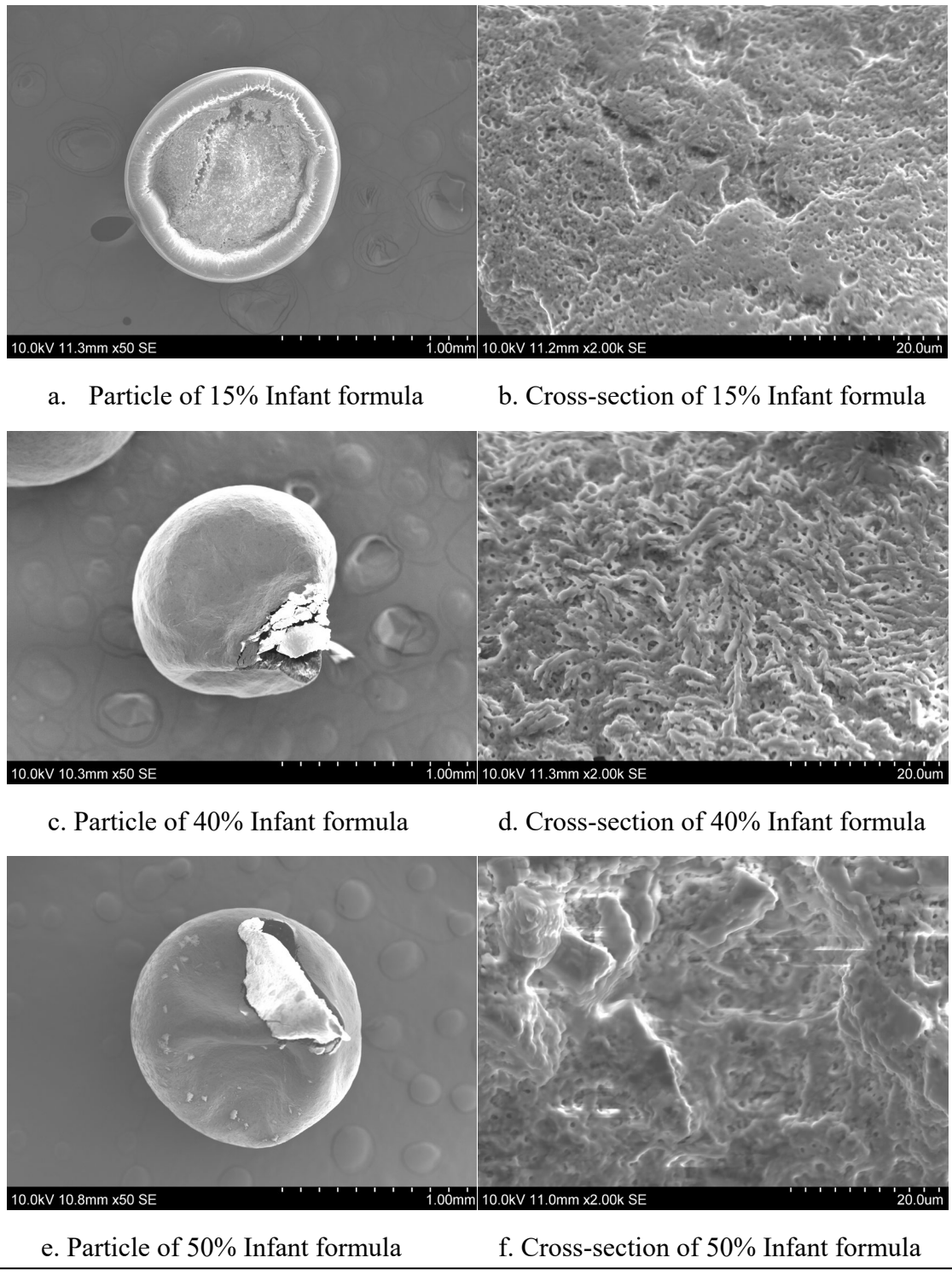

Figure 12. Scanning electron microscopy images of Infant formula standardized at 15%, 40%, and 50% total solids level dried at 70°C with drying air velocity of 0.8 m/s.

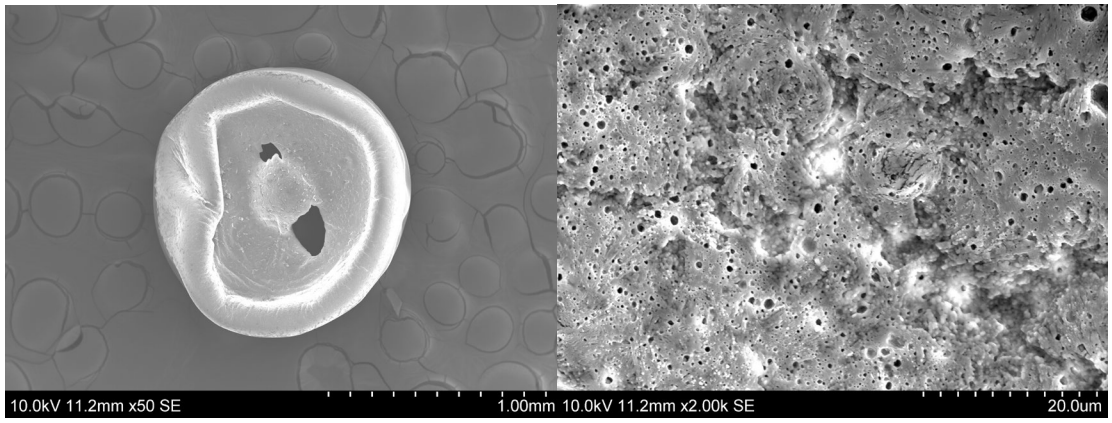

a. Particle of 15% Infant formula b. Cross-section of 15% Infant formula

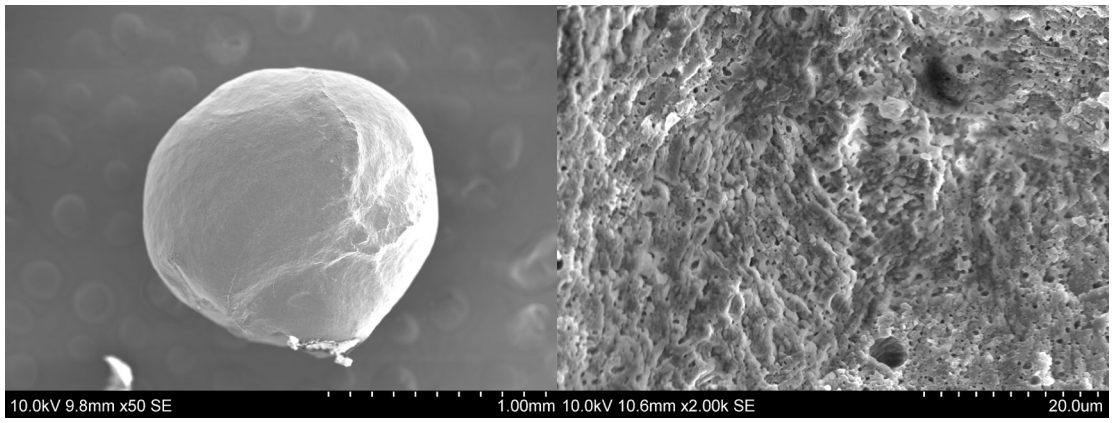

c. Particle of 40% Infant formula d. Cross-section of 40% Infant formula

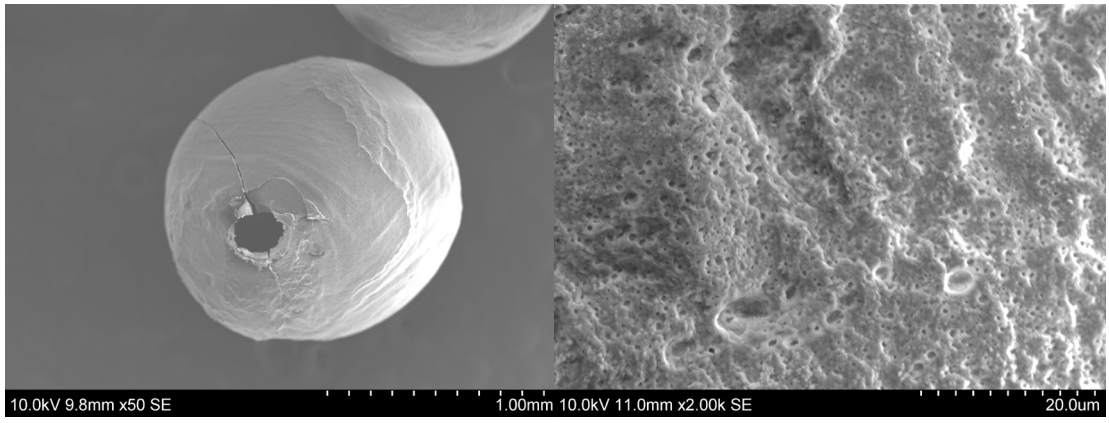

e. Particle of 50% Infant formula f. Cross-section of 50% Infant formula

Figure 13. Scanning electron microscopy images of Infant formula standardized at 15%, 40%, and 50% total solids level dried at 110°C with drying air velocity of 0.8 m/s.

Table 1. Nutritional information of powdered Similac Pro-Advance™ Infant Formula with Iron prepared 1000 ml. as directed on the package.

Parameters	Value
Calories	643
Volume, mL	100
Protein, g	13.31
Fat, g	36.02
Carbohydrate, g	67.53
Water, g	905
Linoleic Acid, mg	6431
Vitamin A, IU	1929
Vitamin D, IU	482
Vitamin E, IU	9.6
Vitamin K, mcg	51.5
Thiamin (Vitamin B1), mcg	643
Riboflavin (Vitamin B2), mcg	1029
Vitamin B6, mcg	405
Vitamin B12, mcg	1.67
Niacin, mcg	7074
Folic Acid (Folacin), mcg	102.9
Pantothenic Acid, mcg	3023
Biotin, mcg	29.6
Vitamin C (Ascorbic Acid), mg	57.9

Choline, mg	154.4
Inositol, mg	31.5
Calcium, mg	527
Calcium, mEq	26.4
Phosphorus, mg	283
Magnesium, mg	38.6
Iron, mg	12.22
Zinc, mg	5.08
Manganese, mcg	32.2
Copper, mcg	611
Iodine, mcg	39
Selenium, mcg	13
Sodium, mg	161
Sodium, mEq	7.1
Potassium, mg	707
Potassium, mEq	18
Chloride, mg	437
Chloride, mEq	12.2

Table 2. The viscosity of Infant formula standardized at three different solid levels.

Product	**Viscosity (Cp)**
Infant Formula 15%	2.66[a]
Infant Formula 40%	16.33[b]
Infant Formula 50%	57.39[c]

Cp = Centipoise

(All values are average values of three replicates obtained from three different trials. For each product, the calculated value of SEM is < 1%. The P-value obtained from one-way ANOVA between the products is $P<0.01$)

[a,b,c] Means within the same column not sharing a common superscript are significantly different ($P<0.01$).

CHAPTER 5

OVERALL CONCLUSIONS

Dairy ingredients account for one of the major export commodities in the global market. However, specific quality, functionality, and process efficiency-related issues currently limit the competitiveness of US-made ingredients in the global market. Major dairy ingredient manufacturers indicated that they are facing challenges related to the optimization of processing/ spray drying conditions to achieve the best quality and functionality of dairy ingredients. One of the primary reasons for this is the lack of a laboratory-scale modeling facility to optimize and tailor spray drying conditions and functionality of dairy ingredients. Therefore, manufacturers rely on trial and error approaches that could be costly and time-consuming. Hence, SDD was installed at SDSU.

A significant part of this research has been directed towards understanding several phenomena associated with a convective droplet drying process using an improved glass filament SDD approach. The SDD rig and experimental procedures were first optimized to achieve an accurate measurement of droplet drying kinetics. The SDD experiments were conducted to study the effect of different total solids/ composition and outlet temperatures of the dryer on the drying kinetics. The SDD experiment was then extended to incorporate dissolution tests, which enabled the evaluation of the rehydration particle functionalities as affected by the drying conditions.

It was interesting to witness the fact that due to differences in the solid concentration of Whey Protein Concentrate resulted in the differences in the drying

kinetics because at the higher solid concentration level, and it was difficult to achieve equilibrium temperatures due to the faster formation crust on the outer surface versus lower solid concentration.

Due to the differences between MCC and Modified MCC in the pH and mineral balance and the presence of the higher amount of de-aggregated casein micelle in the modified MCC, we observed differences in the drying properties (like change in moisture removal pattern and mass change of the particle) of both the materials. Moisture removal was faster in the case of modified MCC as compared to MCC. This is due to the de-aggregation and change in pH from 6.7 to 5.7. The mass change was rapid for Modified MCC compared to MCC. Modified MCC reached the equilibrium temperature faster as compared to MCC.

We observed better rehydration/ higher solubility of the powder particle of Infant Milk formula dried at 70°C temperature as compared to those dried at 110°C. It was also interesting to observe particle throughout the drying and rehydration process. It was thrilling to observe all the particles prepared during the experiments by scanning electron microscopy.

Overall different strategies were applied in this study to evaluate the feasibility of using SDD or bench-top trials.

FUTURE RECOMMENDATIONS

Considering the impact of the improved glass filament SDD technique to study the phenomena associated with drying and mechanisms behind these phenomena, there is a great deal of future work that could be carried out following similar principles. These future works may be divided into three main areas, i.e., the investigations on the drying behaviors of other material systems, the investigations on the three-particle functionalities for other material systems, and the extension of the technique to observe other particle properties. Also, the survival of some desirable microorganisms like probiotics at certain outlet temperatures of drying will be a fascinating study.

The proposed research will undoubtedly lead to new insights and technical developments in functional particle engineering.